Beyond-the-Quark-Model Heavy Hadrons from QCD Sum Rules

A Thesis Submitted to the

College of Graduate and Postdoctoral Studies

in Partial Fulfillment of the Requirements

for the degree of Doctor of Philosophy

in the Department of Physics & Engineering Physics

University of Saskatchewan

Saskatoon

By

Alex Palameta

Permission to Use

In presenting this thesis in partial fulfilment of the requirements for a Postgraduate degree from the University of Saskatchewan, I agree that the Libraries of this University may make it freely available for inspection. I further agree that permission for copying of this thesis in any manner, in whole or in part, for scholarly purposes may be granted by the professor or professors who supervised my thesis work or, in their absence, by the Head of the Department or the Dean of the College in which my thesis work was done. It is understood that any copying or publication or use of this thesis or parts thereof for financial gain shall not be allowed without my written permission. It is also understood that due recognition shall be given to me and to the University of Saskatchewan in any scholarly use which may be made of any material in my thesis.

Requests for permission to copy or to make other use of material in this thesis in whole or part should be addressed to:

Dean
College of Graduate and Postdoctoral Studies
University of Saskatchewan
116 Thorvaldson Building, 110 Science Place
Saskatoon, Saskatchewan S7N 5C9
Canada

Department of Physics & Engineering Physics
University of Saskatchewan
116 Science Place, Rm 163
Saskatoon, SK S7N 5E2
Canada

Abstract

In this thesis, we examine three papers that my coauthors and I have published. The overarching theme of this work will be the use of QCD Laplace sum rules applied to quarkonium or quarkonium-like systems containing heavy quarks in an attempt to explore ideas relating to beyond-the-quark-model hadrons, including hybrids (mesons with gluonic content) and multi-quark meson-like states.

In the first two papers [1, 2], we study mixing between conventional mesons and hybrids in vector and axial vector charmonium-like and bottomonium-like systems. We compute meson-hybrid cross-correlators within the operator product expansion, including condensate contributions up to dimension-six. We then use the measured masses of heavy quarkonium-like states as inputs into a QCD Laplace sum-rules calculation to probe known resonances for nonzero coupling to both the conventional meson and hybrid currents. Nonzero coupling to both of these currents would signal meson-hybrid mixing. We find nonzero mixing in a number of resonances over all four of the mass spectra which we probed. The results from both [1] and [2] are collected and discusses in section 2.7.

In the third paper [3], constituent mass predictions for axial vector cc and bb diquarks are generated using QCD Laplace sum-rule methods. We calculate the diquark correlator within the operator product expansion to next-to-leading-order, including condensate contributions up to dimension-six. We find that the constituent mass of the cc diquark is (3.51 ± 0.35) GeV and the constituent mass of the bb diquark is (8.67 ± 0.69) GeV. We then use these diquark constituent masses as inputs to calculate several tetraquark masses within the Type-II chromomagnetic interaction diquark-antidiquark tetraquark model. The results from the calculations done in [3] are collected in section 3.3.

Acknowledgements

I would like to thank my co-supervisors Dr. Tom Steele and Dr. Derek Harnett for their guidance and insights; a student could not ask for better supervisors. Additionally, I would like to thank my family for their continued support and understanding.

Contents

List of Tables

List of Figures

List of Abbreviations

CMI - chromomagnetic interaction
dim-reg - dimensional regularization
LHS - Left-hand Side
LO - Leading Order
LSR(s) - Laplace sum-rule(s)
NLO - Next-to-leading Order
NOP - Normal Ordered Product
OPE - Operator Product Expansion
QCD - Quantum Chromodynamics
QCDSR(s) - QCD sum-rule(s)
QED - Quantum Electrodynamics
QFT - Quantum Field Theory
RG - Renormalization Group
RHS - Right-hand Side
SSB - Spontaneous Symmetry Breaking
TOP - Time Ordered Product
VEV - Vacuum Expectation Value

Chapter 1

Introduction

1.1 Preamble

In this thesis, we explore several ideas related to beyond-the-quark-model hadrons in the context of QCD sum rules. The research presented here is based on three papers I've published in Physical Review D [1, 2, 3]. The first two papers [1, 2], presented in sections 2.3 and 2.5 of this thesis respectively, explore meson-hybrid mixing in heavy quarkonium using QCD sum rules. In the third paper [3], presented in section 3.2, we use QCD sum rules to predict constituent masses for cc and bb diquarks. We then use these constituent masses to predict tetraquark masses.

In addition to presenting the research articles in chapters 2 and 3, we will include additional background and motivation for these topics as well as any additional discussion that may not have made it to the published works. The goal will be to give context and clarify the motivation for these articles while also expanding on the results and highlighting any novel techniques which may not have been discussed in detail in the final articles. Note that [1] and [2] are grouped and presented together in chapter 2 as the latter is an extension of the former where we explore new quantum numbers. Then [3] is presented separately in chapter 3. Finally at the end of the thesis we include appendices A.1 and A.2 both as a reference and to clarify any convention dependence in the calculations.

Before we get into the research portion of this thesis, we begin with a brief overview of the topics in modern particle physics that will be important in understanding this discussion of beyond-the-quark-model hadrons. Much of the early work for the research presented in [1] was done during my master's degree and was presented in my master's thesis [8]. There I presented the background needed to discuss these topics and the motivations for

exploring meson-hybrid mixing. The motivation and necessary particle physics background information have not changed as the work has progressed and so the following introduction borrows heavily from that earlier work Ref. [8].

1.2 The Quark Model

By the 1950s, the idea that atoms were made up of a positively charged nucleus and some number of negatively charged electrons bound together by the electromagnetic force had been around for decades. The fact that these nuclei were themselves made up of more fundamental nucleons, positively charged protons and neutral neutrons, had also been known for decades.

The discovery of the substructure of the nucleus originally raised questions about how all of these positively charged protons could remain bound considering the electromagnetic repulsion they experience. This problem was solved by introducing the strong nuclear force, which acted as the binding force that provided the attraction for these nucleons. It was understood that this force would need to be strong enough to overpower the electromagnetic repulsion of the protons over short ranges, but it would also need to fall off quickly as distances increased beyond the size of the atomic nucleus. A subatomic particle with a mass consistent with the range of the nuclear force had also been theorized to mediate this strong nuclear force.

By the early 1950s, pions had been discovered; these pions fit neatly into the particle physics of that era as they could act as the carrier particles of the strong nuclear force. In addition to these pions, other particles were being discovered around this time such as the kaon (or K meson) and the lambda baryon. As time went on through the 1950s and early 1960s, more and more of these subatomic particles were being discovered. Around this time, the term "hadron" was coined to serve as a blanket term for all of these particles. So many hadrons were being discovered that it was quickly becoming obvious that they could not be fundamental. A theory that explained all of these hadrons and their substructure was needed, and this is where the quark model came in.

The quark model, which was independently proposed by Murray Gell-Mann [9] and George Zweig [10] in 1964, is a classification scheme for hadrons in terms of their valence

quarks. At this time, the quark model classified hadrons according to their quantum numbers, which are determined by their constituent quarks and antiquarks.

From our current perspective, these quarks come in one of six flavours which are listed here in ascending order by mass: up (u), down (d), strange (s), charm (c), bottom (b), top (t). All of these are spin-$\frac{1}{2}$ fermions, and each of them has an intrinsic fractional electric charge (Q). For the up, charm and top quarks, $Q = \frac{2}{3}e$, and for the down, strange and bottom quarks, $Q = -\frac{1}{3}e$ where e is the elementary charge. Combinations of these quarks and their antiquark counterparts in bound states give us the hadrons. In the quark model, hadrons can be broken down into two categories: baryons, which are a fermionic bound state of three quarks (or antiquarks), and mesons which are a bosonic bound state of a quark and an antiquark (Figure 1.1).

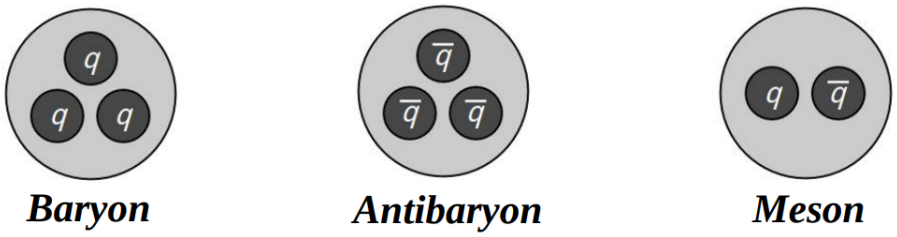

Figure 1.1: Hadrons in the quark model.

1.2.1 The Quark Model and Colour Charge

The quark model was very successful at classifying the hadrons known in that era as well as sorting them into the various geometric patterns of the eightfold way. In addition to giving us a classification scheme for the hadrons and helping explain their substructure, the quark model was also able to predict the existence of new hadrons such as the Ω^-. The quark model enjoyed many other successes including explaining mass splittings between mesons and baryons within their respective multiplets, explaining and predicting the magnetic moments of mesons and baryons, and explaining why there are no spin-1 baryons. The successes of the quark model are well documented in the literature, for a particularly well curated collection of papers on this topic see [11]. For all of its successes, the early quark model did, however, have a couple of serious problems.

One major problem with the early quark model became clear when it was realized that

the Δ^{++} baryon, with its intrinsic spin $S = \frac{3}{2}$ and orbital angular momentum $L = 0$, consisted of three up quarks with parallel spins. It was realized that this would lead to a totally symmetric wave function, violating the Pauli exclusion principle. The best solution to the problem turned out to be the ad hoc introduction of a new quantum number carried by quarks that would come to be known as colour charge. Each quark would now carry a colour: red, green, or blue. Antiquarks would carry anticolour, *i.e.*, anti-red, anti-green, or anti-blue. The colour charge portion of the Δ^{++} wave function could then be constructed as totally antisymmetric. The addition of this new quantum number gave us the anti-symmetric piece of the wave function which we need to satisfy the Pauli exclusion principle and thus fix the problem of the Δ^{++}.

Another serious problem was the question of free quarks. One might expect that, since hadrons are made up of quarks, colliding hadrons with sufficient energy should liberate these quarks, and we should be able to somehow detect these free quarks emerging from the collision event. However, this is not what we find. Instead we see jets of hadrons emerging from these collisions which leads to the following questions: If all hadrons are made up of quarks, why is it that free quarks are never observed? Also, where are these hadrons that make up the jets coming from? Another ad hoc addition to the quark model was needed to address this issue. It was suggested that if free quarks are not observed, they must be confined to these hadrons. Even if these hadrons are collided at sufficient energies to liberate a quark, the free quark would never be observed; instead, these quarks would immediately undergo hadronization (discussed briefly below), and our detectors would only pick up jets of hadrons emerging from the collision event. This phenomenon became known as quark confinement. It was also realized that perhaps this confinement could be characterized in terms of colour charge since all bound states had been observed to be colour singlets. Thus, we refer to confinement as colour confinement. While it can be useful to think of the colours of quarks in a hadron as additive colours in a basic optical sense we should always have the idea that this colour charge emerges from SU(3) gauge theory at the back of our minds.

Incorporating this idea of colour charge into the quark model gives us an updated picture of which hadrons are allowed in the quark model. The three quarks that make up a baryon must now carry one unit of each colour to form a colourless bound state. Likewise, the three

antiquarks in an antibaryon must carry one unit of each of the three anticolours to form a colourless bound state, and mesons can carry any colour and the appropriate anticolour. See Figure 1.2 for hadronic configurations allowed in the quark model.

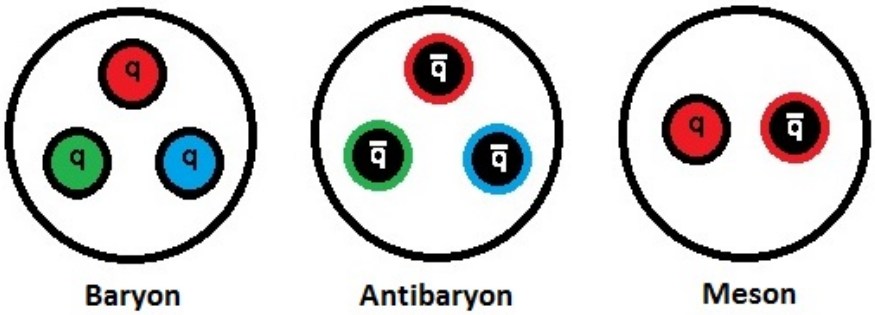

Figure 1.2: Hadrons in the quark model with colour charge.

Perhaps the way in which I have chosen to write about the quark model makes these topics seem more discretized than they should be. In reality, the quark model evolved slowly throughout the 1960s, with individual ideas being developed and incorporated, until it eventually became what we now think of as the quark model. It should also be mentioned that many of the ideas in the quark model (particularly the colour hypothesis) were incorporated into and influenced the development of quantum chromodynamics (QCD) which will be discussed shortly.

1.2.2 Quark Model Mesons

In the quark model, mesons are described as a bound state of a quark-antiquark pair. As we know that all quarks are spin-$\frac{1}{2}$ fermions, we know that mesons must contain intrinsic spins $\vec{S}$ where our quantum numbers are $s = 0$ or $s = 1$. We can then write the total angular momentum $\vec{J}$ of the bound state as

$$\vec{J} = \vec{S} + \vec{L} \tag{1.1}$$

where $\vec{L}$ is the orbital angular momentum. Here $\vec{L} = 0$ corresponds to the ground state of our meson with higher values of $\vec{L}$ (increasing in integer steps) corresponding to excited states. (Note that the excited states are generally considered to be distinct mesons.) Quantization of angular momentum gives $L^2 = l(l+1),\ l \in \{0, 1, 2, ...\}$. Note that for the entirety of this

thesis, we will be using natural units where $\hbar = c = 1$.

There are two other quantum numbers that will be useful to us in classifying mesons. These are parity (P) and C-parity (also known as charge parity or charge conjugation number) (C) which, for mesons, can be written as functions of angular momentum and spin quantum numbers as

$$P = (-1)^{l+1}, \qquad C = (-1)^{l+s}. \tag{1.2}$$

Collectively, we refer to the values J, P, and C as a particle's J^{PC} which gives us a natural way of classifying many particles. Using (1.2), we can show that, for mesons, $J^{PC} \in \{0^{-+}, 0^{++}, 1^{--}, 1^{+-}, 1^{++}, 2^{--}, 2^{++}, \dots\}$. Any other J^{PC} values not appearing in this list would be referred to as exotic quantum numbers for mesons.

1.3 Quantum Chromodynamics

Quantum chromodynamics is the quantum field theory (QFT) of strong interactions. In essence, a QFT can be described as a mathematical framework which allows for the unification of special relativity and quantum mechanics while incorporating the concept of fields and allowing for the creation and annihilation of particles.

By the late 1960s and early 1970s, quantum electrodynamics (QED) was already well established as the QFT of electrodynamics. Quantum electrodynamics mathematically describes all phenomena involving electrically charged, spin-1/2 particles interacting by means of photon exchange. The successes of QED, coupled with the insights gained from the quark model, led to attempts to form a QFT of strong interactions; this theory would become known as QCD.

It was important for QCD to be able to explain experimental results such as deep inelastic scattering (DIS) [12] as well as reproduce the known results from the quark model. It should be mentioned that DIS is an experiment in which protons (or any other sufficiently stable hadrons for that matter) are bombarded with very high energy electrons in an attempt to resolve the substructure of these hadrons. It was experiments like this that provided the first convincing evidence that quarks were, in fact, real particles and not simply a mathematical construct of the theory as some had previously believed them to be. These DIS experiments

also provided evidence that quarks are spin-1/2 particles and that protons are indeed made of a d quark and two u quarks. To match the results of these DIS experiments, it was understood that QCD would need to be an asymptotically free theory. An asymptotically free theory can be described as a theory for which the strength of interactions between particles becomes asymptotically weaker (*i.e.* approaches zero) as energy increases and distance decreases.

It was shown that in four spacetime dimensions, the only asymptotically free renormalizable gauge theories were the class of theories known as Yang-Mills theories [13]. These theories are invariant under local SU(N) transformations. It was also realized that the theory would need to exhibit $\mathrm{SU}(3)_{\mathrm{colour}}$ symmetry as quarks of different colours are indistinguishable from one another. This indicated that QCD should be constructed as an SU(3) Yang-Mills theory. Furthermore, Yang-Mills theories are gauge theories, and, as such, our theory must introduce mediating vector bosons which must carry our colour charge as we have ($N \geq 2$). These vector bosons became known as gluons. There is a rich history surrounding the development of QCD (see e.g., [14] and references therein for a historical perspective); however, we will focus on some of the key concepts of the theory as they are understood today before we move on.

1.3.1 Key Concepts in QCD

Where the strong force was once thought of as the force holding the nucleus together, it is now understood that the strong force is actually the force acting on colour-charged particles (quarks) holding hadrons together. It is just the residual effect of this force that holds the nucleus together, analogous to a dipole force in an electromagnetic context.

As we discussed earlier, all quarks are thought of as having one of three colours (red, green, blue) and all antiquarks come in anticolours (anti-red, anti-green, anti-blue). Or in SU(3) gauge theory terms, quarks in the fundamental 3 representation and antiquarks in the 3^* representation. QCD has now introduced bicoloured gluons which have some combination of colour and anti-colour. Or, again, in SU(3) gauge theory terms they reside in the adjoint 8 representation of SU(3). Hadrons are understood to exist only as colour singlet bound states of these particles.

At close range, quarks are bound loosely inside a hadron. As more energy is put into the system and distances increase, we reach a point where it is more energetically economical

to produce new hadrons than to continue to have the distance between these bound quarks grow. As such, hadron jets are produced and free quarks are never observed. This process is what we call hadronization which was mentioned above.

It is important to note that one strong contrast between QED and QCD is that, unlike photons, gluons (the force carrying vector bosons of QCD) carry colour charge and therefore interact strongly. This will be an important characteristic of gluons for our work in this thesis.

1.3.2 The QCD Lagrangian

We now turn our attention to the fundamental quantity of QCD in its Lagrangian formulation: the Yang-Mills Lagrangian which can be written as

$$\mathcal{L}_{\mathrm{QCD}}(x) = -\frac{1}{4}\left(G^a_{\mu\nu}(x)\right)^2 + \sum_F \bar{Q}_F(x)\left(i\not{D} - m_F\right)Q_F(x) \tag{1.3}$$

where

$$G^a_{\mu\nu}(x) = \partial_\mu A^a_\nu(x) - \partial_\nu A^a_\mu(x) + g_s f^{abc} A^b_\mu(x) A^c_\nu(x) \tag{1.4}$$

is a gluon field strength tensor and

$$\not{D} = D^\mu \gamma_\mu = (\partial^\mu - i g_s t^a A^\mu_a(x))\gamma_\mu \tag{1.5}$$

is a slashed covariant derivative. We will take a moment to go over some of the notation here as much of it will be used repeatedly throughout this thesis. Here the quantities Q_F and A^b_μ are quark and gluon fields respectively, and the subscript F is a quark flavour index. The m indicates the mass of the particle, g_s is our coupling constant, t^a is a generator of SU(3), and f^{abc} are totally antisymmetric structure constants. Finally, any slashed variable is understood to employ Feynman slash notation such as $\not{D} = D^\mu \gamma_\mu$.

We can now expand (1.3) and separate out the free terms from the interaction terms in our Lagrangian. In doing so, and by suppressing the arguments and flavour sums, this gives

us

$$\mathcal{L}_{\text{QCD}} = \mathcal{L}_0 + \frac{g_s}{2}\overline{Q}\gamma^\sigma\lambda^a Q A^a_\sigma - g_s f^{abc}(\partial_\rho A^a_\sigma)A^{\rho b}A^{\sigma c} - \frac{g_s^2}{4}(f^{eab}A^a_\rho A^b_\sigma)(f^{ecd}A^{\rho c}A^{\sigma d}) \tag{1.6}$$

where $\mathcal{L}_0$ is our free Lagrangian and the $\lambda^a = 2t^a$ are Gell-Mann matrices. Having done this expansion, we could now construct the Feynman rules for the theory. By inspection, we can see that the first interaction term will lead to a quark gluon vertex where as the second and third terms will give us three and four gluon vertices respectively (see Figure 1.3).

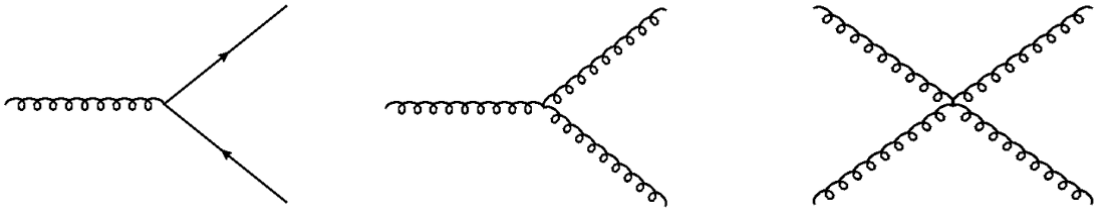

Figure 1.3: Interaction vertices available in QCD, image credit [5]

Details about the vertices shown in Figure 1.3 as well as more discussion on the QCD Lagrangian, can be found in many QFT texts (see e.g., [5]). Note that we use the quantized QCD Lagrangian with a covariant gauge-fixing term and Fadeev-Popov ghosts (also discussed in [5]), this leads to an additional ghost-gluon vertex not shown in Figure 1.3. These additional terms do not enter into the calculations presented in the thesis but would occur in higher-loop extensions of this work. These vertices highlight one of the main differences between QED and QCD; here (in QCD) we have our vector bosons able to have self-interactions where in QED we do not. Moreover, all of these vertices share the same coupling strength as required by SU(3) gauge symmetry. These facts hint that thinking about hadrons with explicit gluonic degrees of freedom is perhaps a sensible thing to do. Some candidates for these hadrons with gluonic degrees of freedom are hybrids and glueballs. Further discussion of hybrids is postponed until Chapter 2 as hybrids are one of the central topics of our first two papers [1, 2], glueballs are not discussed in this thesis.

An important side note: thus far, we have been somewhat careful about the position of indices. This will not be the case in general throughout the thesis. Generally, indices will be raised or lowered purely out of convenience. This will not affect our calculation at all and

will serve to make the notation slightly more aesthetically pleasing. Also, we will make use of a summation convention for repeated indices. All indices that appear twice in a single term will imply summation over all values of that index.

1.3.3 The Correlation Function

Most of the labour intensive work done in all three of the papers that make up this thesis is focused on calculating a specific quantity known as a correlation function. Note that, throughout this thesis, I will use the terms correlator, cross-correlator and correlation function interchangeably to refer to the quantity we are calculating. This quantity can perhaps most simply be described as the vacuum expectation value of the time ordered product of fields. At its simplest, a two point correlation function such as

$$\langle 0|\, T[\phi(x)\phi(y)]\, |0\rangle \tag{1.7}$$

in a free field theory, can be interpreted as the propagation amplitude for the particle from y to x. Here $\phi(x)$ and $\phi(y)$ are simple field operators, T is the time-ordering operator, and $\langle 0|\,|0\rangle$ represent the vacuum in our free theory. In our case, these field operators will be replaced with composite operators containing several fields. These composite operators, which we call currents, will be selected specifically to probe the hadronic states we are interested in examining and will differ in each of the three papers. In general, these currents must be colour singlets (however in [3], where we study diquarks, this requirement is relaxed) and they must have the appropriate quantum numbers for the states we want to probe. We get into the details of these currents when we start the calculation in each of the three papers presented here. But, in principle, for any two point function we will be looking at, eqn. (1.7) will now become

$$\langle \Omega|\, T[\, j^{\mu}_{(a)}(x)\; j^{\nu}_{(b)}(0)]\, |\Omega\rangle \tag{1.8}$$

where $j^{\mu}_{(a)}(x)$ and $j^{\nu}_{(b)}(0)$ are currents at x and 0 respectively which probe the states we are interested in examining (in the Heisenberg picture when written this way) and $\langle \Omega|$ is our

QCD vacuum. This time-ordered product can be written in the interaction picture as

$$\Pi^{\mu\nu}(q) = i\int d^dx\; e^{iq\cdot x}\langle\Omega|T[\, j^{\mu}_{(a)}(x)\; j^{\nu}_{(b)}(0)\; e^{i\int dy\mathcal{L}_{int}(y)}]|\Omega\rangle \tag{1.9}$$

where only connected diagrams are kept on the right-hand side. Here, $e^{i\int dy\mathcal{L}_{int}(y)}$ contains QCD interaction Lagrangian terms we discussed in (1.6), and we have taken the momentum space Fourier transform of the correlation function. Notice that the integral is d dimensional as we will be using dimensional regularization in all three papers presented here (see [5] for details on dimensional regularization). Note also, that all integrals in this thesis where bounds are not explicitly written are taken to be over the full range of their variables.

In this section, we have briefly gone over how we could write our correlator, but we also need to understand what it is and why we want to calculate it. Without introducing several new terms and ideas, perhaps the easiest way to describe the correlator is to describe how it will be used. The correlator is the quantity that contains all the QCD information about our system, and it is what we feed into the dispersion relation which we will discuss shortly in section 1.3.10.

1.3.4 The Operator Product Expansion

We will now take a quick look at some of the tools we will need to simplify our correlator. Substituting the appropriate currents into (1.9) gives us the equation we will now be working with. Remembering that each of the three factors on the right hand side of (1.9) will contain some number of operators in the form of quark and gluon fields, we will need some tools to help us evaluate the products of these non-local fields and their vacuum expectation values (VEV)s. The operator product expansion (OPE) states that, for a product of operators $\mathcal{O}_1$ and $\mathcal{O}_2$ acting at spacetime coordinates x and y, we can write

$$\mathcal{O}_1(x)\mathcal{O}_2(y) \to \sum_n C^n_{12}(x)\mathcal{O}_n(y) \quad \text{as} \quad x \to y \tag{1.10}$$

where the C^n_{12} factors are c-numbered functions known as Wilson coefficients [15]. This, in effect, allows us to write the product of fields at two distinct space-time points in terms of

fields at one of those points in the limit where $x \to y$ [15]. In practice, for our calculation, $\mathcal{O}_1$ and $\mathcal{O}_2$ will be our currents and both sides of the equation will be wrapped in a time-ordered product (TOP) and be inside a VEV. In essence, this will relate our correlation function to the expansion that will allow us to simplify it. The right hand side of this expression will give us a series of local VEVs, including a perturbative contribution and non-perturbative terms that will be characterized by condensates, which we will look at briefly after a quick discussion on Wick's theorem.

1.3.5 Wick's Theorem

Wick's Theorem allows us to write the TOP of some collection of operators in terms of the normal-ordered product (NOP) of the sum of those operators, and their contractions. These contracted fields are then written in terms of propagators. Much more detail about this process is available in most QFT texts including [5] but, in essence, we are now able to write

$$\begin{aligned} T\{\phi_1(x_1)\phi_2(x_2)\ldots\phi_n(x_n)\} = \\ = N\{\phi_1(x_1)\phi_2(x_2)\ldots\phi_n(x_n) + \textit{all possible contractions}\} \end{aligned} \tag{1.11}$$

where N indicates a NOP. Each of the terms in the right hand side of (1.11) can be thought of as representing a Feynman diagram. Those terms, where the fields are fully contracted, and which yield connected diagrams, could be evaluated using the QCD Feynman rules. These diagrams represent the perturbative contribution to our cross-correlator. The terms where fields remain uncontracted, and thus leave us with the VEVs of uncontracted fields, are generally taken to be zero. In the case of QCD however, these VEVs can be non-zero due to the complexity of the QCD vacuum, and, as mentioned above, these terms will be characterized in terms of condensates. Once evaluated, these non-zero VEVs will represent the non-perturbative contribution to our correlator.

1.3.6 Condensates and the QCD Vacuum

As mentioned above, through the application of the OPE and Wick's theorem, we will generate a number of terms that will contain the VEV of uncontracted local operators. In theories

with a simpler vacuum, these terms would be taken to be zero. However the QCD vacuum is more complex and results in non-zero values for these VEVs. See section 2.6.1.1 for a detailed discussion on the calculation of these VEVs. For now however, it will be enough to remember that the complexity of the QCD vacuum and the non-zero nature of these VEVs are driven by spontaneous symmetry breaking (SSB) of global symmetries in QCD. Spontaneous symmetry breaking manifests in a theory where a symmetry associated with the Lagrangian is not shared by the ground state of the theory. Here, our ground state is the QCD vacuum and our Lagrangian is the Yang-Mills QCD Lagrangian. Spontaneous symmetry breaking is a topic that is well covered in most QFT texts including [5]. For our purposes it will be enough to understand that these local VEVs are non-zero, and that their numeric values are external inputs to the theory that need to be extracted phenomenologically.

1.3.7 Regularization

Once we have applied the OPE and Wick's theorem to our correlator and gone through the considerable algebra needed to simplify our expression, we will be left with an expression phrased in terms of an internal momentum integral. These integrals can be complicated and are often divergent in four dimensions. The technique we use to deal with these divergent integrals is known as dimensional regularization (dim-reg). Dim-reg is perhaps the simplest regularization scheme which preserves the symmetries of QCD; it is widely used and well described in many QFT texts including [5]. Put simply, in dim-reg we promote our divergent four dimensional integral to a d dimensional integral that can be evaluated, and this result can be analytically continued to other dimensions. In essence, we compute our integral as a function of the dimensionality of spacetime. Our final expression will be phrased in terms of our spacetime dimension d where we let $d \to 4 + 2\epsilon$, a convention consistent with [16]. Then, the exact result is Laurent-expanded around $\epsilon = 0$ and that the divergences at $d = 4$ show up as poles in this series.

In principle, dim-reg gives us a framework within which all of our integrals can be evaluated, but, in practice, solving these integrals can still be quite complicated. Generally, one-loop integrals can be solved without much trouble, but two-loop integrals often require the application of recurrence relations [17, 18] to simplify the integrals before they are in a

solvable form. We will be using the TARCER [19] Mathematica software package to help in evaluating these two-loop integrals. TARCER can be thought of as a tool which will allow us to write complicated two-loop integrals in terms of master integrals with known solutions, some of which are discussed in [20] and [21].

1.3.8 Renormalization

It is important to note that some of the currents we will be using are not renormalized. Using an unrenormalized current as we do in some of these calculations will result in non-polynomial divergences in our final answer. When doing the sum rules analysis of these correlators, polynomial divergences will not pose a problem as they will be eliminated by a Borel transform [22] defined by

$$\hat{\mathcal{B}} = \lim_{\substack{N,Q^2\to\infty \\ \tau=N/Q^2}} \frac{(-Q^2)^N}{\Gamma(N)} \left(\frac{d}{dQ^2}\right)^N . \tag{1.12}$$

Note that the relation between the Borel transform and the inverse Laplace transform $\hat{\mathcal{L}}^{-1}$ is given by

$$\begin{aligned} \frac{1}{\tau}\hat{\mathcal{B}}\Big\{f(Q^2)\Big\} &= \hat{\mathcal{L}}^{-1}\Big\{f(Q^2)\Big\} \\ &= \frac{1}{2\pi i}\int_{c-i\infty}^{c+i\infty} f(Q^2)e^{Q^2\tau}dQ^2 \end{aligned} \tag{1.13}$$

where c is any real number for which $f(Q^2)$ is analytic for $\mathrm{Re}(Q^2) > c$. This identity (1.13) will be useful shortly. The non-polynomial divergences will still need to be addressed before the correlator is ready for a sum rules analysis. To deal with these non-polynomial divergences, we introduce some notation. If we let a square bracket indicate a renormalized quantity and a quantity with no brackets indicate a bare quantity, as described in [23], we know that

$$\Big[j^\nu_{(a)}\Big] = Z_1 j^\nu_{(a)} + Z_2\mathcal{O}_2 + \cdots + Z_n\mathcal{O}_n. \tag{1.14}$$

In this case, the Z_n are renormalization constants, the $\mathcal{O}_n$ are composite operators with the same quantum numbers as our $j^\nu_{(a)}$ that have dimension less than or equal to that of $j^\nu_{(a)}$ [23].

The ideas about renormalization discussed here are further discussed in [23]. We will make use of these ideas when we come to deal with the non-polynomial divergences in some of our calculations. More details about the specifics of the renormalization used in each of the three papers are included in the papers themselves.

1.3.9 The Dispersion Relation

Once our correlator has been sufficiently simplified and renormalized, we will feed it into the dispersion relation [24]. The dispersion relation can be written as

$$\Pi(Q^2) = \frac{(Q^2)^n}{\pi} \int_{M_Q^2}^{\infty} \frac{\mathrm{Im}[\Pi(t)]}{t^n(t+Q^2)} dt + \cdots, \quad Q^2 > 0, \quad Q^2 = -q^2 \tag{1.15}$$

where the $\cdots$ represent subtraction constants, collectively a polynomial in q^2, and the $\mathrm{Im}[\Pi(t)]$ is our hadronic spectral function. This dispersion relation is an expression of quark/hadron duality. On the left hand side, we have our correlator calculated in terms of quarks via QCD and the dispersion relation relates this quantity to the hadronic spectral function on the right, which contains information about hadrons. In practice, this allows us to calculate in terms of quarks and make predictions about hadrons. Our hadronic spectral function could, in principle, be modelled in terms of Dirac delta functions and Heaviside step functions which would respectively represent the resonances and continuum we would expect to see in the hadronic spectrum. In turn, this would allow us to extract the physical mass of our theorised particle.

1.3.10 The Laplace Sum Rule

Once we have our dispersion relation and the correlator in the necessary form, we apply the Borel transform (1.12) as mentioned above in section 1.3.8. Again, this will eliminate all remaining polynomial divergences, and it will allow us to write the 0^{th}-order Laplace sum rule (LSR) [25] in the form shown in equation (1.16). For a more recent review of QCD sum

rules (QCDSR) see [26].

$$\mathcal{R}(\tau) \equiv \frac{1}{\tau}\hat{\mathcal{B}}\Big\{\Pi(Q^2)\Big\} = \int_{t_0}^{\infty} e^{-t\tau}\frac{1}{\pi}\mathrm{Im}\Pi(t)dt \tag{1.16}$$

We then implement a resonance(s)-plus-continuum model [25] which amounts to setting

$$\frac{1}{\pi}\mathrm{Im}\Pi(t) \to \rho^{(\mathrm{had})}(t) + \frac{1}{\pi}\mathrm{Im}\Pi^{(\mathrm{OPE})}(t)\theta(t-s_0) \tag{1.17}$$

where $\rho^{(\mathrm{had})}$ represents the resonance content of the spectral function, θ is the Heaviside step function, and s_0 is the continuum threshold. Then by subtracting the continuum contribution from the 0^{th}-order LSR (1.16) we can define the continuum-subtracted 0^{th}-order LSR

$$\mathcal{R}(\tau, s_0) \equiv \mathcal{R}(\tau) - \int_{s_0}^{\infty} e^{-t\tau}\frac{1}{\pi}\mathrm{Im}\Pi^{(\mathrm{OPE})}(t)dt = \int_{t_0}^{s_0} e^{-t\tau}\rho^{(\mathrm{had})}(t)dt. \tag{1.18}$$

We then make use of the identity that relates the Borel transform to the inverse Laplace transform (1.13) and proceed with the substitution of the terms that make up $\mathrm{Im}\Pi^{(\mathrm{OPE})}$ into (1.18). Note that the LSR suppresses the high-energy region, reducing our sensitivity to continuum contributions while still allowing the signal from the resonance contributions to persist. We will not write the final form of the 0^{th}-order continuum-subtracted LSR here as it will depend on the specific systems we are trying to model (*i.e.* the specific content of the $\mathrm{Im}\Pi^{(\mathrm{OPE})}$), and so we leave that for the discussions contained in each of the three papers.

This LSR (equation 1.18) is the quantity that we are calculating for all of the QCDSR calculations presented in this thesis. For each paper presented here, once the respective LSR had been prepared, it allowed us to probe the systems in question. In the case of [1, 2] the LSR allowed us to probe resonances for meson-hybrid mixing and in the case of [3] the LSR was used to extract diquark constituent masses. We relegate the discussions of the specific analysis methodologies used in each of these cases to their respective papers. But, at their core, each of these analyses contains an LSR like the one shown in equation (1.18).

1.4 Motivations

We have spent the last few sections introducing some of the key theoretical ideas that frame the work done in this thesis. Let us now turn our attention to the experimental and theoretical findings and predictions that motivated the questions we set out to answer in these three papers.

1.4.1 Motivations from Theory

QCD and colour confinement require only that a bound state be colourless to be a physically observable state. After incorporating colour confinement, the quark model gave us the baryons, antibaryons, and mesons shown in Figure 1.2 as possible hadron configurations. These three configurations of quarks (and antiquarks) are the simplest arrangements that satisfy colour confinement, but they do not form an exhaustive list. We could easily imagine hadrons built out of four, five, or even more quarks. In addition, QCD introduces gluons as a potential building block of hadrons. Again, unlike photons, gluons carry the charge of the theory, they are bicoloured, (in the adjoint 8 representation of SU(3)), and so we may expect that they should be treated similarly to quarks when it comes to building hadrons. With these ideas in mind, we could build a much richer palette of potential beyond-the-quark-model hadron configurations that would satisfy colour confinement. Some of these potential configurations are shown in Figure 1.4.

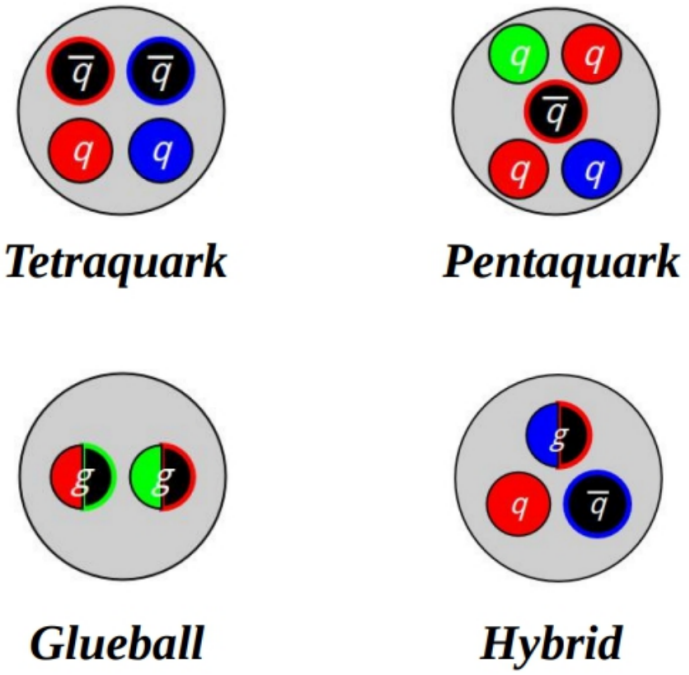

Figure 1.4: Potential configurations for beyond-the-quark-model hadrons.

For the work presented in this thesis, we will be focused first on hybrids, which are central to the first two papers [1, 2], and then on tetraquarks, one of the topics in the third paper [3].

1.4.2 Motivations from Experiment

As we mentioned in section 1.2, a large number of hadrons are now known to exist and this number is growing all the time. Many of these hadrons are well-explained by the quark model, but a growing number of them seem to defy quark model interpretation. In the research presented in this thesis, we focus on the heavy quarkonium spectrum and what are known as the XYZ resonances. These XYZ states are hadrons that have been detected experimentally and have been seen to decay to final states which consist of a heavy quark-antiquark pair but do not fit neatly into the quark model's $q\bar{q}$ scheme [6] (see also [27] for a recent review). As an example of how these XYZ resonances fit into the heavy quarkonium spectra, we now look at the charmonium and charmonium-like meson spectrum in Figure 1.5 It is these XYZ resonances, which seem to defy quark model interpretation, that have motivated much of the research into beyond-the-quark-model hadrons.

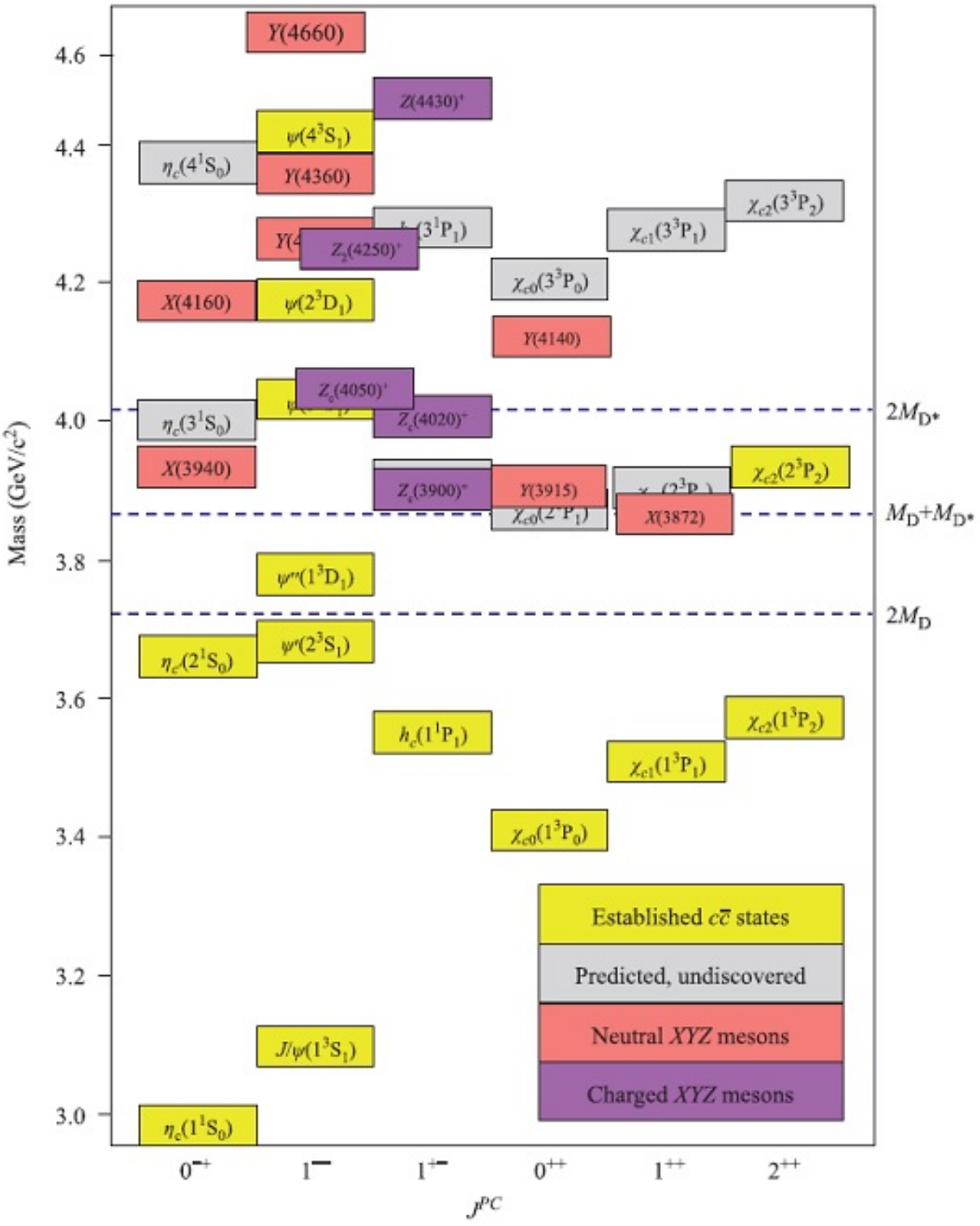

Figure 1.5: The spectrum of charmonium and charmonium like mesons, image credit Olsen, Front. Phys. 10 (2015) 101401 [6].

As we move into the specific research done in each of the three papers presented in this thesis, we will dig deeper into the motivations that drove those specific projects. But to sum up our overall motivations for the work presented here, we are trying to answer key questions concerning the XYZ resonances. In particular, the XYZ resonances have been detected and they seem to defy quark model interpretation. Given that colour confinement and QCD seem to allow for beyond-the-quark-model hadrons, can we explain the XYZ resonances as beyond-the-quark-model hadrons? Also, if our characterization of confinement is correct, we should expect to find all of these beyond-the-quark-model hadrons in nature—so where are they?

In the first two papers [1, 2] we find nonzero mixing parameters in several resonances in the vector and axial vector charmonium and bottomonium sectors. This result suggests that hybrids with non-exotic quantum numbers exist as quantum mechanical superpositions of pure mesonic states and hybrid states. It also suggests that some of the resonances that we've assigned to pure mesonic states are better described as mixed states. In other words, the hybrids are hiding in resonances that we previously thought of as pure mesonic resonances. Then, in the third paper [3], we calculate constituent diquark masses for axial vector $[cc]$ and $[bb]$ diquarks using QCD Laplace sum rules. These mass predictions stabilize and we then use these results to predict tetraquark masses. These mass predictions can be used to guide experimental searches for tetraquarks. Also, if tetraquarks with masses close to those we predict are found it would lend support to the idea that tetraquarks exist with additional substructure in the form of constituent diquarks.

Chapter 2

Meson-Hybrid Mixing

2.1 Meson-Hybrid Mixing

As discussed in Section 1.4.1, QCD seems to allows for looser restrictions on the makeup of hadrons when compared to the conventional quark model, and it also supplies us with more building blocks (gluons). In the quark model, we were only able to build hadrons out of either three quarks, three antiquarks or a quark/antiquark pair (as shown in Figure 1.2). Our present characterization of colour confinement and our understanding of QCD seem to suggest that bound states need only be colourless. Also, QCD supplies us with bicoloured gluons as another potential constituent of our hadrons. Turning our attention back to bound states containing a quark and an antiquark, and considering only the colourless bound state requirement, there is no reason one could not build a bound state out of a quark, an antiquark, and a gluon. Such particles have been theorized for some time and are known as hybrids (as shown in Figure 1.4).

One promising hybrid search strategy would be to look for meson-like bound states with what would be exotic quantum numbers for a quark-antiquark meson. Discovering a meson-like bound state with exotic quantum numbers would point strongly to the existence of beyond-the-quark-model hadrons as it would be difficult to explain these quantum numbers without additional degrees of freedom (extra constituent quarks or constituent gluons). Experimental efforts to find meson-like states with exotic quantum numbers continue with some promising hybrid candidates emerging; however, results are still inconclusive [28].

In the first paper presented in this chapter, we will be exploring charmonium and bottomonium hybrids with $J^{PC} = 1^{--}$, and, in the second paper, we look at similar systems with $J^{PC} = 1^{++}$. As we are dealing with non-exotic quantum numbers for mesons, this makes

finding such particles even more difficult. Some experimental findings that might suggest that these hybrids exist would be the overpopulation of resonances for a particular J^{PC} in a particular spectrum. Also, branching ratios that differ significantly from those predicted by conventional mesonic models would also suggest that hybrids may be present [29, 30, 31]. Detection of these non-exotic hybrids could be further complicated by the fact that they may mix with conventional mesonic states. It is this last point about potential mixing that we will explore further in the first two papers presented in this thesis.

2.2 1^{--} Motivation and Initial Discussion

We began this series of two papers on meson-hybrid mixing in vector heavy quarkonium by first looking at charmonium-like XYZ mesons with $J^{PC} = 1^{--}$. Specifically, we were interested in charmonium-like XYZ mesons with $J^{PC} = 1^{--}$ that do not fit into the $c\bar{c}$ mass spectrum which includes the J/ψ and its radial excitations. The XYZ resonances that fit this description are the $Y(4260)$, $Y(4360)$ and $Y(4660)$. The $Y(4260)$ and $Y(4360)$ were discovered by BaBar in the $\pi^+\pi^- J/\psi$ and $\pi^+\pi^-\psi'$ systems respectively via $e^+e^- \to \gamma_{isr}\pi^+\pi^- J/\psi$ and $e^+e^- \to \gamma_{isr}\pi^+\pi^-\psi'$ [32, 33]. These results were later confirmed by the Belle Collaboration [34, 35] which also found another peak in the $\pi^+\pi^-\psi'$ system, the $Y(4660)$. We can see how these states fit into the charmonium and charmonium-like meson spectrum in Figure 1.5.

It's difficult to interpret these particles in the context of a quark model description of mesons as all of the 1^{--} $c\bar{c}$ states near their detected masses have already been assigned to other resonances. It has been suggested that the $Y(4260)$ is a charmonium hybrid state [36]. Also there have been theoretical explorations of $c\bar{c}g$ hybrid currents with $J^{PC} = 1^{--}$ done using QCDSR resulting in mass predictions in the range of 3.36 ± 0.15 GeV [37]. These unassigned resonances and the fact that QCD allows for mesonic states with an explicit gluonic degree of freedom have served as the motivation for much of the research into charmonium hybrids.

Expanding on some of these ideas, in this first paper, we explored the idea that perhaps some of these resonances do not exist as pure mesonic states, but rather as quantum me-

chanical superpositions of pure $c\bar{c}$ and hybrid states ($c\bar{c}g$). Keeping in mind the findings in [37] where the $c\bar{c}g$ current with $J^{PC} = 1^{--}$ was predicted to have a mass of 3.36 ± 0.15 GeV, it seems plausible that the reason we do not see this resonance in the charmonium spectrum might be because it exists as a quantum mechanical superposition with the J/ψ. Said another way, perhaps the resonance we have assigned to the J/ψ is in fact a mix of pure $c\bar{c}$ with $c\bar{c}g$.

After completing the meson-hybrid mixing analysis of the $J^{PC} = 1^{--}$ charmonium system, we then turned our attention to analyzing the $J^{PC} = 1^{--}$ bottomonium system as well. The results of these analyses were then collected and published as the first paper in this series on meson-hybrid mixing, presented here in Section 2.3.

The following work may be found published in:

A QCD Sum-Rules Analysis of Vector (1^{--}) Heavy Quarkonium Meson-Hybrid Mixing,
A. Palameta, J. Ho, D. Harnett, and T.G. Steele.
Phys. Rev. D **97**, 034001 (2018)
DOI:10.1103/PhysRevD.97.034001

I played a leading role in the work presented in this manuscript. I calculated the cross-correlator, generated the Laplace sum-rule, built models of the hadronic spectra in question and performed the analysis to extract the mixing parameters. I also made significant contributions to the editing of the manuscript.

2.3 Manuscript: A QCD Sum-Rules Analysis of Vector (1^{--}) Heavy Quarkonium Meson-Hybrid Mixing

Abstract: We use QCD Laplace sum-rules to study meson-hybrid mixing in vector (1^{--}) heavy quarkonium. We compute the QCD cross-correlator between a heavy meson current and a heavy hybrid current within the operator product

expansion. In addition to leading-order perturbation theory, we include four- and six-dimensional gluon condensate contributions as well as a six-dimensional quark condensate contribution. We construct several single and multi-resonance models that take known hadron masses as inputs. We investigate which resonances couple to both currents and so exhibit meson-hybrid mixing. Compared to single resonance models that include only the ground state, we find that models that also include excited states lead to significantly improved agreement between QCD and experiment. In the charmonium sector, we find that meson-hybrid mixing is consistent with a two-resonance model consisting of the J/ψ and a 4.3 GeV resonance. In the bottomonium sector, we find evidence for meson-hybrid mixing in the $\Upsilon(1S)$, $\Upsilon(2S)$, $\Upsilon(3S)$, and $\Upsilon(4S)$.

2.3.1 Introduction

Hybrids are hadrons containing explicit gluon degrees of freedom in addition to a constituent quark and antiquark. They are colour singlets and so should be allowed within QCD. However, they have yet to be conclusively identified in experiment (see, e.g., ref. [28] for a comprehensive review).

Hybrids can be broadly classified as having quantum numbers (i.e., J^{PC}) that are exotic or non-exotic. Exotic quantum numbers (e.g., 0^{--}, 0^{+-}, 1^{-+}, 2^{+-}) are those not accessible to conventional quark-antiquark ($q\overline{q}$) mesons; the rest of the quantum numbers are non-exotic and are accessible to both $q\overline{q}$-mesons and hybrids. Looking for resonances with an exotic J^{PC} is a promising hybrid search strategy being used, for example, at GlueX. Furthermore, hybrids with exotic J^{PC} would be unable to quantum mechanically mix with $q\overline{q}$-mesons (as no conventional meson could have the J^{PC} in question), and so could perhaps appear as pure, unmixed states. In contrast, hybrids with non-exotic J^{PC} are expected to mix with $q\overline{q}$-mesons resulting in hadrons that would be superpositions of both conventional meson and hybrid.

In this article, we consider meson-hybrid mixing in (non-exotic) vector (1^{--}) charmonium ($c\bar{c}$) and bottomonium ($b\bar{b}$). The heavy quarkonium sectors have received considerable attention lately due primarily to the discovery of the XYZ resonances (see [38, 39] for reviews and [40] for some recent developments). These XYZ resonances are a collection of hadrons many of whose properties (e.g., masses, widths, and decay rates) do not agree with quark model predictions [41]. Unsurprisingly, the XYZ resonances have generated a lot of discussion concerning outside-the-quark-model hadrons such as hybrids. We focus on 1^{--} rather than some other J^{PC} because more is known about the spectra of 1^{--} heavy quarkonium than is known about the spectra for the other quantum numbers [4].

We investigate meson-hybrid mixing with QCD Laplace sum-rules (LSRs) [25, 42, 43, 44]. Using the operator product expansion (OPE) [15], we compute the cross-correlator between a $q\overline{q}$-meson current and a hybrid current (see (2.3) and (2.4) respectively below). In the cross-correlator calculation, we include leading-order (LO) QCD contributions from perturbation theory and non-perturbative corrections due to the four-dimensional (4d) and 6d gluon condensates as well as the 6d quark condensate. We then analyze several single and multi-resonance models of the hadron mass spectra that take known resonance masses as inputs. We determine which resonances couple to both currents and so can be considered mixed. The QCD sum-rules methodology has been applied to hadron mixing problems in a number of systems including pseudoscalar meson-glueball mixing [45], scalar meson-glueball mixing [46], 1^{++} charmonium hybrid-$\overline{D}D^*$ molecule mixing [47], and open-flavour heavy-light meson-hybrid mixing [48].

We find that multi-resonance models that include excited states in addition to the ground state lead to significantly improved agreement between QCD and experiment when compared to single resonance models that include only the ground state. In addition, we show explicitly that the higher mass excited states make numerically significant contributions to the LSRs despite the tendency of LSRs to suppress such resonances. Finally, we find that meson-hybrid mixing in the charmonium sector is described well by a two-resonance model consisting of the J/ψ and a 4.3 GeV state such as the X(4260). In the bottomonium sector, we find evidence for meson-hybrid mixing in all of the $\Upsilon(1S)$, $\Upsilon(2S)$, $\Upsilon(3S)$, and $\Upsilon(4S)$.

2.3.2 The Correlator

We consider the following cross-correlator

$$\Pi_{\mu\nu}(q) = i\int d^4x\, e^{iq\cdot x}\,\langle 0|\tau\, j_\mu^{(\mathrm{m})}(x)\; j_\nu^{(\mathrm{h})}(0)|0\rangle \tag{2.1}$$

$$= \left(\frac{q_\mu q_\nu}{q^2} - g_{\mu\nu}\right)\Pi(q^2) \tag{2.2}$$

between quarkonium meson current

$$j_\mu^{(\mathrm{m})} = \overline{Q}\gamma_\mu Q \tag{2.3}$$

and quarkonium hybrid current [49]

$$j_\nu^{(\mathrm{h})} = \frac{g_s}{2}\overline{Q}\gamma^\rho\gamma^5\lambda^a\widetilde{G}^a_{\nu\rho}Q \tag{2.4}$$

where

$$\widetilde{G}^a_{\nu\rho} = \frac{1}{2}\epsilon_{\nu\rho\omega\zeta}G^a_{\omega\zeta} \tag{2.5}$$

is the dual gluon field strength tensor and $\epsilon_{\nu\rho\omega\zeta}$ is the totally antisymmetric Levi-Civita symbol. The function Π in (2.2) probes 1^{--} states.

We calculate the correlator (2.1) within the OPE in which perturbation theory is supplemented by non-perturbative terms, each of which is the product of a perturbatively computed Wilson coefficient and a nonzero vacuum expectation value, i.e., a QCD condensate. In addition to perturbation theory, we include OPE terms proportional to the 4d and 6d gluon condensates and the 6d quark condensate defined respectively by

$$\left\langle \alpha G^2 \right\rangle = \alpha_s \left\langle : G^a_{\omega\phi}G^a_{\omega\phi}: \right\rangle \tag{2.6}$$

$$\left\langle g^3G^3 \right\rangle = g_s^3 f^{abc}\left\langle : G^a_{\omega\zeta}\; G^b_{\zeta\rho}G^c_{\rho\omega}: \right\rangle \tag{2.7}$$

$$\left\langle J^2 \right\rangle = \mathrm{Tr}\big(\left\langle : J_\nu J_\nu: \right\rangle\big) \tag{2.8}$$

where

$$J_\nu = \frac{-ig_s^2}{4}\lambda^a \sum_A \overline{q}^A \lambda^a \gamma_\nu q^A. \tag{2.9}$$

In (2.9), the sum on the right-hand side is over quark flavours. We use the vacuum saturation hypothesis [25] to express $\langle J^2 \rangle$ in terms of the 3d quark condensate

$$\langle \overline{q}q \rangle = \langle : \overline{q}_i^\alpha q_i^\alpha : \rangle \tag{2.10}$$

resulting in

$$\langle J^2 \rangle = \frac{2}{3}\,\kappa\, g_s^4 \langle \overline{q}q \rangle^2 \tag{2.11}$$

where κ quantifies deviations from exact vacuum saturation. Throughout, we set $\kappa = 2$ (see, e.g., ref. [44] and references cited therein). The diagrams that contribute to (2.1) at LO in the coupling g_s are shown in Figure 2.1 where we have suppressed a second set of similar diagrams in which the quark line runs clockwise. Wilson coefficients are computed using the fixed-point gauge method (see [50, 51], for example), and divergent integrals are handled using dimensional regularization in $D = 4 + 2\epsilon$ dimensions at $\overline{\text{MS}}$ renormalization scale μ. As in [52], we use the following convention for a dimensionally regularized γ^5:

$$\gamma^5 = \frac{i}{24}\epsilon_{\mu\nu\sigma\rho}\gamma^\mu\gamma^\nu\gamma^\sigma\gamma^\rho. \tag{2.12}$$

We employ TARCER [53], a Mathematica package that implements the recurrence algorithm of [17, 18], to express dimensionally regularized integrals in terms of a small set of master integrals. An exact calculation of each needed master integral is either found in [20, 21] or is a well-known one-loop result. We denote the OPE computation of Π from (2.2) as $\Pi^{(\text{OPE})}$ which we then decompose as

$$\Pi^{(\text{OPE})} = \Pi^{(\text{I})} + \Pi^{(\text{II})} + \Pi^{(\text{III})} + \Pi^{(\text{IV})} + \Pi^{(\text{V})} + \Pi^{(\text{VI})} \tag{2.13}$$

where the superscripts in (2.13) correspond to the labels of the diagrams in Figure 2.1. For $\Pi^{(\text{I})}$, we find an exact ϵ-dependent result

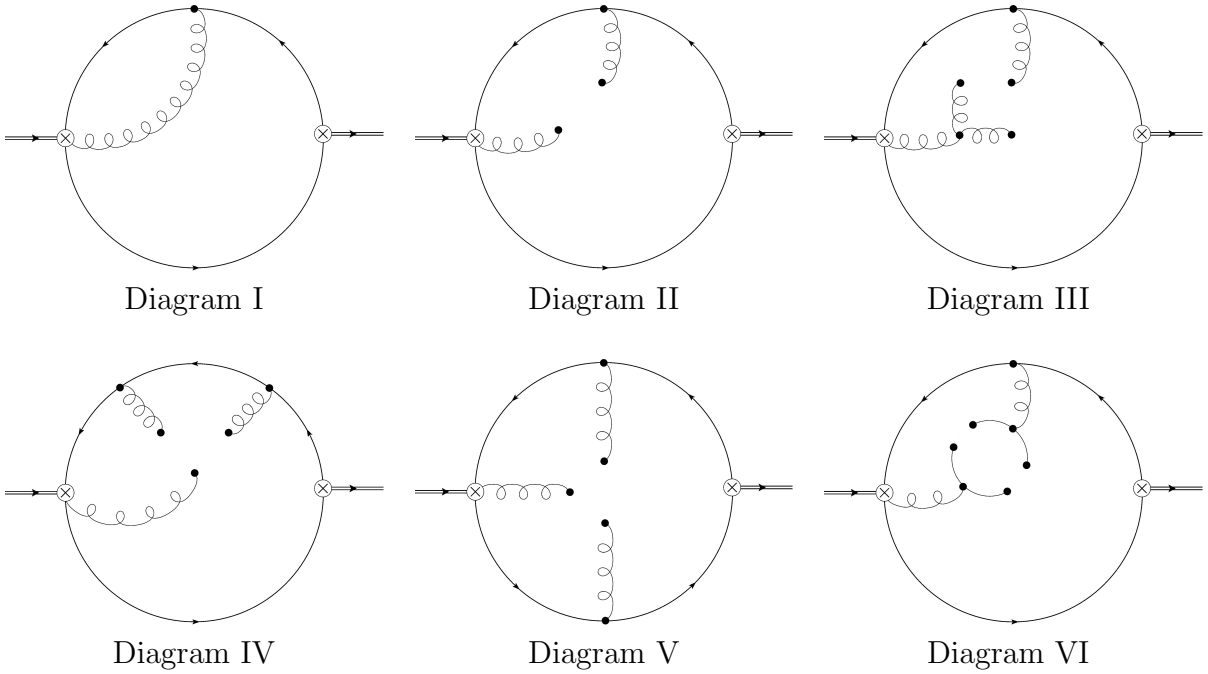

Figure 2.1: The LO Feynman diagrams that contribute to the cross-correlator (2.1) which we decompose in (2.13).

$$\Pi^{(\mathrm{I})}(z;\epsilon) = -\frac{\alpha_s\, e^{-2\epsilon} m^{4(1+\epsilon)} \Gamma(-\epsilon)}{3\pi^3(3+2\epsilon)(4\pi)^{2\epsilon}} \Bigg((1+2\epsilon+4z(1+\epsilon))\Gamma(-\epsilon) \times {}_3F_2\left(1,-1-2\epsilon,-\epsilon;\frac{1}{2}-\epsilon,2+\epsilon;z\right) + \frac{\pi(1+2\epsilon)\mathrm{Csc}(\pi\epsilon)}{\Gamma(1+\epsilon)} \Bigg(-4+3(1+4z(1+\epsilon))\, {}_2F_1\left(1,-\epsilon;\frac{3}{2};z\right) - 2(z-1)\, {}_3F_2\left(1,-2\epsilon,-\epsilon;\frac{1}{2}-\epsilon,2+\epsilon;z\right) \Bigg) \Bigg) \quad (2.14)$$

where

$$z = \frac{q^2}{4m^2}, \quad (2.15)$$

m is a heavy quark mass (i.e., m_c or m_b), Γ is the gamma function, and ${}_pF_q(\cdots;\cdots;z)$ are generalized hypergeometric functions (see [54], for example). Expanding (2.14) in ϵ and dropping terms polynomial in z as they will not contribute to the LSR, we find

$$\Pi^{(\mathrm{I})}(z) = \frac{2\alpha_s m^4 z(1+4z)\, {}_2F_1\left(1,1;\frac{5}{2};z\right)}{9\pi^3}\frac{1}{\epsilon} + \frac{d}{d\epsilon}\Pi^{(\mathrm{I})}(z;\epsilon)\Big|_{\epsilon=0}. \quad (2.16)$$

For the sake of brevity, we do not include an explicit expression for the derivative term on the right-hand side of (2.16). (Note that (2.16) is ultimately superseded by (2.27), and we provide a complete expression for the latter.) Expanding the remaining terms on the right hand side of (2.13) in ϵ, we find

$$\Pi^{(\mathrm{II})}(z) = \frac{z\Big(-3 + {}_2F_1\big(1,1;\frac{5}{2};z\big)\Big)}{18\pi(z-1)}\big\langle \alpha G^2\big\rangle \tag{2.17}$$

$$\Pi^{(\mathrm{III})}(z) = \frac{\Big(2+5z-4z^2-(2-7z+10z^2-4z^3)\,{}_2F_1\big(1,1;\frac{5}{2};z\big)\Big)}{2304\pi^2m^2(z-1)^3}\big\langle g^3G^3\big\rangle \tag{2.18}$$

$$\Pi^{(\mathrm{IV})}(z) = \frac{\big\langle g^3G^3\big\rangle}{4608\pi^2m^2(z-1)^3}\left(-22+41z-16z^2+(10-25z+22z^2-8z^3)\,{}_2F_1\big(1,1;\tfrac{5}{2};z\big)\right) \tag{2.19}$$

$$\Pi^{(\mathrm{V})}(z) = \frac{\big\langle g^3G^3\big\rangle}{4608\pi^2m^2(z-1)^2}\left(-15+12z+(3-2z)\,{}_2F_1\big(1,1;\tfrac{5}{2};z\big)\right) \tag{2.20}$$

$$\Pi^{(\mathrm{VI})}(z) = \frac{2\alpha_s^2\big\langle\overline{q}q\big\rangle^2}{81m^2(z-1)^3}\left(2+5z-4z^2+(-2+7z-10z^2+4z^3)\,{}_2F_1\big(1,1;\tfrac{5}{2};z\big)\right). \tag{2.21}$$

Perturbation theory (2.16) contains a nonlocal divergence. Following [47, 48], this divergence is eliminated via operator mixing under renormalization. The meson current (2.3) is renormalization-group (RG) invariant and so we only need consider the operator mixing of the hybrid current (2.4) which induces operator mixing with (2.3) and with

$$j_\nu^{(c)} = \overline{Q}iD_\nu Q \tag{2.22}$$

where $D_\nu = \partial_\nu - \frac{i}{2}g_s\lambda^a A_\nu^a$ is the covariant derivative. Thus,

$$j_\nu^{(\mathrm{h})} \to j_\nu^{(\mathrm{h})} + \frac{C_1}{\epsilon}j_\nu^{(\mathrm{m})} + \frac{C_2}{\epsilon}j_\nu^{(\mathrm{c})} \tag{2.23}$$

where C_1 and C_2 are as-yet-undetermined renormalization constants. Substituting (2.23) into (2.1) (in D rather than four dimensions) gives

$$i\int d^Dx\; e^{iq\cdot x}\langle\Omega|\tau j_\mu^{(\mathrm{m})}j_\nu^{(\mathrm{h})}|\Omega\rangle \to i\int d^Dx\; e^{iq\cdot x}\langle\Omega|\tau j_\mu^{(\mathrm{m})}j_\nu^{(\mathrm{h})}|\Omega\rangle$$

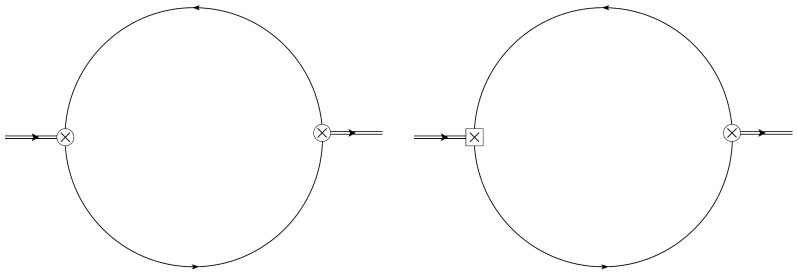

Figure 2.2: Renormalization-induced Feynman diagrams that provide a LO perturbative contribution to the mixed correlator. The square insertion denotes the current (2.22).

$$+\,i\frac{C_1}{\epsilon}\int d^Dx\; e^{iq\cdot x}\langle\Omega|\tau j_\mu^{(\mathrm{m})} j_\nu^{(\mathrm{m})}|\Omega\rangle + i\frac{C_2}{\epsilon}\int d^Dx\; e^{iq\cdot x}\langle\Omega|\tau j_\mu^{(m)} j_\nu^{(\mathrm{c})}|\Omega\rangle. \quad (2.24)$$

The last two terms on the right-hand side of (2.24) each generate a new renormalization-induced Feynman diagram, the pair of which are shown in Figure 2.2. Note that a square insertion represents the current (2.22). Evaluating these two diagrams and choosing C_1 and C_2 such that the right-hand side of (2.24) is free of nonlocal divergences, we find

$$C_1 = -\frac{10m^2\alpha_s}{9\pi} \quad (2.25)$$

$$C_2 = \frac{4m\alpha_s}{9\pi} \quad (2.26)$$

as well as an updated expression for $\Pi^{(\mathrm{I})}$ from (2.13) that is free of nonlocal divergences

$$\Pi^{(\mathrm{I})}(z) = \frac{2\alpha_s m^4 z}{81\pi^3}\Bigg(18(z-1)\,{}_3F_2\big(1,1,1;\tfrac{3}{2},3;z\big) - 2z(4z+1)\,{}_3F_2\big(1,1,2;\tfrac{5}{2},4;z\big) + 3\bigg(3(4z+1)\log\left(\frac{m^2}{\mu^2}\right) + 26z + 6\bigg)\,{}_2F_1\big(1,1;\tfrac{5}{2};z\big)\Bigg) \quad (2.27)$$

where, again, we have omitted polynomials in z as they will not contribute to the LSR.

In summary, taking operator mixing into account, the LO QCD expression $\Pi^{(\mathrm{OPE})}$ can be decomposed as in (2.13) with the terms on the right-hand side given by (2.27) & (2.17)–(2.21).

2.3.3 QCD Laplace Sum-Rules

The function Π from (2.2) satisfies a dispersion relation

$$\Pi(Q^2) = \frac{Q^6}{\pi}\int_{t_0}^{\infty}\frac{\mathrm{Im}\Pi(t)}{t^3(t+Q^2)}dt + \cdots\,,\ Q^2 = -q^2 > 0 \tag{2.28}$$

where Π on the left-hand side is to be identified with the QCD prediction $\Pi^{(\mathrm{OPE})}$; $\mathrm{Im}\Pi(t)$ is the hadronic spectral function; t_0 is the hadron threshold parameter; and $\cdots$ represents subtraction constants, collectively a quadratic polynomial in Q^2. To eliminate these subtraction constants as well as local divergences in $\Pi^{(\mathrm{OPE})}$ and to accentuate the resonance contributions of the hadronic spectral function to the integral on the right-hand side of (2.28), we apply the Borel transform

$$\hat{\mathcal{B}} = \lim_{\substack{N,Q^2\to\infty \\ \tau = N/Q^2}} \frac{\big(-Q^2\big)^N}{\Gamma(N)}\left(\frac{d}{dQ^2}\right)^N \tag{2.29}$$

with Borel parameter τ to formulate the 0^{th}-order LSR [25]

$$\mathcal{R}(\tau) \equiv \frac{1}{\tau}\hat{\mathcal{B}}\Big\{\Pi(Q^2)\Big\} = \int_{t_0}^{\infty} e^{-t\tau}\frac{1}{\pi}\mathrm{Im}\Pi(t)dt. \tag{2.30}$$

On the right-hand side of (2.30), we use a "resonance(s) plus continuum" model

$$\frac{1}{\pi}\mathrm{Im}\Pi(t) = \rho^{(\mathrm{had})}(t) + \frac{1}{\pi}\mathrm{Im}\Pi^{(\mathrm{OPE})}(t)\theta(t-s_0) \tag{2.31}$$

where $\rho^{(\mathrm{had})}$ represents the resonance content of the spectral function (to be discussed further in Section 2.3.4), θ is the Heaviside step function, and s_0 is the continuum threshold. Then, we define the continuum-subtracted 0^{th}-order LSR

$$\mathcal{R}(\tau, s_0) \equiv \mathcal{R}(\tau) - \int_{s_0}^{\infty} e^{-t\tau}\frac{1}{\pi}\mathrm{Im}\Pi^{(\mathrm{OPE})}(t)dt = \int_{t_0}^{s_0} e^{-t\tau}\rho^{(\mathrm{had})}(t)dt. \tag{2.32}$$

To compute $\mathcal{R}(\tau,\, s_0)$, we use the following identity relating the Borel transform to the inverse Laplace transform $\hat{\mathcal{L}}^{-1}$ [25]:

$$\frac{1}{\tau}\hat{\mathcal{B}}\Big\{f(Q^2)\Big\} = \hat{\mathcal{L}}^{-1}\Big\{f(Q^2)\Big\} = \frac{1}{2\pi i}\int_{c-i\infty}^{c+i\infty} f(Q^2)e^{Q^2\tau}dQ^2 \tag{2.33}$$

where c is any real number for which $f(Q^2)$ is analytic for $\mathrm{Re}(Q^2) > c$. Generalized hypergeometric functions of the form ${}_pF_{p-1}$ have a branch cut along the positive real semi-axis originating at the branch point $z = 1$. As such, in the complex Q^2-plane, $\Pi^{(\mathrm{OPE})}(Q^2)$ is analytic except for a branch cut along the negative real semi-axis originating at a branch point $Q^2 = -4m^2$. In (2.33), we let $f(Q^2) = \Pi^{(\mathrm{OPE})}(Q^2)$ and deform the integration contour on the right-hand side to that shown in Figure 2.3. Then, we apply definitions (2.30) and (2.32) to find

$$\mathcal{R}(\tau,\, s_0) = \int_{4m^2(1+\eta)}^{s_0} e^{-t\tau}\frac{1}{\pi}\mathrm{Im}\Pi^{(\mathrm{OPE})}(t)dt + \frac{1}{2\pi i}\int_{\Gamma_\eta} e^{Q^2\tau}\Pi^{(\mathrm{OPE})}(Q^2)dQ^2 \quad \text{for} \quad \eta \to 0^+ \tag{2.34}$$

where

$$\mathrm{Im}\Pi^{(\mathrm{OPE})}(t) = \sum_{i=I}^{VI} \mathrm{Im}\Pi^{(\mathrm{i})}(t) \tag{2.35}$$

and, from (2.27) and (2.17)–(2.21), we get

$$\begin{aligned}\mathrm{Im}\Pi^{(\mathrm{I})}(t) = \frac{\alpha_s}{18\pi^2 t\sqrt{t-4m^2}}\Bigg(&24m^3\sqrt{\frac{t}{4m^2}-1}\left(2m^4-2m^2t+t^2\right)\sinh^{-1}\left(\sqrt{\frac{t}{4m^2}-1}\right)\\ &+\sqrt{t}\left(t-4m^2\right)\Big(18m^4+8m^2t-t^2+6m^2(t+m^2)\Big)\log\left(\frac{m^2}{\mu^2}\right)\Bigg)\end{aligned} \tag{2.36}$$

$$\mathrm{Im}\Pi^{(\mathrm{II})}(t) = \frac{m^2}{3\sqrt{t(t-4m^2)}}\left\langle \alpha G^2\right\rangle \tag{2.37}$$

$$\mathrm{Im}\Pi^{(\mathrm{III})}(t) = \frac{t^3-10m^2t^2+28m^4t-32m^6}{96\pi t^{3/2}(t-4m^2)^{5/2}}\left\langle g^3G^3\right\rangle \tag{2.38}$$

$$\mathrm{Im}\Pi^{(\mathrm{IV})}(t) = \frac{-t^3+11m^2t^2-50m^4t+80m^6}{96\pi t^{3/2}(t-4m^2)^{5/2}}\left\langle g^3G^3\right\rangle \tag{2.39}$$

$$\mathrm{Im}\Pi^{(\mathrm{V})}(t) = \frac{-t+6m^2}{96\pi t^{3/2}(t-4m^2)^{3/2}}\left\langle g^3G^3\right\rangle \tag{2.40}$$

$$\mathrm{Im}\Pi^{(\mathrm{VI})}(t) = \frac{16\pi\alpha_s^2(t^3-10m^2t^2+28m^4t-32m^6)}{27t^{3/2}(t-4m^2)^{5/2}}\left\langle \bar{q}q\right\rangle^2. \tag{2.41}$$

For both $\Pi^{(\mathrm{I})}$ and $\Pi^{(\mathrm{II})}$, the first integral on the right-hand side of (2.34) converges and the second vanishes for $\eta \to 0^+$. For $\Pi^{(\mathrm{III})}$–$\Pi^{(\mathrm{VI})}$, however, each integral diverges although their sum is finite. To isolate this finite contribution, we first expand the imaginary parts (2.38)–

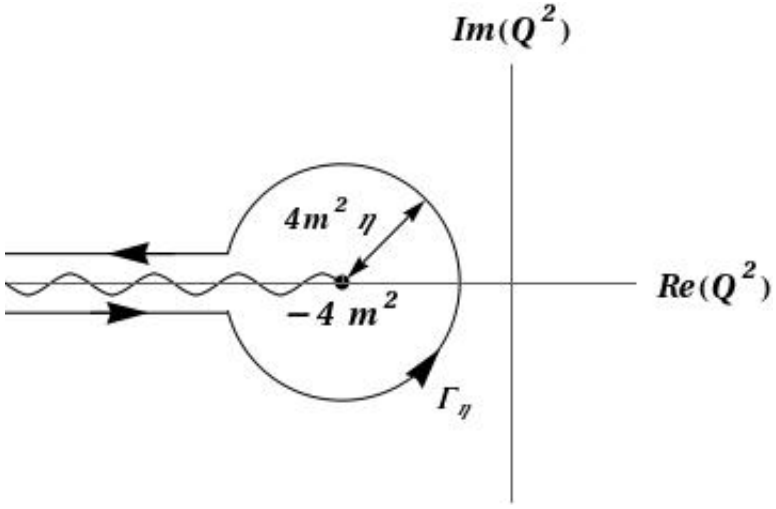

Figure 2.3: The integration contour used to compute the LSR (2.34)

(2.41) near $t = 4m^2$:

$$\mathrm{Im}\Pi^{(\mathrm{III})}(t) + \mathrm{Im}\Pi^{(\mathrm{IV})}(t) + \mathrm{Im}\Pi^{(\mathrm{V})}(t) + \mathrm{Im}\Pi^{(\mathrm{VI})}(t) = \frac{-m}{864\pi\sqrt{t-4m^2}}\left(\frac{m^2\left(27\langle g^3G^3\rangle + 1024\pi^2\alpha_s^2\langle\overline{q}q\rangle^2\right)}{(t-4m^2)^2} + \frac{27\langle g^3G^3\rangle - 1024\pi^2\alpha_s^2\langle\overline{q}q\rangle^2}{8(t-4m^2)} + p(t)\right) \tag{2.42}$$

where

$$p(t) = \frac{-27}{8(2m+\sqrt{t})^2t^{3/2}}\left(16m^3 + 16m^2\sqrt{t} + 4mt + t^{3/2}\right)\langle g^3G^3\rangle + \frac{1024\pi^2\alpha_s^2}{8m(2m+\sqrt{t})^2t^{3/2}}\left(32m^4 + 32m^3\sqrt{t} - 4m^2t - 15mt^{3/2} - 4t^2\right)\langle\overline{q}q\rangle^2 \tag{2.43}$$

is analytic in a neighbourhood about $t = 4m^2$. When (2.42) is inserted into the first integral on the right-hand side of (2.34), the part of the result stemming from the $p(t)$ term converges whereas the parts stemming from the $(t-4m^2)^{-2}$ and $(t-4m^2)^{-1}$ terms diverge. Focusing on these divergent parts, we have

$$\int_{4m^2(1+\eta)}^{s_0} e^{-t\tau}\frac{1}{\pi}\left(\frac{-m}{864\pi\sqrt{t-4m^2}}\left(\frac{m^2\left(27\langle g^3G^3\rangle + 1024\pi^2\alpha_s^2\langle\overline{q}q\rangle^2\right)}{(t-4m^2)^2}\right.\right.$$

$$+\frac{27\langle g^3G^3\rangle - 1024\pi^2\alpha_s^2\langle\overline{q}q\rangle^2}{8(t-4m^2)}\Big)\Big)dt$$
$$=\frac{e^{-4m^2\tau}}{10368\pi^2}\Big(-\frac{27\langle g^3G^3\rangle + 1024\pi^2\alpha_s^2\langle\overline{q}q\rangle^2}{\eta^{3/2}}$$
$$+\frac{3\Big(27(8m^2\tau-1)\langle g^3G^3\rangle + 1024(8m^2\tau+1)\pi^2\alpha_s^2\langle\overline{q}q\rangle^2\Big)}{2\eta^{1/2}}\Big)$$
$$+\frac{m\,e^{-4m^2\tau}}{384\pi^2}\Big(\sqrt{\pi\tau}\Big(3-8m^2\tau\Big)\mathrm{erf}\Big(\sqrt{(s_0-4m^2)\tau}\Big)+\frac{e^{-s_0\,\tau}}{(s_0-4m^2)^{3/2}}\Big($$
$$-8e^{s_0\,\tau}m^2\sqrt{\pi}\big((s_0-4m^2)\tau\big)^{3/2}+e^{4m^2\,\tau}\big(3s_0+32m^4\tau-8m^2(1+s_0\tau)\big)$$
$$+6e^{s_0\,\tau}m^2\,\mathrm{E}_{5/2}\big((s_0-4m^2)\tau\big)\Big)\Big)\langle g^3G^3\rangle$$
$$+\frac{8\,\alpha_s\,m\,e^{-4m^2\tau}}{81}\Big(-\sqrt{\pi\tau}\Big(3-8m^2\tau\Big)\mathrm{erf}\Big(\sqrt{(s_0-4m^2)\tau}\Big)+\frac{e^{-s_0\,\tau}}{(s_0-4m^2)^{3/2}}\Big($$
$$-24e^{s_0\,\tau}m^2\sqrt{\pi}\big((s_0-4m^2)\tau\big)^{3/2}+e^{4m^2\,\tau}\big(-3s_0+8m^2(1-4m^2\tau+s_0\tau)\big)$$
$$+18e^{s_0\,\tau}m^2\,\mathrm{E}_{5/2}\big((s_0-4m^2)\tau\big)\Big)\Big)\langle\overline{q}q\rangle^2 \quad (2.44)$$

for $\eta\to 0^+$. In (2.44), erf is the error function and E_n is the exponential integral function

$$\mathrm{erf}(z)=\frac{2}{\sqrt{\pi}}\int_0^z e^{-t^2}dt \quad (2.45)$$

$$\mathrm{E}_n(z)=\int_1^\infty\frac{e^{-zt}}{t^n}dt. \quad (2.46)$$

On the right-hand side of (2.44), note that the terms proportional to $\eta^{-3/2}$ and $\eta^{-1/2}$ diverge whereas the remaining terms are finite. Next, we consider the contributions of $\Pi^{(\mathrm{III})}$–$\Pi^{(\mathrm{VI})}$ to the second integral on the right-hand side of (2.34). Parameterizing

$$Q^2=-4m^2+4m^2\eta e^{i\theta} \quad (2.47)$$

for $\theta_i=-\pi^+$ to $\theta_f=\pi^-$, we find that

$$\frac{1}{2\pi i}\int_{\Gamma_\eta}e^{Q^2\tau}\Big(\Pi^{(\mathrm{III})}(Q^2)+\Pi^{(\mathrm{IV})}(Q^2)+\Pi^{(\mathrm{V})}(Q^2)+\Pi^{(\mathrm{VI})}(Q^2)\Big)dQ^2$$

$$= -\frac{e^{-4m^2\tau}}{10368\pi^2}\Bigg(-\frac{27\big\langle g^3G^3\big\rangle + 1024\pi^2\alpha_s^2\big\langle\overline{q}q\big\rangle^2}{\eta^{3/2}}$$
$$+\frac{3\Big(27(8m^2\tau-1)\big\langle g^3G^3\big\rangle + 1024(8m^2\tau+1)\pi^2\alpha_s^2\big\langle\overline{q}q\big\rangle^2\Big)}{2\eta^{1/2}}\Bigg) + \frac{e^{-4m^2\tau}}{384\pi^2}\big\langle g^3G^3\big\rangle \quad (2.48)$$

for $\eta \to 0^+$. When (2.44) and (2.48) are added together, the divergent terms which go like $\eta^{-3/2}$ and $\eta^{-1/2}$ cancel leaving a finite result. Finally, collecting together (2.34), (2.35), (2.42), (2.44), and (2.48), we have

$$\mathcal{R}(\tau,\, s_0) = \int_{4m^2}^{s_0} e^{-t\tau}\frac{1}{\pi}\Bigg(\mathrm{Im}\Pi^{(\mathrm{I})}(t) + \mathrm{Im}\Pi^{(\mathrm{II})}(t) - \frac{m\; p(t)}{864\pi\sqrt{t-4m^2}}\Bigg)dt$$
$$+\frac{m\; e^{-4m^2\tau}}{384\pi^2}\Bigg(\frac{1}{m} + \sqrt{\pi\tau}\Big(3-8m^2\tau\Big)\mathrm{erf}\Big(\sqrt{(s_0-4m^2)\tau}\Big) + \frac{e^{-s_0\,\tau}}{(s_0-4m^2)^{3/2}}\Bigg($$
$$-8e^{s_0\,\tau}m^2\sqrt{\pi}\big((s_0-4m^2)\tau\big)^{3/2} + e^{4m^2\,\tau}\big(3s_0 + 32m^4\tau - 8m^2(1+s_0\tau)\big)$$
$$+6e^{s_0\,\tau}m^2\,\mathrm{E}_{5/2}\big((s_0-4m^2)\tau\big)\Bigg)\Bigg)\big\langle g^3G^3\big\rangle$$
$$+\frac{8\;\alpha_s\;m\;e^{-4m^2\tau}}{81}\Bigg(-\sqrt{\pi\tau}\Big(3-8m^2\tau\Big)\mathrm{erf}\Big(\sqrt{(s_0-4m^2)\tau}\Big) + \frac{e^{-s_0\,\tau}}{(s_0-4m^2)^{3/2}}\Bigg($$
$$-24e^{s_0\,\tau}m^2\sqrt{\pi}\big((s_0-4m^2)\tau\big)^{3/2} + e^{4m^2\,\tau}\big(-3s_0 + 8m^2(1-4m^2\tau+s_0\tau)\big)$$
$$+18e^{s_0\,\tau}m^2\,\mathrm{E}_{5/2}\big((s_0-4m^2)\tau\big)\Bigg)\Bigg)\big\langle\overline{q}q\big\rangle^2 \quad (2.49)$$

where, again, $p(t)$ is given in (2.43), and the imaginary parts $\mathrm{Im}\Pi^{(\mathrm{I})}$ and $\mathrm{Im}\Pi^{(\mathrm{II})}$ are given in (2.36) and (2.37). The integral on the right-hand side of (2.49) can be evaluated analytically; however, the result is long and so we omit it for the sake of brevity.

Renormalization-group improvement [55] implies that the strong coupling and quark mass in the simplified (2.34) get replaced by corresponding running quantities evaluated at renormalization scale μ, i.e., $\alpha_s \to \alpha_s(\mu)$ and $m \to m_{c,b}(\mu)$. At one-loop in the $\overline{\mathrm{MS}}$ renormalization scheme, we have for charmonium

$$\alpha_s(\mu) = \frac{\alpha_s(M_\tau)}{1 + \frac{25\alpha_s(M_\tau)}{12\pi}\log\Big(\frac{\mu^2}{M_\tau^2}\Big)} \quad (2.50)$$

$$m_c(\mu) = \overline{m}_c \left(\frac{\alpha_s(\mu)}{\alpha_s(\overline{m}_c)} \right)^{12/25} \tag{2.51}$$

and for bottomonium

$$\alpha_s(\mu) = \frac{\alpha_s(M_Z)}{1 + \frac{23\alpha_s(M_Z)}{12\pi} \log\left(\frac{\mu^2}{M_Z^2}\right)} \tag{2.52}$$

$$m_b(\mu) = \overline{m}_b \left(\frac{\alpha_s(\mu)}{\alpha_s(\overline{m}_b)} \right)^{12/23} \tag{2.53}$$

where [4]

$$\alpha_s(M_\tau) = 0.330 \pm 0.014 \tag{2.54}$$

$$\alpha_s(M_Z) = 0.1185 \pm 0.0006 \tag{2.55}$$

$$\overline{m}_c = (1.275 \pm 0.025)\ \text{GeV} \tag{2.56}$$

$$\overline{m}_b = (4.18 \pm 0.03)\ \text{GeV}. \tag{2.57}$$

For charmonium, we set μ to $\overline{m}_c$; for bottomonium, we set μ to $\overline{m}_b$. Finally, we use the following values for the gluon and quark condensates [56, 57, 58]:

$$\left\langle \alpha G^2 \right\rangle = (0.075 \pm 0.02)\ \text{GeV}^4 \tag{2.58}$$

$$\left\langle g^3 G^3 \right\rangle = ((8.2 \pm 1.0)\ \text{GeV}^2) \left\langle \alpha G^2 \right\rangle \tag{2.59}$$

$$\left\langle \overline{q} q \right\rangle = -(0.23 \pm 0.03)^3\ \text{GeV}^3. \tag{2.60}$$

2.3.4 Analysis and Results

To extract hadron properties from the LSR (2.49) we must first select an acceptable range of τ values, i.e., a Borel interval (τ_{min}, τ_{max}). To do so, we follow the same methodology as in [47, 48, 59, 60]. To choose τ_{max}, we demand that the LSR converge in the following sense: the magnitude of the 4d gluon condensate contribution (stemming from $\Pi^{(\text{II})}$) must be less than one-third that of the perturbative contribution (stemming from $\Pi^{(\text{I})}$), and the magnitude of the sum of the 6d gluon and quark condensate contributions (stemming from $\Pi^{(\text{III})}$–$\Pi^{(\text{VI})}$)

must be less than one-third that of 4d gluon condensate contribution. For charmonium, we find $\tau_{\rm max} = 0.6$ GeV^{-2}; for bottomonium, we find $\tau_{\rm max} = 0.2$ GeV^{-2}. To choose $\tau_{\rm min}$, we consider the pole contribution

$$\frac{\mathcal{R}(\tau,\, s_0)}{\mathcal{R}(\tau,\, \infty)}, \tag{2.61}$$

i.e., the ratio of the LSR's hadron contribution to its hadron plus continuum contribution, and demand that it be at least 10%. In both the charmonium and bottomonium analyses, the value of $\tau_{\rm min}$ selected using this prescription depends weakly on s_0, a parameter not known at the outset. Hence, we first choose reasonable seed values for s_0: $s_0 = 25$ GeV^2 for charmonium and $s_0 = 130$ GeV^2 for bottomonium. When input into (2.61), these two seed values correspond to $\tau_{\rm min} = 0.1$ GeV^{-2} for charmonium and $\tau_{\rm min} = 0.01$ GeV^{-2} for bottomonium. After making predictions for s_0 through the optimization procedure explained below, we then update $\tau_{\rm min}$ using the new, predicted value of s_0. In all cases considered, the effect on $\tau_{\rm min}$ was insignificant.

Next, we turn our attention to $\rho^{\rm (had)}$ from (2.31). As $\rho^{\rm (had)}$ represents the resonance(s) portion of the hadronic spectral function, it contains those hadrons which couple to both the meson current (2.3) and the hybrid current (2.4). Such hadrons can be thought of as mixtures that have a $\overline{q}q$-meson and a hybrid component. Our analysis approach is to input known vector heavy quarkonium resonances into $\rho^{\rm (had)}$ in order to test them for meson-hybrid mixing. In Table 2.1, we list all vector charmonium resonances that have a Particle Data Group entry in [4], and in Table 2.2, we do the same for bottomonium. (Note that, in Table 2.1, states named with a ψ or J/ψ have $I^G = 0^-$ whereas those named with an X have unknown I^G.) All resonances listed in the two tables have widths $\lesssim 100$ MeV. In general, LSRs are insensitive to resonance widths of up to several hundred MeV, and so, we ignore the widths of individual resonances. But, for a cluster of resonances for which the mass difference between successively heavier states is $\lesssim 250$ MeV, we amalgamate the cluster into a single resonance with nonzero effective width. And so, we consider a variety of $\rho^{\rm (had)}$ of the form

$$\rho^{\rm (had)}(t) = \sum_{i=1}^{n} \rho_i^{\rm (had)}(t) \tag{2.62}$$

where n is the number of distinct resonances (or clusters of resonances) and where each $\rho_i^{\rm (had)}$

Table 2.1: Particle Data Group masses of vector charmonium resonances [4].

Name	Mass (GeV)
J/ψ	3.10
$\psi(2S)$	3.69
$\psi(3770)$	3.77
$\psi(4040)$	4.04
$\psi(4160)$	4.19
$X(4230)$	4.23
$X(4260)$	4.23
$X(4360)$	4.34
$\psi(4415)$	4.42
$X(4660)$	4.64

is either a narrow ($\Gamma_i = 0$) resonance

$$\rho_i^{(\mathrm{had})}(t) = \xi_i \delta(t - m_i^2) \tag{2.63}$$

or, for a resonance cluster, a rectangular pulse

$$\rho_i^{(\mathrm{had})}(t) = \frac{\xi_i}{2m_i\Gamma_i}\theta\big(t - m_i(m_i - \Gamma_i)\big)\theta\big(m_i(m_i + \Gamma_i) - t\big) \tag{2.64}$$

with effective width $\Gamma_i \neq 0$ in which the resonance strength is uniformly distributed over $m_i(m_i - \Gamma_i) < t < m_i(m_i + \Gamma_i)$. The $\{\xi_i\}_{i=1}^n$ are mixing parameters related to the combined effect of coupling to the hybrid and $q\overline{q}$-meson currents. A state with both $q\overline{q}$-meson and hybrid components has $\xi_i \neq 0$; a pure $q\overline{q}$-meson or pure hybrid state has $\xi_i = 0$. The specific models for which we present results are defined for the charmonium and bottomonium sectors in Tables 2.3 and 2.4 respectively.

Substituting (2.62) into (2.32) gives

$$\mathcal{R}(\tau,\, s_0) = \sum_{i=1}^{n} \int_{4m^2}^{s_0} e^{-t\tau} \rho_i^{(\mathrm{had})}(t) dt \tag{2.65}$$

Table 2.2: Particle Data Group masses of vector bottomonium resonances [4].

Name	Mass (GeV)
$\Upsilon(1S)$	9.46
$\Upsilon(2S)$	10.02
$\Upsilon(3S)$	10.34
$\Upsilon(4S)$	10.58
$\Upsilon(10860)$	10.89
$\Upsilon(11020)$	10.99

Table 2.3: A representative collection of hadron models analyzed in the charmonium sector.

Model	m_1 (GeV)	Γ_1 (GeV)	m_2 (GeV)	Γ_2 (GeV)	m_3 (GeV)	Γ_3 (GeV)
1	3.10	0	-	-	-	-
2	3.10	0	3.73	0	-	-
3	3.10	0	3.73	0	4.30	0
4	3.10	0	3.73	0	4.30	0.30
5	3.10	0	3.73	0.05	4.30	0.30
6	3.10	0	-	-	4.30	0
7	3.10	0	-	-	4.30	0.30

Table 2.4: A representative collection of hadron models analyzed in the bottomonium sector.

Model	m_1 (GeV)	Γ_1 (GeV)	m_2 (GeV)	Γ_2 (GeV)	m_3 (GeV)	Γ_3 (GeV)
1	9.46	0	-	-	-	-
2	9.46	0	10.02	0	-	-
3	9.46	0	10.02	0	10.47	0
4	9.46	0	10.02	0	10.47	0.22

where

$$\int_{4m^2}^{s_0} e^{-t\tau}\rho_i^{(\text{had})}(t)dt = \begin{cases} \xi_i e^{-m_i^2\tau},\ \Gamma_i = 0 \\ \xi_i e^{-m_i^2\tau}\frac{\sinh\left(m_i\Gamma_i\tau\right)}{m_i\Gamma_i\tau},\ \Gamma_i \neq 0 \end{cases}. \tag{2.66}$$

As a specific example, consider a $\rho^{(\text{had})}$ that has three resonances with masses $\{m_1,\, m_2,\, m_3\}$. If the first two resonances are narrow (i.e., $\Gamma_1 = \Gamma_2 = 0$) and the third has $\Gamma_3 \neq 0$, then

$$\rho^{(\text{had})}(t) = \xi_1\delta(t-m_1^2) + \xi_2\delta(t-m_2^2) + \frac{\xi_3}{2m_3\Gamma_3}\theta\big(t-m_3(m_3-\Gamma_3)\big)\theta\big(m_3(m_3+\Gamma_3)-t\big) \tag{2.67}$$

and

$$\mathcal{R}(\tau,\, s_0) = \xi_1 e^{-m_1^2\tau} + \xi_2 e^{-m_2^2\tau} + \xi_3 e^{-m_3^2\tau}\frac{\sinh\left(m_3\Gamma_3\tau\right)}{m_3\Gamma_3\tau}. \tag{2.68}$$

For particular choices of $\{m_i\}_{i=1}^n$ and $\{\Gamma_i\}_{i=1}^n$, the quantities $\{\xi_i\}_{i=1}^n$ and s_0 are extracted as best-fit parameters to (2.65). More precisely, we partition the Borel interval $(\tau_{\min},\, \tau_{\max})$ into $N = 20$ equal length subintervals with $\{\tau_j\}_{j=0}^N$ and define

$$\chi^2(\xi_1, \ldots, \xi_n,\, s_0) = \sum_{j=0}^{N}\left(\mathcal{R}(\tau_j,\, s_0) - \sum_{i=1}^{n}\int_{4m^2}^{s_0} e^{-t\tau_j}\rho_i^{(\text{had})}(t)dt\right)^2. \tag{2.69}$$

With the specific $\rho^{(\text{had})}(t)$ given in (2.67), for example, eqn. (2.69) becomes

$$\chi^2(\xi_1,\, \xi_2,\, \xi_3,\, s_0) = \sum_{j=0}^{N}\left(\mathcal{R}(\tau_j,\, s_0) - \xi_1 e^{-m_1^2\tau_j} - \xi_2 e^{-m_2^2\tau_j} - \xi_3 e^{-m_3^2\tau_j}\frac{\sinh\left(m_3\Gamma_3\tau_j\right)}{m_3\Gamma_3\tau_j}\right)^2. \tag{2.70}$$

Minimizing (2.69) gives predictions for $\{\xi_i\}_{i=1}^n$ and s_0 corresponding to the best fit agreement between QCD and the hadronic model in question. For the models defined in Tables 2.3 and 2.4, our results are shown in Tables 2.5 and 2.6 respectively. Rather than present each ξ_i, we instead present ζ and $\frac{\xi_i}{\zeta}$ where

$$\zeta = \sum_{i=1}^{n}|\xi_i|. \tag{2.71}$$

The errors included are associated with the strong coupling reference values (2.54)–(2.55), the quark mass parameters (2.56)–(2.57), the condensates (2.58)–(2.60), and an allowed

Table 2.5: Predicted mixing parameters with their theoretical uncertainties and continuum thresholds for hadron models defined in Table 2.3.

Model	s_0 (GeV^2)	$\chi^2 \times 10^6$ (GeV^{12})	ζ (GeV^6)	$\frac{\xi_1}{\zeta}$	$\frac{\xi_2}{\zeta}$	$\frac{\xi_3}{\zeta}$
1	12.5	4.33	0.514(21)	1	-	-
2	13.9	3.17	0.734(40)	0.726(34)	0.274(34)	-
3	24.1	0.164	2.88(25)	0.215(12)	−0.022(49)	0.762(30)
4	24.2	0.162	2.97(26)	0.210(12)	−0.032(48)	0.758(25)
5	24.2	0.162	2.97(26)	0.210(12)	−0.032(48)	0.758(25)
6	23.7	0.184	2.68(25)	0.228(19)	-	0.772(19)
7	23.6	0.204	2.66(25)	0.228(20)	-	0.772(19)

Table 2.6: Predicted mixing parameters with their theoretical uncertainties and continuum thresholds for hadron models defined in Table 2.4.

Model	s_0 (GeV^2)	$\chi^2 \times 10^4$ (GeV^{12})	ζ (GeV^6)	$\frac{\xi_1}{\zeta}$	$\frac{\xi_2}{\zeta}$	$\frac{\xi_3}{\zeta}$
1	107	42.0	140(3)	1	-	-
2	100	36.5	189(9)	0.774(14)	−0.226(14)	-
3	132	0.0860	1377(33)	0.203(2)	−0.380(3)	0.418(5)
4	132	0.0879	1375(32)	0.203(2)	−0.379(3)	0.418(5)

± 0.1 GeV variability in the renormalization scale [61]. We also allow for the end points of the Borel interval to vary by half the value of $\tau_{\min}$, i.e., 0.05 GeV^{-2} in the charmonium sector and 0.005 GeV^{-2} in the bottomonium sector. We don't vary κ from (2.11) as the numerical contribution to the LSR (2.49) stemming from the 6d quark condensate diagram is negligible. Our results are most sensitive to varying the quark mass parameters.

2.3.5 Discussion

As can be seen from Tables 2.5 and 2.6, in both the charmonium and bottomonium sectors, the inclusion of a third heavy resonance cluster in the analysis significantly improves the fit between QCD and experiment as measured by (2.69). The improvement is particularly dramatic for bottomonium. It is important to note that these third resonance clusters make large contributions to the LSR, i.e., the right-hand side of (2.65), despite the fact that high mass states are suppressed relative to low mass states due to the exponentially decaying

kernel. As a quantitative measure of the excited state signal strength, consider

$$\frac{\int_{4m^2}^{s_0} e^{-t\tau}\rho_3^{(\mathrm{had})}(t)dt}{\sum_{i=1}^{3}\left|\int_{4m^2}^{s_0} e^{-t\tau}\rho_i^{(\mathrm{had})}(t)dt\right|}, \tag{2.72}$$

the ratio of the third resonance's net contribution to the LSR to the sum (of the magnitudes) of the contributions made by all three resonances. In the charmonium sector, evaluating (2.72) for model 3 from Table 2.5 gives 0.43. In the bottomonium sector, evaluating (2.72) for model 3 from Table 2.6 gives 0.35. Thus the signal strength of the excited state is significant, as expected by its clear effect of reducing the χ^2-values in Tables 2.5 and 2.6.

Including one or more resonance widths in the analysis has almost no impact on the quality of fit between QCD and experiment as can be seen from the value of the minimized χ^2 of model 3–5 in Table 2.5 and models 3–4 in Table 2.6. This is unsurprising given the general insensitivity of LSRs to resonance width.

In both charmonium and bottomonium sectors, including a fourth resonance or resonance cluster in $\rho^{(\mathrm{had})}$ leads to a χ^2 that minimizes at $s_0 \approx m_4^2$, i.e., the heaviest resonance essentially merges with the continuum, contrary to the initial assumption articulated in (2.31) that there is a separation between resonance physics and the continuum. Furthermore, as can be seen from both Tables 2.5 and 2.6, the two-resonance scenario model 2 also suffers from this problem which gives us another reason to disfavour it compared to the three-resonance models.

Focusing on the three-resonance models in the charmonium sector (model 3–5 in Table 2.5), we find a nonzero mixing parameter for the J/ψ; essentially no evidence for mixing in the $\psi(2S)$, $\psi(3770)$ resonance cluster; and a large mixing parameter corresponding to a resonance (or resonance cluster) of mass (or average mass) 4.3 GeV. We investigated the effect of varying the mass of the third resonance, m_3, from 4.0 GeV–4.6 GeV. We found that the minimum value of the χ^2 was indeed lowest for $m_3 = 4.3$ GeV, about one-third the value for either $m_3 = 4.0$ GeV or $m_3 = 4.6$ GeV.

Given the lack of evidence for meson-hybrid mixing in the $\psi(2S)$, $\psi(3770)$ resonance cluster, it is reasonable to exclude it from $\rho^{(\mathrm{had})}$. As can be seen from models 6–7 in Table 2.5, doing so has a small effect on the fitted values of ξ_1, ξ_3, and s_0 as well as the minimum value

of the χ^2.

Focusing on the three-resonance models in the bottomonium sector (models 3–4 in Table 2.6), we find a nonzero mixing parameter for all three resonances, i.e., the $\Upsilon(1S)$, the $\Upsilon(2S)$, and the $\Upsilon(3S)$, $\Upsilon(4S)$ resonance cluster, indicating that all have $q\overline{q}$-meson and hybrid components.

In summary, the best agreement between our QCD predictions and experiment is achieved with three-resonance models in both the charmonium and the bottomonium sectors although, in the charmonium sector, omitting the second heaviest resonance cluster has minimal effect on the results. In fact, $q\overline{q}$-meson-hybrid mixing in the charmonium sector is well-described by a two resonance model consisting of the J/ψ and a second state with mass 4.3 GeV. It has been hypothesized that the $X(4260)$ might be a resonance with a significant hybrid component [62, 63, 36]. Our results are certainly consistent with this idea. In the bottomonium sector, our results indicate that there is nonzero $q\overline{q}$-meson-hybrid mixing in the $\Upsilon(1S)$, the $\Upsilon(2S)$, and in the $\Upsilon(3S)$, $\Upsilon(4S)$ pair.

Acknowledgments

We are grateful for financial support from the National Sciences and Engineering Research Council of Canada (NSERC).

2.4 1^{++} Initial Discussion

In the second paper in this series, we turn our attention to meson-hybrid mixing in $J^{PC} = 1^{++}$ heavy quarkonium. In Tables 2.7 and 2.8, we can see the known resonance masses that we will use as inputs into our model. It is these resonances that will now be probed for meson-hybrid mixing. The computation of the cross-correlator and subsequent generation of the LSR in [2] follow quite closely from the work done in [1].

The following work may be found published in:

Meson-Hybrid Mixing in $J^{PC} = 1^{++}$ Heavy Quarkonium from QCD Sum-Rules,
A. Palameta, D. Harnett, and T.G. Steele.
Phys. Rev. D **98**, 074014 (2018)
DOI:10.1103/PhysRevD.98.074014

I played a leading role in the work presented in this manuscript. In the second paper in this series I again calculated the cross-correlator, generated the Laplace sum-rule, built models of the hadronic spectra in question and performed the analysis to extract the mixing parameters. However here I also wrote the first draft of the manuscript and made significant contributions to subsequent edits.

2.5 Manuscript: Meson-Hybrid Mixing in $J^{PC} = 1^{++}$ Heavy Quarkonium from QCD Sum-Rules

Abstract: We explore conventional meson-hybrid mixing in $J^{PC} = 1^{++}$ heavy quarkonium using QCD Laplace sum-rules. We calculate the cross-correlator between a heavy conventional meson current and heavy hybrid current within the operator product expansion, including terms proportional to the four- and six-dimensional gluon condensates and the six-dimensional quark condensate. Using experimentally determined hadron masses, we construct models of the 1^{++} charmonium and bottomonium mass spectra. These models are used to investigate which resonances couple to both currents and thus exhibit conventional meson-hybrid mixing. In the charmonium sector, we find almost no conventional meson-hybrid mixing in the $\chi_{c1}(1P)$, minimal mixing in the $X(3872)$, and significant mixing in both the $X(4140)$ and $X(4274)$. In the bottomonium sector, we find minimal conventional meson-hybrid mixing in the $\chi_{b1}(1P)$ and significant mixing

in both the $\chi_{b1}(2P)$ and $\chi_{b1}(3P)$.

2.5.1 Introduction

Hybrids are hadrons which consist of a quark-antiquark pair and exhibit explicit gluon degrees of freedom. Hybrids are allowed by QCD as they are colour singlets; however, they have not yet been definitively experimentally identified [28].

Hybrids can be classified by J^{PC}, quantum numbers that can be separated into two categories, non-exotic and exotic, depending on whether the quantum numbers are accessible to conventional (quark-antiquark) mesons or not. Hybrids with exotic J^{PC} would not be able to quantum mechanically mix with conventional mesons; however, hybrids with non-exotic quantum numbers can potentially mix with conventional mesons. This mixing would result in hadrons that are superpositions of both conventional meson and hybrid.

In this article, we extend our work from [64] on vector (i.e., 1^{--}) conventional meson-hybrid mixing to axial vector (i.e., 1^{++}) charmonium ($c\bar{c}$) and bottomonium ($b\bar{b}$). Of particular interest in the charmonium sector is the $X(3872)$ [65, 4], the first of the XYZ resonances [66, 67, 68, 69, 38], a collection of charmonium-like hadrons many of which are not easily accommodated by the constituent quark model. The $X(3872)$ has been studied in the context of conventional meson-tetraquark mixing [70] as well as tetraquark-hybrid mixing [71] (see also [72, 73] for other approaches to mixing). Our analysis complements these two by considering conventional meson-hybrid mixing. At present, the 1^{++} channel is the only channel other then the 1^{--} with enough experimentally observed resonances to allow for the multi-resonance analysis methods of [64].

We use the operator product expansion (OPE) [15] to compute the cross-correlator between a heavy conventional meson current and a heavy hybrid current. In this calculation we include leading-order (LO) contributions from perturbation theory and non-perturbative corrections proportional to the four-dimensional (4d) and 6d gluon condensates as well as the 6d quark condensate. Then, using QCD Laplace sum-rules (LSRs) [25, 42, 43, 44], we analyze several single and multi-resonance models of the 1^{++} charmonium and bottomonium mass spectra. These models take known resonance masses as inputs and allow us to probe

the resonances to determine whether they couple to both the conventional meson current and the hybrid current. Resonances which couple to both currents are considered to be quantum mechanical mixtures of conventional meson and hybrid. The QCD sum-rules methodology has been applied to hadron mixing in a number of systems [64, 45, 46, 47, 74].

We find that multi-resonance models which include excited states in addition to the ground state lead to a significant improvement in agreement between QCD and experiment when compared to single resonance models. We show explicitly that the higher mass states make numerically significant contributions to the LSRs despite the LSR's exponential suppression of such resonances. In the charmonium sector, we find very little conventional meson-hybrid mixing in the $\chi_{c1}(1P)$, minimal mixing in the $X(3872)$, and large mixing in both the $X(4140)$ and the $X(4274)$. In the bottomonium sector, we find minimal conventional meson-hybrid mixing in the $\chi_{b1}(1P)$ and large mixing in both the $\chi_{b1}(2P)$ and $\chi_{b1}(3P)$.

2.5.2 The Correlator

For the conventional meson current

$$j_\mu^{(\mathrm{m})} = \overline{Q}\gamma_\mu\gamma^5 Q \tag{2.73}$$

and the hybrid current [49]

$$j_\nu^{(\mathrm{h})} = \frac{g_s}{2}\overline{Q}\gamma^\rho\lambda^a\widetilde{G}^a_{\nu\rho}Q \tag{2.74}$$

where Q is a heavy quark (i.e., charm or bottom) field and

$$\widetilde{G}^a_{\nu\rho} = \frac{1}{2}\epsilon_{\nu\rho\omega\zeta}G^a_{\omega\zeta} \tag{2.75}$$

is the dual gluon field strength tensor, we consider the cross-correlator

$$\Pi_{\mu\nu}(q) = i\int d^4x\; e^{iq\cdot x}\,\langle 0|\tau\, j_\mu^{(\mathrm{m})}(x)\; j_\nu^{(\mathrm{h})}(0)|0\rangle \tag{2.76}$$

$$= \frac{q_\mu q_\nu}{q^2}\Pi_0(q^2) + \left(\frac{q_\mu q_\nu}{q^2} - g_{\mu\nu}\right)\Pi_1(q^2). \tag{2.77}$$

In (2.77), the function $\Pi_0(q^2)$ probes spin-0 states and $\Pi_1(q^2)$ probes spin-1 states. We focus on $\Pi_1(q^2)$ as we are interested in probing 1^{++} states.

We evaluate the cross-correlator (2.76) within the OPE where perturbation theory is supplemented by non-perturbative corrections. Each of these non-perturbative corrections is the product of a perturbatively computed Wilson coefficient and a QCD condensate. We include terms proportional to the 4d and 6d gluon condensates and the 6d quark condensate defined respectively as follows:

$$\left\langle \alpha G^2 \right\rangle = \alpha_s \left\langle : G^a_{\omega\phi} G^a_{\omega\phi} : \right\rangle \tag{2.78}$$

$$\left\langle g^3 G^3 \right\rangle = g_s^3 f^{abc} \left\langle : G^a_{\omega\zeta}\, G^b_{\zeta\rho} G^c_{\rho\omega} : \right\rangle \tag{2.79}$$

$$\left\langle J^2 \right\rangle = \mathrm{Tr}\Big(\left\langle : J_\nu J_\nu : \right\rangle \Big) \tag{2.80}$$

with

$$J_\nu = \frac{-i g_s^2}{4} \lambda^a \sum_A \overline{q}^A \lambda^a \gamma_\nu q^A \tag{2.81}$$

where, in (2.81), q is a light quark (i.e., up, down, or strange) field and the sum is over flavours. We use the vacuum saturation hypothesis [25] to express $\langle J^2 \rangle$ in terms of the 3d quark condensate

$$\left\langle \overline{q} q \right\rangle = \left\langle : \overline{q}^\alpha_i q^\alpha_i : \right\rangle \tag{2.82}$$

resulting in

$$\left\langle J^2 \right\rangle = \frac{2}{3}\, \kappa\, g_s^4 \left\langle \overline{q} q \right\rangle^2 \tag{2.83}$$

where κ quantifies deviations from vacuum saturation. As in [64], we set $\kappa = 2$ [44].

The diagrams that contribute to (2.76) at LO are given in Figure 2.4. Each diagram is multiplied by two to account for additional diagrams in which the quark lines run in the opposite directions. Diagram IV gets another factor of two due to symmetry under exchange of the two interaction vertices. We calculate Wilson coefficients via fixed-point gauge methods [50, 51], and divergent integrals are dealt with through dimensional regularization in $D = 4 + 2\epsilon$ dimensions at $\overline{\mathrm{MS}}$-scale μ. The Mathematica package TARCER [53] which implements the recurrence relations of [17, 18] is used to express results in terms of known master

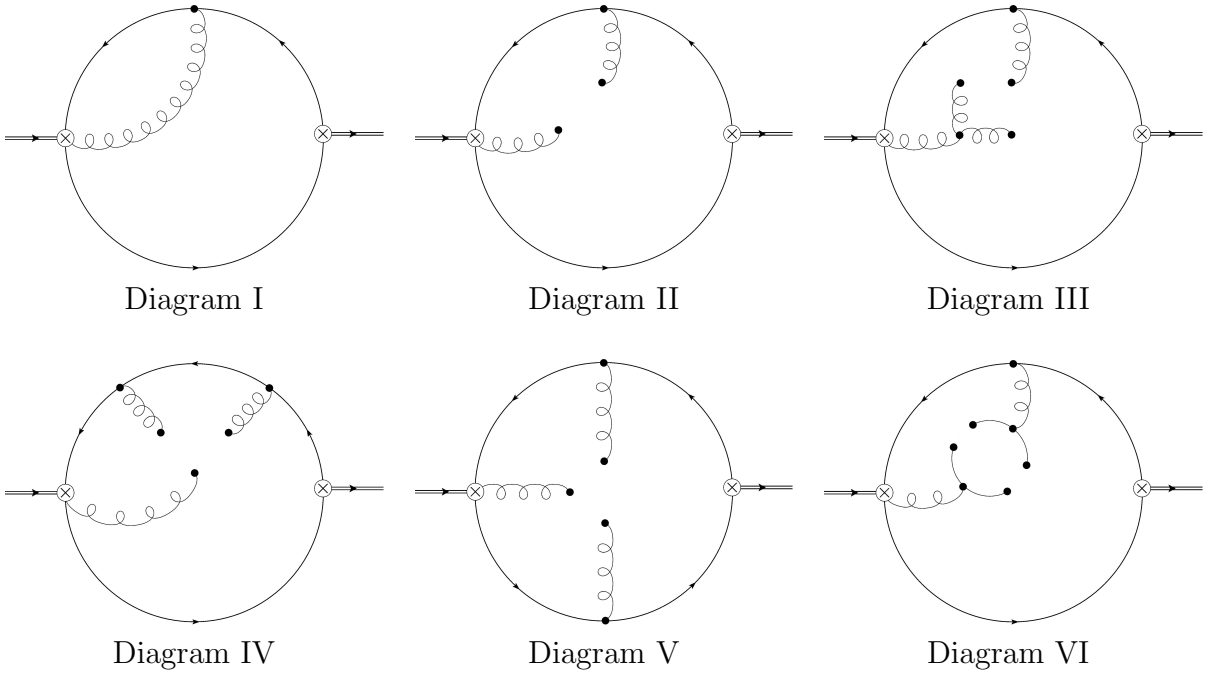

Figure 2.4: Feynman diagrams that contribute to the cross-correlator (2.76) at LO.

integrals including those of [20, 21]. Following [52] we use the γ^5 convention

$$\gamma^5 = \frac{i}{24}\epsilon_{\mu\nu\sigma\rho}\gamma^\mu\gamma^\nu\gamma^\sigma\gamma^\rho. \tag{2.84}$$

The OPE computation of Π_1 from (2.77), denoted $\Pi^{(\mathrm{OPE})}$, is decomposed as

$$\Pi^{(\mathrm{OPE})} = \Pi^{(\mathrm{I})} + \Pi^{(\mathrm{II})} + \Pi^{(\mathrm{III})} + \Pi^{(\mathrm{IV})} + \Pi^{(\mathrm{V})} + \Pi^{(\mathrm{VI})} \tag{2.85}$$

where the superscripts in (2.85) correspond to the labels of the diagrams in Figure 2.4. For $\Pi^{(\mathrm{I})}$, the ϵ-dependent result is given by

$$\begin{aligned}\Pi^{(\mathrm{I})}(z;\epsilon) = \frac{\alpha_s\, m^{4(1+\epsilon)}(1+\epsilon)\Gamma^2(-1-\epsilon)}{6\pi^3 z(3+2\epsilon)^2(4+3\epsilon)(4\pi)^{2\epsilon}}\Bigg(&\\ -12z(\epsilon+1)(2\epsilon+1)(3\epsilon+4)\left(z(4\epsilon+5)-2\epsilon^2-7\epsilon-5\right){}_2F_1\left(1,-\epsilon;\frac{3}{2};z\right)&\\ +\left(4z^2(\epsilon+1)(2\epsilon+3)(7\epsilon+8)+z(2\epsilon+1)(\epsilon(4\epsilon+7)+4)+(\epsilon+2)(2\epsilon+1)(4\epsilon+5)\right)&\end{aligned}$$

$$\times\ {}_3F_2\left(1,-2\epsilon-1,-\epsilon;\frac{1}{2}-\epsilon,\epsilon+2;z\right)$$
$$+2(z-1)(2\epsilon+1)(z(\epsilon(8\epsilon+19)+12)+(\epsilon+2)(4\epsilon+5))\,{}_3F_2\left(1,-2\epsilon,-\epsilon;\frac{1}{2}-\epsilon,\epsilon+2;z\right)\Bigg) \tag{2.86}$$

where

$$z=\frac{q^2}{4m^2}, \tag{2.87}$$

and all polynomials in z have been omitted as they will not contribute to the LSR. In (2.86), m is a heavy quark mass, Γ is the Gamma function, and ${}_pF_q(\cdots;\cdots;z)$ are generalized hypergeometric functions [54]. Expanding (2.86) in ϵ, we find

$$\Pi^{(\mathrm{I})}(z)=\frac{20\alpha_s m^4 z(z-1)\,{}_2F_1\left(1,1;\frac{5}{2};z\right)}{27\pi^3}\frac{1}{\epsilon}+\frac{d}{d\epsilon}\Pi^{(\mathrm{I})}(z;\epsilon)\Big|_{\epsilon=0}. \tag{2.88}$$

We do not include an explicit expression for the derivative term on the right-hand side of (2.88) as it will be replaced by (2.99) shortly. Expanding the remaining terms from (2.85) in ϵ, we find

$$\Pi^{(\mathrm{II})}(z)=\frac{z\Big(3-{}_2F_1\big(1,1;\frac{5}{2};z\big)\Big)}{36\pi(z-1)}\big\langle\alpha G^2\big\rangle \tag{2.89}$$

$$\Pi^{(\mathrm{III})}(z)=\frac{\Big(-3\left(44z^2-108z+73\right)+\left(24z^3-56z^2+38z+3\right)\,{}_2F_1\big(1,1;\frac{5}{2};z\big)\Big)}{13824\pi^2m^2(z-1)^3}\big\langle g^3G^3\big\rangle \tag{2.90}$$

$$\Pi^{(\mathrm{IV})}(z)=\frac{\big\langle g^3G^3\big\rangle}{13824\pi^2m^2(z-1)^2}\left(132z-183+\left(-24z^2+38z+3\right)\,{}_2F_1\big(1,1;\tfrac{5}{2};z\big)\right) \tag{2.91}$$

$$\Pi^{(\mathrm{V})}(z)=\frac{\big\langle g^3G^3\big\rangle}{4608\pi^2m^2(z-1)^2}\left(12z-15-(2z-3)\,{}_2F_1\big(1,1;\tfrac{5}{2};z\big)\right) \tag{2.92}$$

$$\Pi^{(\mathrm{VI})}(z)=\frac{4\alpha_s^2\big\langle\overline{q}q\big\rangle^2}{243m^2(z-1)^3}\left(3\left(44z^2-108z+73\right)-\left(24z^3-56z^2+38z+3\right)\,{}_2F_1\big(1,1;\tfrac{5}{2};z\big)\right). \tag{2.93}$$

The perturbative result (2.88) contains a nonlocal divergence. We eliminate this nonlocal

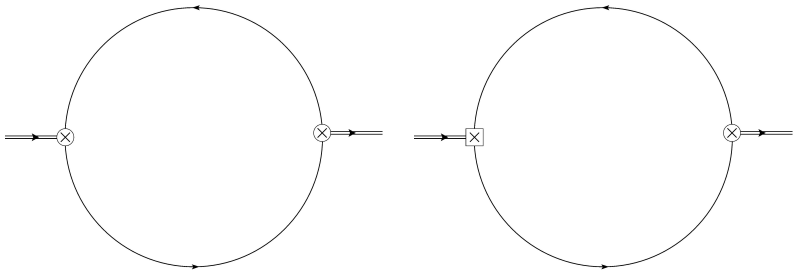

Figure 2.5: Renormalization-induced Feynman diagrams resulting from (2.96). The square insertion denotes the current (2.94).

divergence through operator mixing under renormalization as in [64, 47, 74]. The meson current (2.73) is renormalization-group (RG) invariant, and so we only need to consider the operator mixing of the hybrid current (2.74). The only operators that can mix with (2.74) and possibly generate nonzero contributions to the LO renormalized correlator are $j_\nu^{(m)}$ given in (2.73) and

$$j_\nu^{(c)} = \overline{Q} i\gamma^5 D_\nu Q \tag{2.94}$$

where $D_\nu = \partial_\nu - \frac{i}{2} g_s \lambda^a A_\nu^a$ is the covariant derivative. Then, the replacement

$$j_\nu^{(\mathrm{h})} \to j_\nu^{(\mathrm{h})} + Z_1\, j_\nu^{(\mathrm{m})} + Z_2\, j_\nu^{(\mathrm{c})} \tag{2.95}$$

for renormalization constants Z_1 and Z_2 must result in a perturbative contribution free of nonlocal divergences. Substituting (2.95) into (2.76) in D dimensions gives

$$\begin{aligned} i\int d^D x\; e^{iq\cdot x}\langle\Omega|\tau j_\mu^{(\mathrm{m})} j_\nu^{(\mathrm{h})}|\Omega\rangle \to{}& i\int d^D x\; e^{iq\cdot x}\langle\Omega|\tau j_\mu^{(\mathrm{m})} j_\nu^{(\mathrm{h})}|\Omega\rangle \\ &+ i\,Z_1\int d^D x\; e^{iq\cdot x}\langle\Omega|\tau j_\mu^{(\mathrm{m})} j_\nu^{(\mathrm{m})}|\Omega\rangle + i\,Z_2\int d^D x\; e^{iq\cdot x}\langle\Omega|\tau j_\mu^{(m)} j_\nu^{(\mathrm{c})}|\Omega\rangle. \end{aligned} \tag{2.96}$$

The two terms in (2.96) containing Z_1 and Z_2 each generate a renormalization-induced diagram, both of which are shown in Figure 2.5. Evaluating these two diagrams and selecting Z_1 and Z_2 such that the right-hand side of (2.96) is free of nonlocal divergences, we find

$$Z_1 = -\frac{10m^2\alpha_s}{9\pi\epsilon} \tag{2.97}$$

$$Z_2 = -\frac{4m\alpha_s}{9\pi\epsilon}. \tag{2.98}$$

Substituting (2.97) and (2.98) into (2.96) and expanding in ϵ gives a renormalized expression

$$\Pi^{(\mathrm{I})}(z) = \frac{m^4\alpha_s}{243\pi^3}\Bigg(9(6z^2-z-5)\,{}_3F_2\big(1,1,1;\tfrac{3}{2},3;z\big) - z\left(48z^2+2z+5\right)\,{}_3F_2\big(1,1,2;\tfrac{5}{2},4;z\big) + 9z\left(20(z-1)\log\left(\frac{m^2}{\mu^2}\right)+8z+5\right)\,{}_2F_1\big(1,1;\tfrac{5}{2};z\big)\Bigg) \tag{2.99}$$

where, again, we have omitted polynomials in z as they will not contribute to the LSR.

Finally, collecting (2.89)–(2.93) and (2.99) and then substituting them into (2.85) gives us the LO expression for $\Pi^{(\mathrm{OPE})}$ up to 6d condensates.

2.5.3 QCD Laplace Sum-Rules

For Euclidean momentum $Q^2 = -q^2 > 0$, the quantity Π_1 from (2.77) satisfies the dispersion relation

$$\Pi(Q^2) = \frac{Q^6}{\pi}\int_{t_0}^{\infty}\frac{\mathrm{Im}\Pi(t)}{t^3(t+Q^2)}dt + \cdots \tag{2.100}$$

where Π on the left-hand side represents the QCD result $\Pi^{(\mathrm{OPE})}$ and $\mathrm{Im}\Pi(t)$ on the right-hand side is the hadronic spectral function. Equation (2.100) is a statement of quark-hadron duality and allows us to interpret QCD information contained in the cross-correlator in the context of hadrons. In (2.100), t_0 is the hadron production threshold and the $\cdots$ represents unknown subtraction constants (a polynomial in Q^2). To eliminate these subtraction constants, eliminate local divergences in $\Pi^{(\mathrm{OPE})}$, and accentuate the resonance contributions of the hadronic spectral function, we apply to (2.100) the Borel transform

$$\hat{\mathcal{B}} = \lim_{\substack{N,Q^2\to\infty \\ \tau=N/Q^2}} \frac{\big(-Q^2\big)^N}{\Gamma(N)}\left(\frac{d}{dQ^2}\right)^N \tag{2.101}$$

where τ is the Borel parameter. This results in the formation of the 0^{th}-order LSR [25]

$$\mathcal{R}(\tau) \equiv \frac{1}{\tau}\hat{\mathcal{B}}\Big\{\Pi(Q^2)\Big\} = \int_{t_0}^{\infty} e^{-t\tau}\frac{1}{\pi}\text{Im}\Pi(t)dt. \tag{2.102}$$

We then introduce a "resonance(s) plus continuum" model

$$\frac{1}{\pi}\text{Im}\Pi(t) \to \rho^{(\text{had})}(t) + \frac{1}{\pi}\text{Im}\Pi^{(\text{OPE})}(t)\theta(t - s_0) \tag{2.103}$$

where $\rho^{(\text{had})}$ represents the resonance portion of the spectral function, θ is the Heaviside step function, and s_0 is the continuum threshold, and define the continuum-subtracted 0^{th}-order LSR

$$\mathcal{R}(\tau, s_0) \equiv \mathcal{R}(\tau) - \int_{s_0}^{\infty} e^{-t\tau}\frac{1}{\pi}\text{Im}\Pi^{(\text{OPE})}(t)dt = \int_{t_0}^{s_0} e^{-t\tau}\rho^{(\text{had})}(t)dt. \tag{2.104}$$

To compute $\mathcal{R}(\tau,\, s_0)$, we exploit the following relation between the Borel transform and the inverse Laplace transform $\hat{\mathcal{L}}^{-1}$ [25]:

$$\begin{aligned}\frac{1}{\tau}\hat{\mathcal{B}}\Big\{f(Q^2)\Big\} &= \hat{\mathcal{L}}^{-1}\Big\{f(Q^2)\Big\} \\ &= \frac{1}{2\pi i}\int_{c-i\infty}^{c+i\infty} f(Q^2)e^{Q^2\tau}dQ^2\end{aligned} \tag{2.105}$$

where $c \in \mathbb{R}$ is selected such that $f(Q^2)$ is analytic for $\text{Re}(Q^2) > c$. Generalized hypergeometric functions of the form ${}_pF_{p-1}(z)$, (such as those appearing in $\Pi^{(\text{OPE})}$) have a branch cut originating at the branch point $z = 1$ that extends along the positive real semi-axis. As such, in the complex Q^2-plane, $\Pi^{(\text{OPE})}$ is analytic everywhere except along the negative real semi-axis for $z < -Q^2/(4m^2)$. In (2.105), we let $f \to \Pi^{(\text{OPE})}$ and warp the contour of integration to that shown in Figure 2.6. We then apply definitions (2.102) and (2.104) to get

$$\mathcal{R}(\tau,\, s_0) = \int_{4m^2(1+\eta)}^{s_0} e^{-t\tau}\frac{1}{\pi}\text{Im}\Pi^{(\text{OPE})}(t)dt + \frac{1}{2\pi i}\int_{\Gamma_\eta} e^{Q^2\tau}\Pi^{(\text{OPE})}(Q^2)dQ^2 \quad \text{for} \quad \eta \to 0^+ \tag{2.106}$$

where

$$\text{Im}\Pi^{(\text{OPE})}(t) = \sum_{i=I}^{VI}\text{Im}\Pi^{(\text{i})}(t) \tag{2.107}$$

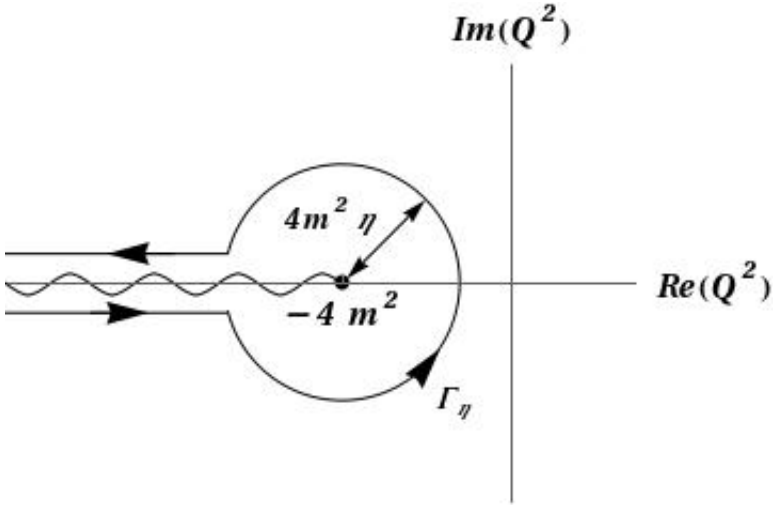

Figure 2.6: The contour of integration used in the evaluation of the LSR (2.106)

and, from (2.89)–(2.93) and (2.99)

$$\mathrm{Im}\Pi^{(\mathrm{I})}(t) = \frac{\alpha_s}{108\pi^2 t^2\sqrt{t-4m^2}}\Bigg(12m^2\sqrt{t-4m^2}\left(20m^6-6m^4t-6m^2t^2+5t^3\right)\sinh^{-1}\left(\frac{1}{2m}\sqrt{t-4m^2}\right)$$
$$+\sqrt{t}\left(t-4m^2\right)\left(60m^6+22m^4t-7m^2t^2+30m^2t\left(t-4m^2\right)\log\left(\frac{m^2}{\mu^2}\right)-6t^3\right)\Bigg) \tag{2.108}$$

$$\mathrm{Im}\Pi^{(\mathrm{II})}(t) = \frac{-m^2}{6\sqrt{t(t-4m^2)}}\left\langle\alpha G^2\right\rangle \tag{2.109}$$

$$\mathrm{Im}\Pi^{(\mathrm{III})}(t) = \frac{24m^6+76m^4t-28m^2t^2+3t^3}{288\pi t^{3/2}(t-4m^2)^{5/2}}\left\langle g^3G^3\right\rangle \tag{2.110}$$

$$\mathrm{Im}\Pi^{(\mathrm{IV})}(t) = \frac{6m^4+19m^2t-3t^2}{288\pi t^{3/2}(t-4m^2)^{3/2}}\left\langle g^3G^3\right\rangle \tag{2.111}$$

$$\mathrm{Im}\Pi^{(\mathrm{V})}(t) = \frac{m^2(6m^2-t)}{96\pi t^{3/2}(t-4m^2)^{3/2}}\left\langle g^3G^3\right\rangle \tag{2.112}$$

$$\mathrm{Im}\Pi^{(\mathrm{VI})}(t) = \frac{-64\pi\alpha_s^2(24m^6+76m^4t-28m^2t^2+3t^3)}{81t^{3/2}(t-4m^2)^{5/2}}\left\langle\bar{q}q\right\rangle^2. \tag{2.113}$$

Evaluating the integrals on the right-hand side of (2.106) for all six OPE terms leads to several divergences in η that, when summed, delicately cancel leaving us with a finite LSR. A detailed treatment of the evaluation of (2.106) for similar inputs is available in [64]. Here, for the sake of brevity, we omit these details and present the LSR:

$$\mathcal{R}(\tau,\, s_0) = \int_{4m^2}^{s_0} e^{-t\tau}\frac{1}{\pi}\Bigg(\mathrm{Im}\Pi^{(\mathrm{I})}(t) + \mathrm{Im}\Pi^{(\mathrm{II})}(t) + p(t)\Bigg)dt$$
$$- \frac{m\; e^{-4m^2\tau}}{384\pi^2}\Bigg(\sqrt{\pi\tau}\Big(3 - 8m^2\tau\Big)\mathrm{erf}\Big(\sqrt{(s_0-4m^2)\tau}\Big) + \frac{162e^{-s_0\,\tau}}{(s_0-4m^2)^{3/2}}\Bigg($$
$$- 8e^{s_0\,\tau}m^2\sqrt{\pi}\big((s_0-4m^2)\tau\big)^{3/2} + e^{4m^2\,\tau}\big(3s_0 + 32m^4\tau - 8m^2(1+s_0\tau)\big)$$
$$+ 6e^{s_0\,\tau}m^2\,\mathrm{E}_{5/2}\big((s_0-4m^2)\tau\big)\Bigg)\Bigg)\big\langle g^3G^3\big\rangle$$
$$- \frac{8\; m\; \alpha_s^2\; e^{-8m^2\tau}}{243}\Bigg(196m^2\tau^{3/2}e^{4m^2\tau}\left(4\sqrt{\pi} - 3\;\Gamma\left(-\frac{3}{2}, \big(s_0-4m^2\big)\,\tau\right)\right) + \frac{31e^{-s_0\,\tau}}{(s_0-4m^2)^{3/2}}\Bigg($$
$$2e^{8m^2\tau}\left(32m^4\tau - 8m^2(s_0\tau+1) + 3s_0\right)$$
$$- 2\sqrt{\pi\tau}\left(s_0-4m^2\right)^{3/2}\left(8m^2\tau - 3\right)e^{\tau\left(4m^2+s_0\right)}\mathrm{erf}\left(\sqrt{\tau\left(s_0-4m^2\right)}\right)\Bigg)\Bigg)\big\langle\overline{q}q\big\rangle^2 \quad (2.114)$$

where

$$p(t) = \frac{-1}{20736\pi t^{3/2}\left(\sqrt{t}+2m\right)^2\sqrt{t-4m^2}}\Bigg(81m\left(16m^3 + 16m^2\sqrt{t} + 4mt + t^{3/2}\right)\big\langle g^3G^3\big\rangle$$
$$+ 2048\pi^2\alpha_s^2\left(48m^4 + 48m^3\sqrt{t} + 188m^2t + 127mt^{3/2} + 24t^2\right)\big\langle\overline{q}q\big\rangle^2\Bigg) \quad (2.115)$$

and the imaginary parts $\mathrm{Im}\Pi^{(\mathrm{I})}$ and $\mathrm{Im}\Pi^{(\mathrm{II})}$ are given in (2.108) and (2.109) respectively. The integral on the right-hand side of (2.114) can be evaluated analytically; however, we omit the result for the sake of brevity.

Renormalization-group improvement [55] requires that the strong coupling and quark mass get replaced by their corresponding running quantities evaluated at renormalization scale μ. At one-loop in the $\overline{\mathrm{MS}}$ renormalization scheme, for charmonium we have

$$\alpha_s \to \alpha_s(\mu) = \frac{\alpha_s(M_\tau)}{1 + \frac{25\alpha_s(M_\tau)}{12\pi}\log\left(\frac{\mu^2}{M_\tau^2}\right)} \quad (2.116)$$

$$m \to m_c(\mu) = \overline{m}_c\left(\frac{\alpha_s(\mu)}{\alpha_s(\overline{m}_c)}\right)^{12/25} \quad (2.117)$$

and for bottomonium

$$\alpha_s \to \alpha_s(\mu) = \frac{\alpha_s(M_Z)}{1 + \frac{23\alpha_s(M_Z)}{12\pi}\log\left(\frac{\mu^2}{M_Z^2}\right)} \tag{2.118}$$

$$m \to m_b(\mu) = \overline{m}_b\left(\frac{\alpha_s(\mu)}{\alpha_s(\overline{m}_b)}\right)^{12/23} \tag{2.119}$$

where [4]

$$\alpha_s(M_\tau) = 0.330 \pm 0.014 \tag{2.120}$$

$$\alpha_s(M_Z) = 0.1185 \pm 0.0006 \tag{2.121}$$

$$\overline{m}_c = (1.275 \pm 0.025)\ \text{GeV} \tag{2.122}$$

$$\overline{m}_b = (4.18 \pm 0.03)\ \text{GeV}. \tag{2.123}$$

For charmonium, $\mu \to \overline{m}_c$ and for bottomonium, $\mu \to \overline{m}_b$. Finally, the following values are used for the gluon and quark condensates [56, 57, 58]:

$$\left\langle \alpha G^2 \right\rangle = (0.075 \pm 0.02)\ \text{GeV}^4 \tag{2.124}$$

$$\left\langle g^3 G^3 \right\rangle = ((8.2 \pm 1.0)\ \text{GeV}^2)\left\langle \alpha G^2 \right\rangle \tag{2.125}$$

$$\left\langle \overline{q}q \right\rangle = -(0.23 \pm 0.03)^3\ \text{GeV}^3. \tag{2.126}$$

2.5.4 Analysis and Results

We now turn our attention to $\rho^{(\text{had})}$ (recall (2.103)) which represents the resonance portion of the hadronic spectral function and contains the experimentally determined resonances we wish to probe for conventional meson-hybrid mixing. Resonances in $\rho^{(\text{had})}$ which couple to both the conventional meson current (2.73) and the hybrid current (2.74) can be thought of as meson-hybrid mixtures.

Our analysis approach is to build a variety of models of the 1^{++} heavy quarkonium mass spectra (i.e. a variety of choices for $\rho^{(\text{had})}$) that take known resonance masses as inputs, and test them for conventional meson-hybrid mixing. In Table 2.7, we list all 1^{++} charmonium resonances that have a Particle Data Group entry in [4], and in Table 2.8, we do the same

Table 2.7: Particle Data Group masses of 1^{++} charmonium resonances [4].

Name	Mass (GeV)
$\chi_{c1}(1P)$	3.51
$X(3872)$	3.87
$X(4140)$	4.15
$X(4274)$	4.27

Table 2.8: Particle Data Group masses of 1^{++} bottomonium resonances [4].

Name	Mass (GeV)
$\chi_{b1}(1P)$	9.89
$\chi_{b1}(2P)$	10.26
$\chi_{b1}(3P)$	10.51

for bottomonium. Note that, in Table 2.7 and Table 2.8, all entries have $I^G = 0^+$.

Laplace sum-rules are generally insensitive to resonance widths, and so we consider $\rho^{(\text{had})}$ to be a sum of narrow resonances, i.e.,

$$\rho^{(\text{had})}(t) = \sum_{i=1}^{n} \xi_i \delta(t - m_i^2) \tag{2.127}$$

where n is the number of resonances in the model. The $\{\xi_i\}_{i=1}^n$ are mixing parameters (products of hadron masses, signed hadronic couplings, and mixing angle factors) which are a measure of the combined coupling to both the conventional meson current and hybrid current. For example, in a simple case of two-state mixing, we would have $\xi_1 = m_H^2 m_M^2 f_H f_M \sin^2\theta$ and $\xi_2 = -m_H^2 m_M^2 f_H f_M \cos^2\theta$ where θ is a mixing angle between pure hybrid and meson states with corresponding couplings f_H and f_M. A state with both conventional meson and hybrid components has $\xi_i \neq 0$. A pure conventional meson state or pure hybrid state has $\xi_i = 0$. The specific models for which we present results are given for the charmonium and bottomonium sectors in Tables 2.9 and 2.10 respectively.

Substituting (2.127) into (2.104) gives

$$\mathcal{R}(\tau,\, s_0) = \sum_{i=1}^{n} \xi_i e^{-m_i^2 \tau}. \tag{2.128}$$

Table 2.9: A representative collection of hadron models analyzed in the charmonium sector.

Model	m_1 (GeV)	m_2 (GeV)	m_3 (GeV)	m_4 (GeV)
C1	3.51	-	-	-
C2	3.51	3.87	-	-
C3	3.51	3.87	4.15	-
C4	3.51	3.87	4.15	4.27

Table 2.10: A representative collection of hadron models analyzed in the bottomonium sector.

Model	m_1 (GeV)	m_2 (GeV)	m_3 (GeV)
B1	9.89	-	-
B2	9.89	10.26	-
B3	9.89	10.26	10.51

To extract hadronic properties from (2.128) together with LSR (2.114), we must first, for each model, select an acceptable range of τ values, i.e., a Borel window $(\tau_{\min}, \tau_{\max})$. To determine the Borel window, we follow the same methodology as in [47, 74, 59, 60]. To select $\tau_{\min}$, we consider

$$\frac{\mathcal{R}(\tau, s_0)}{\mathcal{R}(\tau, \infty)}, \tag{2.129}$$

i.e., the ratio of the LSR's hadron contribution to its hadron plus continuum contribution. We demand that this ratio be at least 10%. To select $\tau_{\max}$, we demand that the LSR converge where convergence is taken to mean that the magnitude of successive OPE terms be at most one-third that of any previous term. This means that we require the magnitude of the 4d gluon condensate contribution be less than one-third that of the perturbative contribution. We also require that the magnitude of the sum of the 6d gluon and quark condensate contributions be less than one-third that of 4d gluon condensate contribution.

For particular choices of $\{m_i\}_{i=1}^n$, the quantities $\{\xi_i\}_{i=1}^n$ and s_0 are extracted as best fit parameters to (2.128). To do so, we partition the Borel window into $N = 20$ equal length

subintervals with $\{\tau_j\}_{j=0}^{N}$, and define

$$\chi^2(\xi_1, \ldots, \xi_n,\, s_0) = \sum_{j=0}^{N} \left(\mathcal{R}(\tau_j,\, s_0) - \sum_{i=1}^{n} \xi_i e^{-m_i^2 \tau_j} \right)^2 . \tag{2.130}$$

Minimizing (2.130) gives predictions for $\{\xi_i\}_{i=1}^{n}$ and s_0 corresponding to the best fit agreement between QCD and the hadronic model in question.

The procedure described above for selecting a Borel window depends on s_0. However, s_0 is not known at the outset. It is one of the parameters that emerges from the minimization of (2.130). But the definition of (2.130) requires a Borel window. Hence, we determine both the Borel window and s_0 iteratively. We start with a seed value of $s_0 = 2m_{\text{max}}^2$ where m_{max} is the mass of the heaviest resonance in the model. This seed value separates the continuum from the resonances by a generous margin. We generate a Borel window for this s_0 value according to the criteria outlined above. Minimization of (2.130) then yields an updated value for s_0. This process is iteratively repeated until s_0 and the Borel window settle. For all the models examined in the charmonium sector, we found that the Borel window settled to $\tau_{\text{min}} = 0.17$ GeV^{-2} to $\tau_{\text{max}} = 0.41$ GeV^{-2}, and, in the bottomonium sector, all of the models have Borel windows that settled to $\tau_{\text{min}} = 0.02$ GeV^{-2} to $\tau_{\text{max}} = 0.12$ GeV^{-2}. These persistent values for the Borel window across different models in each sector demonstrates the LSR's insensitivity to changes in s_0 and is consistent with our findings in [64].

We extract $\{\xi_i\}_{i=1}^{n}$ and s_0 for each of the models defined in Tables 2.9 and 2.10, and present our results in Tables 2.11 and 2.12 respectively. Instead of presenting each ξ_i, we present ζ and $\frac{\xi_i}{\zeta}$ where

$$\zeta = \sum_{i=1}^{n} |\xi_i|. \tag{2.131}$$

The errors included are associated with the strong coupling values (2.120)–(2.121), the quark masses (2.122)–(2.123), the condensates (3.33)–(3.35), and an allowed ± 0.1 GeV variability in the renormalization scale [61]. We also allow for the end points of the Borel window to vary by 0.1 GeV^{-2} in the charmonium sector and 0.01 GeV^{-2} in the bottomonium sector. The vacuum saturation parameter κ from (3.7) is not varied because the numerical contribution to the LSR (2.114) stemming from the 6d quark condensate diagram is negligible. Our results are

Table 2.11: Continuum thresholds and χ^2 values for hadron models defined in Table 2.9 and their resulting extracted mixing parameters with their theoretical uncertainties.

Model	s_0 (GeV^2)	$\chi^2 \times 10^9$ (GeV^{12})	ζ (GeV^6)	$\frac{\xi_1}{\zeta}$	$\frac{\xi_2}{\zeta}$	$\frac{\xi_3}{\zeta}$	$\frac{\xi_4}{\zeta}$
C1	18.8	7990	0.18(1)	1	-	-	-
C2	28.8	76.3	0.83(7)	0.47(2)	−0.53(2)	-	-
C3	18.8	27.4	2.6(4)	0.21(2)	−0.45(1)	0.34(2)	-
C4	31.7	0.0586	44(6)	0.03(1)	−0.16(1)	0.46(1)	−0.35(1)

Table 2.12: Continuum thresholds and χ^2 values for hadron models defined in Table 2.10 and their resulting extracted mixing parameters with their theoretical uncertainties.

Model	s_0 (GeV^2)	$\chi^2 \times 10^6$ (GeV^{12})	ζ (GeV^6)	$\frac{\xi_1}{\zeta}$	$\frac{\xi_2}{\zeta}$	$\frac{\xi_3}{\zeta}$
B1	128	2580	49(1)	1	-	-
B2	282	1980	70(4)	0.30(1)	0.70(1)	-
B3	241	0.832	1905(28)	0.16(1)	−0.48(1)	0.36(1)

most sensitive to varying the value of $\tau_{\min}$ and varying the value of the quark masses (2.122) and (2.123). In Figure 2.7, we plot relative residuals representing the difference between the QCD prediction and the resonance plus continuum hadronic model,

$$r(\tau) = \frac{\mathcal{R}(\tau,\, s_0) - \sum_{i=1}^{n} \xi_i e^{-m_i^2 \tau}}{\mathcal{R}(\tau,\, s_0)}, \tag{2.132}$$

(the numerator in (2.132) is the difference between the left- and right-hand sides of (2.128)) for models C2–C4 using the optimized values of s_0 and $\{\xi_i\}$ from Table 2.11. In Figure 2.8, we do the same for models B1–B3 using the optimized values from Table 2.12.

2.5.5 Discussion

As shown in Tables 2.11 and 2.12, the inclusion of heavy resonances beyond the ground state significantly improves agreement between QCD and experiment in both the charmonium and bottomonium sectors. In particular, in the charmonium sector, going from three to

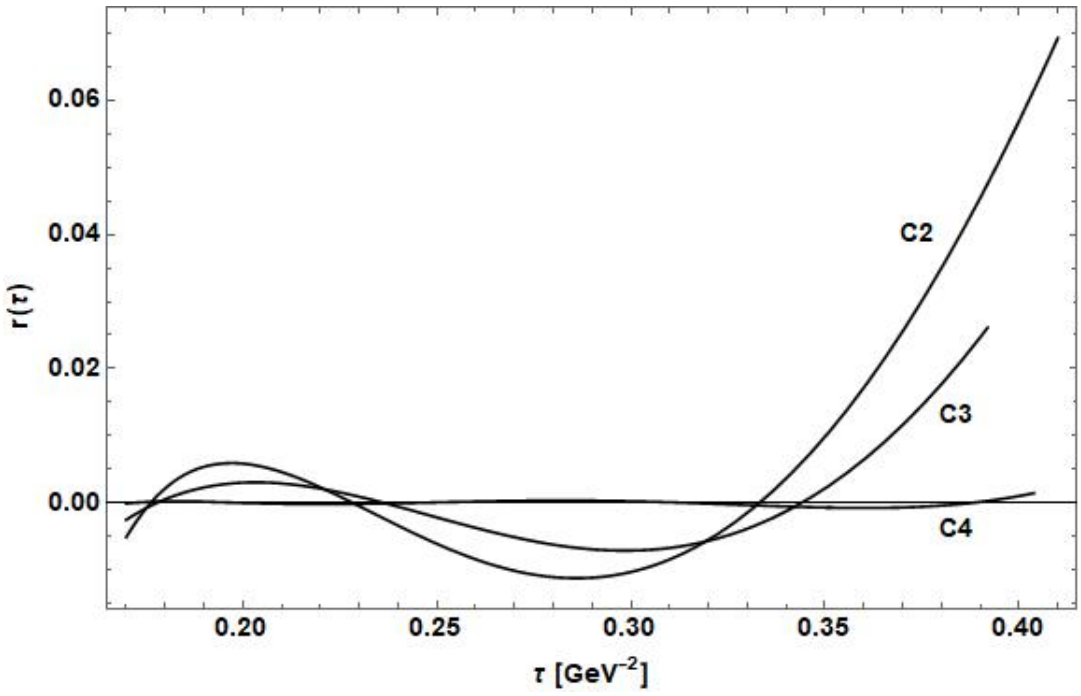

Figure 2.7: Relative residuals (2.132) for models C2–C4 using the optimized values of s_0 and ξ_i from Table 2.11. Residuals for model C1 are not shown because they are much larger than the scales of the figure.

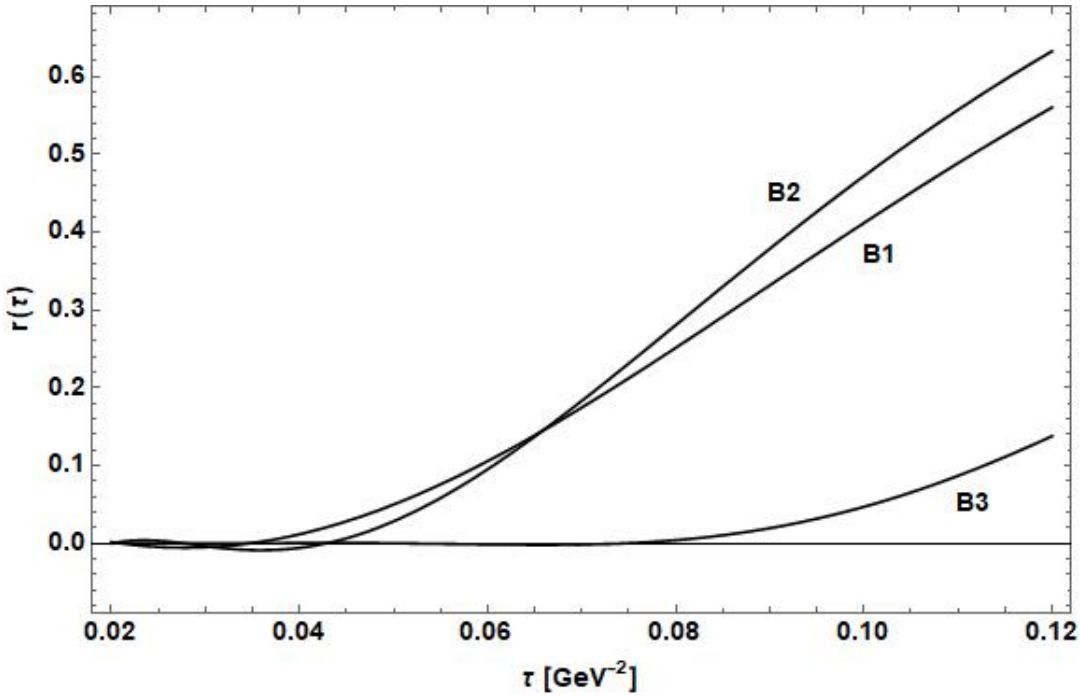

Figure 2.8: Relative residuals (2.132) for models B1–B3 using the optimized values of s_0 and ξ_i from Table 2.12.

four resonances (i.e., from model C3 to C4 in Table 2.11) decreases the value of the χ^2 (recall (2.130)) by a factor of 468 while in the bottomonium sector, going from two to three resonances (i.e., from model B2 to B3 in Table 2.12) decreases the χ^2 by a factor of 2380. This improvement can also be seen from the trend of decreasing magnitude of relative residuals with increasing number of resonances depicted in Figures 2.7 and 2.8. For the highest mass resonance in a given model we define a measure of its contribution to the LSR as in [64]:

$$\frac{\left|\int_{\tau_{\min}}^{\tau_{\max}} \xi_n e^{-m_n^2\tau} d\tau\right|}{\sum_{i=1}^{n}\left|\int_{\tau_{\min}}^{\tau_{\max}} \xi_i e^{-m_i^2\tau} d\tau\right|} \tag{2.133}$$

where n is the number of resonances in the model. The highest mass resonances make substantial contributions to the LSRs in spite of the exponential suppression inherent in LSRs: in the charmonium sector, evaluating (2.133) for model C4 gives 0.25, and in the bottomonium sector, evaluating (2.133) for model B3 gives 0.30. These results, coupled with the dramatic improvement in χ^2-values when compared to models containing less resonances, indicate the significant impact that the highest mass resonances have on the LSRs, and cause us to favour models C4 and B3.

In the charmonium sector, model C4 indicates that there is almost no conventional meson-hybrid mixing in the $\chi_{c1}(1P)$, minimal mixing in the $X(3872)$, and significant mixing in both the $X(4140)$ and $X(4274)$. Assuming the $\chi_{c1}(1P)$, the lightest known resonance in this sector, has a large conventional meson component [75], then our results indicate that it has very little hybrid component. Regarding the interpretation of the $X(3872)$, if the $X(3872)$ does have a significant hybrid component, a possibility put forth in [71], then our results indicate that it does not have a significant conventional meson component. However, if the $X(3872)$ does have a large conventional meson component as argued in [70], then our results indicate that it does not have a large hybrid component. In addition, our results imply that the $X(4140)$ and the $X(4274)$ both contain significant conventional meson and hybrid components.

In the bottomonium sector, model B3 indicates that there is minimal conventional meson-hybrid mixing in the $\chi_{b1}(1P)$ and significant mixing in both the $\chi_{b1}(2P)$ and the $\chi_{b1}(3P)$. Thus, assuming the $\chi_{b1}(1P)$, the lightest observed resonance in this sector, contains a significant conventional meson component [75], our results imply that it does not have a large

hybrid component. Also, our results indicate that the $\chi_{b1}(2P)$ and the $\chi_{b1}(3P)$ each contain significant conventional meson and hybrid components.

Acknowledgments

We are grateful for financial support from the National Sciences and Engineering Research Council of Canada (NSERC).

2.6 Meson-Hybrid Mixing Discussion

Now that we've reviewed the two papers [1, 2] which present our findings on the topic of meson-hybrid mixing in vector heavy quarkonium, we will discuss a few interesting intermediate details of the calculation before we get to the conclusion where we summarize our findings.

2.6.1 Non-perturbative Contributions

In this section, we're going to take a closer look at one technical detail involved in the calculation of the correlators (2.1) and (2.76). In the discussion about Wick's theorem in Section 1.3.5, we mentioned that the VEVs of uncontracted fields can be non-zero due to the nature of the QCD vacuum. We will now consider the contribution to the cross-correlators from these terms containing non-zero VEVs. In both [1] and [2], these contributions correspond to the contributions from Diagrams II–VI in Figures 2.1 and 2.4. While computing the contributions from these diagrams, we will encounter several non-local VEVs which take the following forms

$$\left\langle : G^a_{\omega\zeta}(0)\, A^b_\sigma(z) : \right\rangle \tag{2.134}$$

$$\left\langle : A^a_\alpha(y)\, G^b_{\beta\gamma}(0)\, A^c_\delta(z) : \right\rangle \tag{2.135}$$

$$\left\langle : G^a_{\alpha\beta}(0)\, A^b_\gamma(y)\, A^c_\delta(z) : \right\rangle. \tag{2.136}$$

The first non-local VEV (2.134) will emerge from diagrams where a single interaction vertex is present, such as diagrams II, III and VI from Figure 2.1 and 2.4, and will yield a 4d and

a 6d gluon condensate contribution as well as a 6d quark condensate contribution. The next two VEVs (2.135) and (2.136) will emerge from diagrams with two interaction vertices such as diagrams IV and V and will yield 6d gluon condensate contributions in these calculations.

In the previously mentioned master's thesis [8], we included a detailed discussion of how the 4d and 6d gluon condensate contributions (from diagrams II, III of Figure 2.1) were calculated and a discussion of how the needed VEVs could be evaluated. I will include the discussion of how these VEVs are evaluated here. I will then, for the sake of brevity, skip a detailed discussion of how the rest of these VEVs are evaluated and simply present the substitutions which are necessary to proceed with the calculation and evaluate the remaining diagrams.

2.6.1.1 Expansion of the Non-local VEV

Including a pre-factor from elsewhere in the calculation, we will want to evaluate

$$g_s^2 \, \mathrm{Tr}[\lambda^a \lambda^b] \big\langle : G^a_{\omega\zeta}(0) \, A^b_\sigma(z) : \big\rangle. \tag{2.137}$$

We are going to want to start by expanding this non-local VEV into an infinite series of local VEVs. To do that we can use the ideas discussed in [16]. Specifically, we know that working in the fixed point gauge where $x^\mu A_\mu(x) = 0$, we can write our gluon field at z as an infinite series of terms involving the commutator of covariant derivatives D and gluon field strength tensors G at the origin as follows:

$$A_\sigma(z) = \sum_{n=0}^{\infty} \frac{1}{n!(n+2)} z^\phi z^{\rho_1} z^{\rho_2} \dots z^{\rho_n} [D_{\rho_1}(0), [D_{\rho_2}(0), [\dots [D_{\rho_n}(0), G_{\phi\sigma}(0)] \dots]]]. \tag{2.138}$$

Note that in the perturbative calculation, when contracting gluon fields, we chose to work in the Feynman gauge; however, here we have chosen to work in the fixed point gauge. Perhaps the easiest way to think about why we are free to do this is to realize that for each gauge invariant contribution to our correlator, we are free to make whatever gauge choice we wish. A more detailed discussion on this topic is available in [76]. It will also be useful to note that

we can write our gluon field strength tensor $G_{\mu\nu}$ in the following form:

$$G_{\mu\nu} = \frac{ig_s}{2}\lambda^a G^a_{\mu\nu}. \tag{2.139}$$

Also, we can write individual gluon fields A_μ similarly as follows:

$$A_\mu = \frac{ig_s}{2}\lambda^a A^a_\mu. \tag{2.140}$$

Now, substituting (2.139) and (2.140) into (2.138) and then substituting the result into (2.137) will give us

$$\begin{aligned} g_s^2\ \mathrm{Tr}[\lambda^a\lambda^b]\big\langle :G^a_{\omega\zeta}(0)\, A^b_\sigma(z): \big\rangle &= \\ &= g_s^2\ \mathrm{Tr}[\lambda^a\lambda^b]\Big\{\frac{1}{2}z^\phi\big\langle :G^a_{\omega\zeta}(0)\, G^b_{\phi\sigma}(0): \big\rangle + \frac{1}{3}z^\phi z^{\rho_1}\big\langle :G^a_{\omega\zeta}(0)[D_{\rho_1}(0), G^b_{\phi\sigma}(0)]: \big\rangle \\ &\qquad + \frac{1}{8}z^\phi z^{\rho_1} z^{\rho_2}\big\langle :G^a_{\omega\zeta}(0)[D_{\rho_1}(0), [D_{\rho_2}(0), G^b_{\phi\sigma}(0)]]: \big\rangle + \dots\Big\} \\ &= -2\ z^\phi\ \mathrm{Tr}[\big\langle :G_{\omega\zeta}(0)\, G_{\phi\sigma}(0): \big\rangle] - \frac{4}{3}\ z^\phi z^{\rho_1}\ \mathrm{Tr}[\big\langle :G_{\omega\zeta}(0)[D_{\rho_1}(0), G_{\phi\sigma}(0)]: \big\rangle] \\ &\qquad - \frac{1}{2}\ z^\phi z^{\rho_1} z^{\rho_2}\ \mathrm{Tr}[\big\langle :G_{\omega\zeta}(0)[D_{\rho_1}(0), [D_{\rho_2}(0), G_{\phi\sigma}(0)]]: \big\rangle] - \dots \end{aligned} \tag{2.141}$$

where the second equality holds because of another application of (2.139). The VEV in the first term on the right will give us our term proportional to what we will call the 4d gluon condensate. The second term on the right will go to zero. An easy way to see this is there are an odd number of Lorentz indices in this term, and there would be no way to write this term using only metric tensors. The VEV in the third term will give us a term proportional to what we will call the 6d gluon condensate. This third term will also yield the 6d quark condensate contribution which we will discuss shortly. We truncate the series at this point ignoring higher order terms which will be increasingly suppressed by factors of $\frac{1}{m}$ and $\frac{1}{q}$.

2.6.1.2 Evaluating the 4d VEV

The 4d VEV can be written in terms of metric tensors as follows:

$$\mathrm{Tr}[\big\langle :G_{\omega\zeta}G_{\phi\sigma}: \big\rangle] = Ag_{\omega\zeta}g_{\phi\sigma} + Bg_{\phi\zeta}g_{\omega\sigma} + Cg_{\omega\phi}g_{\sigma\zeta} \tag{2.142}$$

where A, B and C are unknown constants we will need to solve for. But we know that our gluon field strength tensors are antisymmetric under the exchange of their indices, so $A \to 0$. Now we can group the remaining two terms while maintaining antisymmetry under $\omega \leftrightarrow \zeta$ and $\phi \leftrightarrow \sigma$ with a new arbitrary constant F as follows:

$$\mathrm{Tr}[\langle : G_{\omega\zeta} G_{\phi\sigma} : \rangle] = F\big[g_{\omega\sigma} g_{\zeta\phi} - g_{\omega\phi} g_{\zeta\sigma}\big]. \tag{2.143}$$

We can now start solving for F by contracting both sides of the equation with $g_{\omega\sigma} g_{\zeta\phi}$ giving us

$$\mathrm{Tr}[\langle : G_{\omega\phi} G_{\phi\omega} : \rangle] = F\big[d^2 - d\big]. \tag{2.144}$$

Then, by again using (2.139) and evaluating the remaining trace using $\mathrm{Tr}[\lambda^a \lambda^b] = 2\delta^{ab}$, we can solve for F. We find that

$$F = \frac{\langle g_s^2 G^2 \rangle}{2d(d-1)} \tag{2.145}$$

where

$$\langle g_s^2 G^2 \rangle = g_s^2 \langle : G^a_{\omega\phi} G^a_{\omega\phi} : \rangle \tag{2.146}$$

is the 4d gluon condensate. We can now substitute (2.145) back into (2.143) and, using (2.139), rewrite the left hand side (LHS) of the expression. If we then substitute this back into the first term in (2.141) and, keeping just that first term, this results in an expression proportional to the 4d gluon condensate contribution. This result is the contribution to the correlator that corresponds to diagram II in Figures 2.1 and 2.4.

2.6.1.3 Evaluating the 6d VEV (gluonic contribution only)

Now, returning back to equation (2.141), we have one more term in our series that will contribute. To get at the 6d gluon condensate contribution, we will need to simplify the trace in the last term in (2.141). We could again write out all of the combinations of metrics that this 6d term could depend on like we did in the 4d case in equation (2.142). If we did, we would find 15 possible combinations of metrics. After taking into account the antisymmetric nature of the gluon field strength tensors, we could immediately eliminate five of these leaving us with ten terms. We could then start to carefully group these terms so that the symmetries

of the gluon field strength tensors are preserved until we found that this expression could be written as follows:

$$\begin{aligned}\mathrm{Tr}[\big\langle : G_{\omega\zeta}(0)[D_{\rho_1}(0),&[D_{\rho_2}(0), G_{\phi\sigma}(0)]]: \big\rangle] = \\ &= A\ g_{\rho_1\rho_2}(g_{\omega\phi}g_{\zeta\sigma} - g_{\phi\zeta}g_{\omega\sigma}) + \\ &\quad + B\ \left[g_{\phi\rho_2}(g_{\omega\rho_1}g_{\zeta\sigma} - g_{\rho_1\zeta}g_{\omega\sigma}) - g_{\sigma\rho_2}(g_{\phi\zeta}g_{\omega\rho_1} - g_{\omega\phi}g_{\zeta\rho_1})\right] + \\ &\quad + C\ \left[g_{\rho_1\sigma}(g_{\omega\rho_2}g_{\phi\zeta} - g_{\omega\phi}g_{\zeta\rho_2}) - g_{\rho_1\phi}(g_{\omega\rho_2}g_{\zeta\sigma} - g_{\omega\sigma}g_{\rho_2\zeta})\right]\end{aligned} \tag{2.147}$$

where A, B and C are unknown constants for which we will need to solve. We will now need to generate three equations to solve for our three unknowns. The easiest way to do this is to select three different contraction schemes that will fully contract the right hand side (RHS) of the equation without sending it to zero. We will then apply these contraction schemes to both sides of the equation to generate the three equations in three unknowns. We have selected the following three products of metrics to contract both sides

$$\begin{aligned} &g_{\rho_1\rho_2}g_{\omega\phi}g_{\zeta\sigma} \\ &g_{\phi\rho_2}g_{\omega\rho_1}g_{\zeta\sigma} \\ &g_{\rho_1\sigma}g_{\omega\rho_2}g_{\phi\zeta}. \end{aligned} \tag{2.148}$$

The simplification of the RHSs of our three new expressions is fairly straightforward. We simply contract the indices and make use of the fact that $g_{\mu\mu} = d$. The simplification of the LHSs will be a bit more involved. To simplify the LHSs we will need to make use of the Jacobi identity [16] which in this context can be stated as follows:

$$[D_\mu, [D_\nu, D_\rho]] + [D_\rho, [D_\mu, D_\nu]] + [D_\nu, [D_\rho, D_\mu]] = 0. \tag{2.149}$$

We will also make use of the definition $[D_\mu, D_\nu] = -G_{\mu\nu}$, and we will set $[D^\mu, G_{\mu\nu}] = J_\nu \to 0$. The reason for setting $J_\nu \to 0$ is that these terms will lead to the 6d quark condensate contribution and we want to keep those separated for the moment. We will now take a look at how the simplification of the LHS would work for the first contraction scheme found in (2.148). The other two contractions would follow similarly. Applying the metrics in

contraction scheme (1) to the LHS of (2.147) and making use of (2.149) while suppressing the arguments and the trace allows us to write

$$\big\langle\!\!\big\langle : G_{\omega\zeta}[D_{\rho_1},[D_{\rho_1},G_{\omega\zeta}]] : \big\rangle\!\!\big\rangle = -\big\langle\!\!\big\langle : G_{\omega\zeta}[D_{\rho_1},[D_{\zeta},G_{\rho_1\omega}]] : \big\rangle\!\!\big\rangle - \big\langle\!\!\big\langle : G_{\omega\zeta}[D_{\rho_1},[D_{\omega},G_{\zeta\rho_1}]] : \big\rangle\!\!\big\rangle. \tag{2.150}$$

We can also use (2.149) to show that

$$[D_{\rho_1},[D_{\zeta},G_{\rho_1\omega}]] = [G_{\rho_1\omega},G_{\rho_1\zeta}] \;\text{ and }\; [D_{\rho_1},[D_{\omega},G_{\zeta\rho_1}]] = [G_{\zeta\rho_1},G_{\rho_1\omega}]. \tag{2.151}$$

Substituting these results back into (2.150) and flipping commutators in one factor and indices in another to pick up some minus signs gives us

$$\begin{aligned}\big\langle\!\!\big\langle : G_{\omega\zeta}[D_{\rho_1},[D_{\rho_1},G_{\omega\zeta}]] : \big\rangle\!\!\big\rangle &= \big\langle\!\!\big\langle : G_{\omega\zeta}[G_{\rho_1\zeta},G_{\rho_1\omega}] : \big\rangle\!\!\big\rangle + \big\langle\!\!\big\langle : G_{\omega\zeta}[G_{\rho_1\zeta},G_{\rho_1\omega}] : \big\rangle\!\!\big\rangle \\ &= -4\,\big\langle\!\!\big\langle : G_{\omega\zeta}\; G_{\zeta\rho_1}G_{\rho_1\omega} : \big\rangle\!\!\big\rangle\end{aligned} \tag{2.152}$$

where the second equality is realized by expanding the commutators, rearranging indices and grouping terms. Now, wrapping both sides of the equation in a trace (as we must to regain (2.147)) and making use of (2.139) allows us to write

$$\mathrm{Tr}\big[\big\langle\!\!\big\langle : G_{\omega\zeta}[D_{\rho_1},[D_{\rho_1},G_{\omega\zeta}]] : \big\rangle\!\!\big\rangle\big] = -4\Big(\frac{ig_s}{2}\Big)^3\mathrm{Tr}[\lambda^a\lambda^b\lambda^c]\big\langle\!\!\big\langle : G^a_{\omega\zeta}\; G^b_{\zeta\rho_1}G^c_{\rho_1\omega} : \big\rangle\!\!\big\rangle. \tag{2.153}$$

The identity $\mathrm{Tr}[\lambda^a\lambda^b\lambda^c] = 2(d_{abc} + if_{abc})$, which can be found in [16], where the d_{abc} is real and totally symmetric and the f_{abc} is again a totally antisymmetric structure constants, can be used to simplify this expression. Then, using the totally symmetric nature of d_{abc} and the fact that $G^a_{\mu\nu}$ is antisymmetric in μ and ν to argue away the first term, we can write

$$\mathrm{Tr}\big[\big\langle\!\!\big\langle : G_{\omega\zeta}[D_{\rho_1},[D_{\rho_1},G_{\omega\zeta}]] : \big\rangle\!\!\big\rangle\big] = -\big\langle g_s^3G^3\big\rangle \tag{2.154}$$

where

$$\big\langle g_s^3G^3\big\rangle = g_s^3f_{abc}\big\langle\!\!\big\langle : G^a_{\omega\zeta}\; G^b_{\zeta\rho_1}G^c_{\rho_1\omega} : \big\rangle\!\!\big\rangle. \tag{2.155}$$

We can now perform similar simplifications using all three of the contraction schemes in (2.148) on (2.147). Doing so generates the following system of equations:

$$\begin{aligned} d(d-1)(dA+2B-2C) &= -\langle g_s^3 G^3 \rangle \\ d(d-1)(A+(d-1)B-C) &= 0 \\ -d(d-1)(A+B-(d-1)C) &= \frac{\langle g_s^3 G^3 \rangle}{2}. \end{aligned} \tag{2.156}$$

Then, solving this system for our three unknowns A, B and C and substituting the results back into (2.147) with some simplification will give us

$$\begin{aligned} &\mathrm{Tr}\big[\langle : G_{\omega\zeta}(0)[D_{\rho_1}(0),[D_{\rho_2}(0),G_{\phi\sigma}(0)]]: \rangle\big] = \\ &\quad = \frac{\langle g_s^3 G^3 \rangle}{2d(d^2-4)}\Bigg[-2\, g_{\rho_1\rho_2}(g_{\omega\phi}g_{\zeta\sigma} - g_{\phi\zeta}g_{\omega\sigma}) + \\ &\qquad + \frac{3}{d-1}\left[g_{\phi\rho_2}(g_{\omega\rho_1}g_{\zeta\sigma} - g_{\rho_1\zeta}g_{\omega\sigma}) - g_{\sigma\rho_2}(g_{\phi\zeta}g_{\omega\rho_1} - g_{\omega\phi}g_{\zeta\rho_1})\right] + \\ &\qquad + \left[g_{\rho_1\sigma}(g_{\omega\rho_2}g_{\phi\zeta} - g_{\omega\phi}g_{\zeta\rho_2}) - g_{\rho_1\phi}(g_{\omega\rho_2}g_{\zeta\sigma} - g_{\omega\sigma}g_{\rho_2\zeta})\right]\Bigg]. \end{aligned} \tag{2.157}$$

Here, we have highlighted the calculation of two of the VEVs needed in simplifying the correlators in [1, 2]. In addition to the ones we've discussed here, there is a 6d quark condensate and versions of the 6d gluon condensate emerging from two interaction vertices as seen in 2.135 and 2.136 all of these would be derived using the techniques discusses above.

2.7 Meson-Hybrid Mixing Summary

We will now collect our results and present some final reflections or our exploration of meson-hybrid mixing in vector heavy quarkonium. In [1, 2], we explore meson-hybrid mixing in the $J^{PC} = 1^{--}$ and $J^{PC} = 1^{++}$ charmonium-like and bottomonium-like mass spectra. Using the experimentally determined resonance masses listed in Tables 2.1, 2.2 and Tables 2.7, 2.8 and again collected here in Figure 2.9, we employ QCDSRs and a multi-resonance analysis methodology to probe these resonances for meson-hybrid mixing.

Focusing in on each of the models in the four sectors we examined that showed the best

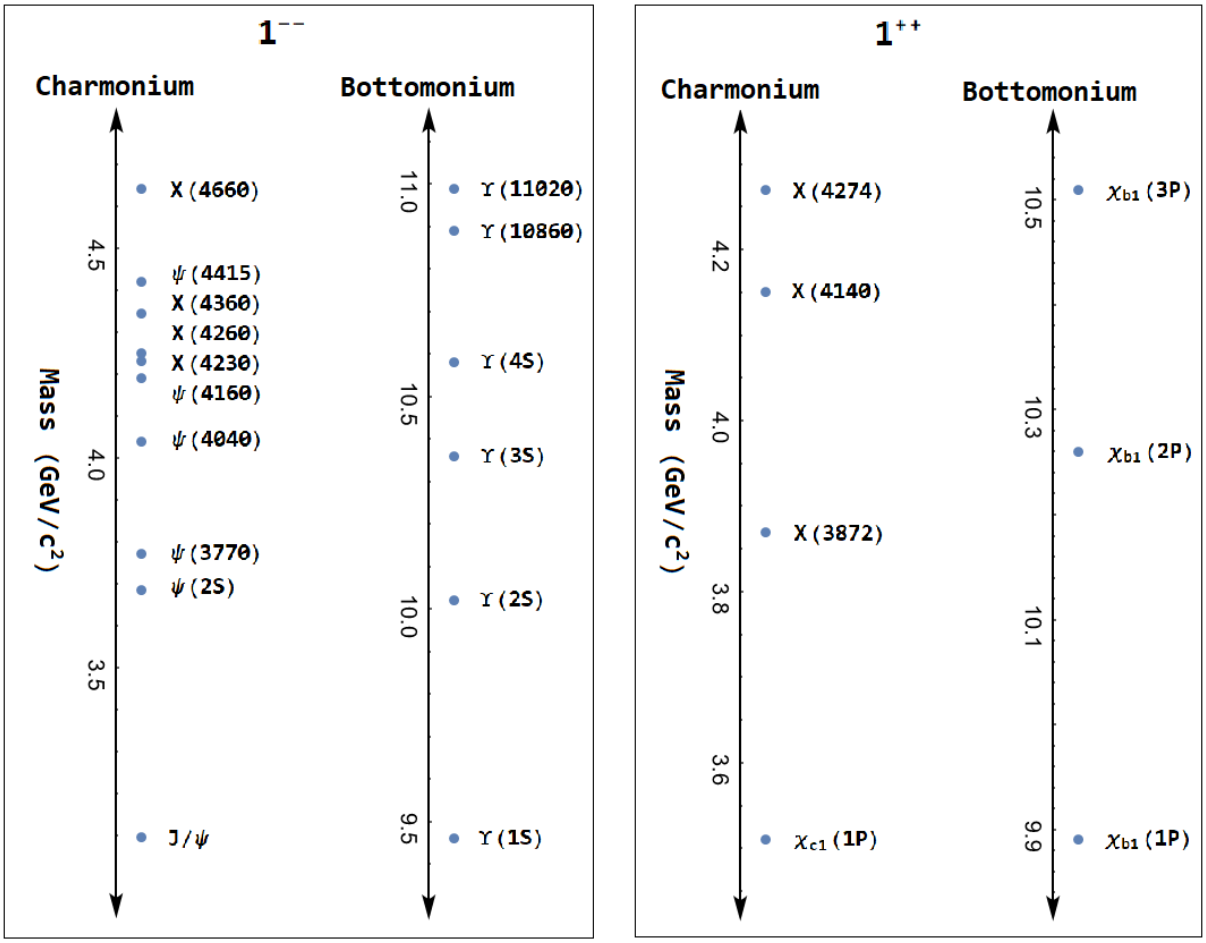

Figure 2.9: $J^{PC} = 1^{--}$ and $J^{PC} = 1^{++}$ charmonium and bottomonium mass spectra.

agreement between QCD and experiment (Model 3 from Table 2.3 and Table 2.5, Model 3 from Table 2.4 and Table 2.6, Model C4 from Table 2.11 and Model B3 from Table 2.12), we can draw several conclusions. First we collect all of these models and present them in Figure 2.10.

m_1	m_2	m_3	m_4	ζ (GeV^6)	$\frac{\xi_1}{\zeta}$	$\frac{\xi_2}{\zeta}$	$\frac{\xi_3}{\zeta}$	$\frac{\xi_4}{\zeta}$
3.10	3.73	4.30	-	2.88 ± 0.25	0.215 ± 0.012	-0.022 ± 0.049	0.762 ± 0.030	-
9.46	10.02	10.47	-	1377 ± 33	0.203 ± 0.002	-0.380 ± 0.003	0.418 ± 0.005	-
3.51	3.87	4.15	4.27	44 ± 6	0.03 ± 0.01	-0.16 ± 0.01	0.46 ± 0.01	-0.35 ± 0.01
9.89	10.26	10.51	-	1905 ± 28	0.16 ± 0.01	-0.48 ± 0.01	0.36 ± 0.01	-

Figure 2.10: From the top row to the bottom row, these entries correspond to the following models respectively: Model 3 from Table 2.3 and Table 2.5 (1^{--} charmonium results), Model 3 from Table 2.4 and Table 2.6 (1^{--} bottomonium results), Model C4 from Table 2.11 (1^{++} charmonium results) and Model B3 from Table 2.12 (1^{++} bottomonium results). All of these models represent the best fit between QCD and experiment in their respective sectors. Note that the masses are given in GeV.

- In the 1^{--} charmonium sector (corresponding to the top row in Figure 2.10), we see non-zero mixing in the J/ψ, no evidence for mixing in the $\psi(2S), \psi(3770)$ cluster, and a large mixing parameter in the 4.3 GeV cluster. Note that, as mentioned in [1], the $X(4260)$, which would be a member of the cluster at 4.3 GeV, has often been interpreted as having significant hybrid content and our results are consistent with this idea.

- In the 1^{--} bottomonium sector (corresponding to the second row in Figure 2.10), we see non-zero mixing in all three resonances, the $\Upsilon(1S)$, the $\Upsilon(2S)$ and the two-state cluster containing the $\Upsilon(3S)$ and $\Upsilon(4S)$.

- In the 1^{++} charmonium sector (corresponding to the third row in Figure 2.10), we see almost no mixing in the $\chi_{c1}(1P)$, minimal mixing in the $X(3872)$ and significant mixing in both the $X(4140)$ and the $X(4274)$. Note that (as mentioned in [2]) the $X(3872)$ has been interpreted as having significant tetraquark content and our result is consistent with that idea.

- In the 1^{++} bottomonium sector (corresponding to the bottom row in Figure 2.10), we see minimal mixing in the $\chi_{b1}(1P)$ and significant mixing in both the $\chi_{b1}(2P)$ and the $\chi_{b1}(2P)$.

Chapter 3

Diquarks and Tetraquarks

3.1 Tetraquarks from Diquarks

Again, as discussed in Section 1.4.1, QCD and colour confinement allow for looser restrictions on the makeup of hadrons than the quark model does. Considering only the restriction that hadrons must be colourless, we saw in Section 1.4.1 that we could construct bound states consisting of two quarks and two antiquarks, so-called tetraquarks. In the paper presented in Section 3.2, we explored one potential interpretation of what the underlying substructure of these tetraquarks may resemble and what implications that would have for particular tetraquark masses. The introduction in Subsection 3.2.1 mentions three potential configurations for what the substructure of these tetraquarks might look like. Here, we include a schematic diagram in Figure 3.1 to illustrate these ideas.

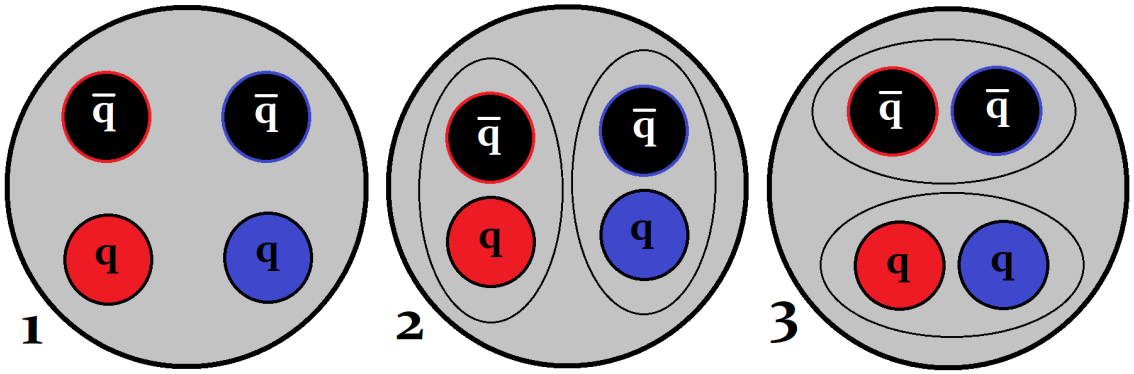

Figure 3.1: Potential configurations of tetraquark substructure: (1) No additional substructure. (2) Meson-meson molecular state. (3) Quarks and antiquarks pair off to form a diquark and an antidiquark.

In the first model, the two quarks and two antiquarks have no additional substructure. The four objects exist with no additional strong correlations between them ($qq\bar{q}\bar{q}$). In the second

model, the quarks and antiquarks pair off to form meson-like substructures. This leads to a tetraquark that resembles a meson-meson molecule ($[q\bar{q}][q\bar{q}]$). Finally, in the third model, the antiquarks and quarks pair off to form an antidiquark and a diquark ($[\bar{q}\bar{q}][qq]$).

In the following manuscript, we briefly point to some of the literature involving models (1) and (2) from Figure 3.1, but all of our work focuses on model (3), the diquark-antidiquark model of tetraquarks. We begin by using QCD and the OPE to calculate the constituent masses of these diquarks/antidiquarks. Once the constituent masses are calculated, they are used as inputs into a chromomagnetic interaction (CMI) model of diquark-antidiquark tetraquarks [77]. We discuss this model in subsection 3.2.4, and additional information is available in the papers cited in that section including [77]. The CMI model is then used to predict the masses of the tetraquarks we are examining. Note that the diquarks and antidiquarks are not colourless, they must carry net colour charge, and so they must be thought of as the building blocks of hadrons and not hadrons themselves. Constituent masses that we generate in this paper must therefore be used as inputs in some intermediate step on the way to producing a physically measurable quantity (a tetraquark mass in this case).

The following work may be found published in:

Axial Vector *cc* and *bb* Diquark Masses from QCD Laplace Sum-Rules,
S. Esau, A. Palameta, R.T. Kleiv, D. Harnett, and T.G. Steele
Phys. Rev. D **100**, 074025 (2019)
DOI:10.1103/PhysRevD.100.074025

My involvement in this paper again had me playing a leading role in the work presented in this manuscript. I calculated the correlator, generated the Laplace sum-rule and performed the analysis to extract the diquark constituent masses. I again wrote the first draft of the manuscript here and made significant contributions to subsequent edits.

3.2 Manuscript: Axial Vector cc and bb Diquark Masses from QCD Laplace Sum-Rules

Abstract: Constituent mass predictions for axial vector (*i.e.* $J^P = 1^+$) cc and bb colour-antitriplet diquarks are generated using QCD Laplace sum rules. We calculate the diquark correlator within the operator product expansion to next-to-leading-order, including terms proportional to the four- and six-dimensional gluon and six-dimensional quark condensates. The sum-rules analyses stabilize, and we find that the constituent mass of the cc diquark is (3.51 ± 0.35) GeV and the constituent mass of the bb diquark is (8.67 ± 0.69) GeV. Using these diquark constituent masses as inputs, we calculate several tetraquark masses within the Type-II diquark-antidiquark tetraquark model.

3.2.1 Introduction

Outside-the-quark-model hadrons consisting of four (or more) valence quarks have been theorized for decades. For example, the concept of tetraquarks, hadrons composed of four quarks ($qq\overline{q}\overline{q}$), was introduced in [78, 79] in 1977. Jump forward to 2003 and the discovery of the X(3872) by the Belle collaboration [65] and its subsequent confirmation by several other experimental collaborations [80, 81, 82, 83] places us in a new era of hadron spectroscopy. Since then more and more of these hadrons have been discovered in the heavy quarkonium spectra. These hadrons, now collectively referred to as the XYZ resonances, are difficult to explain within the quark model [75]. These XYZ resonances have served as a strong motivator for research into beyond-the-quark-model hadrons. See [84, 85] for a review of experimental findings and [86, 87] for a review of several multiquark systems.

Looking at four-quark states in particular, there are several interpretations of what their internal quark structure might resemble. One possibility is that there are no particularly strong correlations between any of the quarks. However, another possible interpretation is

that these states could be meson-meson molecule states in which two colour-singlet mesons form a weakly bound conglomerate state. See [88, 89, 90, 91, 92, 93, 94, 95] for discussions about the X(3872) in this configuration. Yet another possible interpretation is that four-quark states are diquark-antidiquark states. Diquarks are strongly correlated, colour antitriplet pairs of quarks within a hadron. (As such, their colour configurations are identical to those of antiquarks.) See [96] for applications of diquarks and [97] for a discussion of possible diquark configurations. In a diquark-antidiquark configuration, the diquark constituents are strongly bound together in a four-quark configuration. See [98, 99, 100, 101, 102] for discussions about the X(3872) in the diquark-antidiquark configuration. Also, see [103] for additional discussions on the differences between the molecular and tetraquark models in the context of a QCD sum-rules analysis.

QCD sum-rules analyses of diquarks in several channels have been presented in [104, 105, 106, 107, 108, 109]. Lattice QCD analyses of light diquarks have also been performed [110, 111, 112]. In this paper, we use QCD Laplace sum-rules (LSRs) to calculate the constituent masses of axial vector (*i.e.* $J^P = 1^+$) cc and bb diquarks. The axial vector is the only quantum number that can be realized for colour antitriplet diquarks of identical flavours in an S-wave configuration. We use the operator product expansion (OPE) [15] to compute the correlation function between a pair of diquark currents (3.1)–(3.2). In this calculation, in addition to leading-order (LO) pertubative contributions, we also include next-to-leading-order (NLO) perturbative contributions and non-perturbative corrections proportional to the four-dimensional (4d) and 6d gluon condensates as well as the 6d quark condensate. The results of these calculations are summarized in Table 3.1. In particular, we find that the constituent mass of the cc diquark is (3.51 ± 0.35) GeV and the constituent mass of the bb diquark is (8.67 ± 0.69) GeV. Substituting these diquark constituent masses into the Type-II diquark-antidiquark tetraquark model of Ref. [77], we calculate masses of several $[cc][\overline{c}\overline{c}]$, $[cc][\overline{b}\overline{b}]$, and $[bb][\overline{b}\overline{b}]$ tetraquarks.

3.2.2 The Correlator

The axial vector, colour antitriplet diquark current is given by [105, 106]

$$j_{\mu,\alpha} = \epsilon_{\alpha\beta\gamma} Q_\beta^T C\gamma_\mu Q_\gamma \tag{3.1}$$

with adjoint

$$j_{\mu,\alpha}^\dagger = -\epsilon_{\alpha\beta\gamma} \overline{Q}_\beta \gamma_\mu C \overline{Q}_\gamma^T \tag{3.2}$$

where C denotes the charge conjugation operator, $\epsilon_{\alpha\beta\gamma}$ is a Levi-Civita symbol in quark colour space, and Q is a heavy (charm or bottom) quark field.

Using (3.2), we consider the diquark correlator

$$\Pi(q^2) = \frac{i}{D-1}\left(\frac{q_\mu q_\nu}{q^2} - g_{\mu\nu}\right)\int d^D x\, e^{iq\cdot x}\, \langle 0|\tau[\, j_{\mu,\alpha}(x)\; S_{\alpha\omega}(x,0)\; j_{\nu,\omega}^\dagger(0)]|0\rangle \tag{3.3}$$

where D is the spacetime dimension. In (3.3), $S_{\alpha\omega}(x,0)$ is a path-ordered exponential, or Schwinger string, given by

$$S_{\alpha\omega}(x,0) = \hat{\mathcal{P}} \exp\left[ig_s \frac{\lambda^a_{\alpha\omega}}{2}\int_0^x dz^\mu A^a_\mu(z)\right] \tag{3.4}$$

where $\hat{\mathcal{P}}$ is the path-ordering operator. The Schwinger string allows gauge-invariant information to be extracted from the gauge-dependent current (3.1) [105, 106]. The explicit cancellation of the gauge parameter has been shown for perturbative contributions up to NLO [113], and in Landau gauge the NLO contributions from the Schwinger string are zero [105, 106]; hence $S_{\alpha\omega}(x,0) \to \delta^{\alpha\omega}$. For non-perturbative contributions of QCD condensates, gauge-invariance of the correlator (3.3) implies that fixed-point gauge methods used to obtain OPE coefficients are equivalent to other methods [114]. As observed in Refs. [105, 106], the Schwinger string will not contribute to the QCD condensate contributions in the fixed-point gauge, and hence $S_{\alpha\omega}(x,0) \to \delta^{\alpha\omega}$. Thus, using Landau gauge for pertubative contributions and fixed-point gauge methods for QCD condensate contributions, we can simplify (3.3) by setting $S_{\alpha\omega}(x,0) \to \delta^{\alpha\omega}$ (as in [103]). Lattice QCD analyses of constituent light diquark masses are also based on correlation functions of (coloured) diquark operators [110, 111, 112].

Instead of the Schwinger string, gauge dependence of the correlation function is addressed in lattice analyses either through gauge fixing or coupling to a heavy colour source.

We evaluate the correlator (3.3) within the OPE to NLO in perturbation theory and include non-perturbative corrections proportional to the 4d and 6d gluon condensates and the 6d quark condensate. Each non-perturbative correction is the product of a LO perturbatively computed Wilson coefficient and a QCD condensate. The 4d and 6d gluon and 6d quark condensates are defined respectively by

$$\left\langle \alpha G^2 \right\rangle = \alpha_s \left\langle : G^a_{\omega\phi} G^a_{\omega\phi} : \right\rangle \tag{3.5}$$

$$\left\langle g^3 G^3 \right\rangle = g_s^3 f^{abc} \left\langle : G^a_{\omega\zeta}\, G^b_{\zeta\rho} G^c_{\rho\omega} : \right\rangle \tag{3.6}$$

$$\left\langle J^2 \right\rangle = \frac{D}{6}\, \kappa\, g_s^4 \left\langle \overline{q} q \right\rangle^2 \tag{3.7}$$

where κ in (3.7) quantifies deviation from vacuum saturation. As in [64, 115], we set $\kappa = 2$ for the remainder of this calculation, *e.g.* see [44] and references contained therein.

The diagrams computed in the simplification of (3.3) are given in Figure 3.2. Each diagram has a (base) multiplicity of two associated with interchanging the quark fields contracted on the top and bottom quark lines. Diagrams II, IV, VI, VIII, X, and XI receive an additional factor of two to account for vertical reflections. As noted earlier, Wilson coefficients are calculated in the Landau gauge. Divergent integrals are handled using dimensional regularization in $D = 4 + 2\epsilon$ dimensions at $\overline{\text{MS}}$ renormalization scale μ. We use a dimensionally regularized γ^5 satisfying $(\gamma^5)^2 = 1$ and $\{\gamma^\mu, \gamma^5\} = 0$ [116]. The recurrence relations of Refs. [17, 18] are implemented via the Mathematica package TARCER [53] resulting in expressions phrased in terms of master integrals with known solutions including those of [20, 21].

The OPE computation of Π, denoted Π^{OPE}, can be written as

$$\Pi^{\text{OPE}}(q^2) = \sum_{\text{i=I}}^{\text{XI}} \Pi^{(\text{i})}(q^2) \tag{3.8}$$

where the superscript in (3.8) corresponds to the labels of the diagrams in Figure 3.2. Eval-

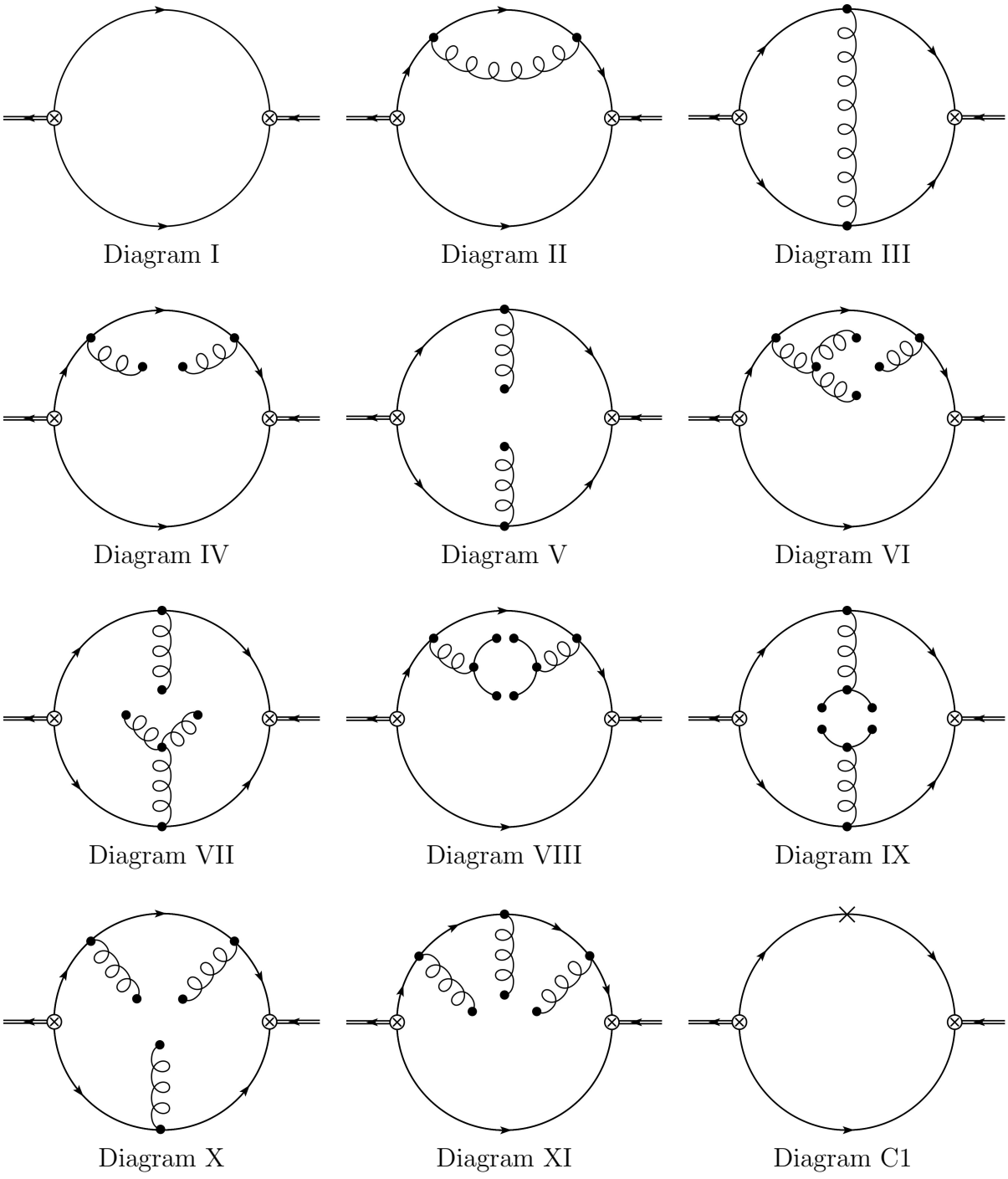

Figure 3.2: Feynman diagrams that contribute to the correlator (3.3) to NLO and up to dimension-six in the QCD condensates. Diagram C1 is the counterterm diagram used to eliminate the non-local divergence in Diagram II. Feynman diagrams were created using JaxoDraw [7].

uating the first term in this sum, $\Pi^{(\mathrm{I})}$, expanding the result in ϵ, and dropping a polynomial in q^2 (which does not contribute to the sum rules—see Section 3.2.3), we find

$$\Pi^{(\mathrm{I})}(z) = \frac{4m^2}{3\pi^2} z(2z+1)\mathrm{H}_1(z) \tag{3.9}$$

where m is a heavy quark mass and

$$z = \frac{q^2}{4m^2}. \tag{3.10}$$

Also,

$$\mathrm{H}_1(z) = {}_2F_1\left(1, 1; \frac{5}{2}; z\right), \tag{3.11}$$

where functions of the form ${}_pF_q\left(\cdots;\cdots;z\right)$ are generalized hypergeometric functions, *e.g.,* [54]. Note that hypergeometric functions of the form ${}_pF_{p-1}(\cdots;\cdots;z)$ have a branch point at $z = 1$ and a branch cut extending along the positive real semi-axis. In evaluating $\Pi^{(\mathrm{II})}(z)$, we find a nonlocal divergence which is eliminated through the inclusion of the counterterm diagram, Diagram C1, of Figure 3.2. From this point forward, we refer to the renormalized contribution arising from the sum of Diagrams II and C1 as $\Pi^{(\mathrm{II})}(z)$. Note that, in Landau gauge, Diagram III does not have a nonlocal divergence corresponding to the fact that the (multiplicative) vector diquark renormalization constant is trivial [113]. The Mathematica package HypExp [117] is used to generate the ϵ-expansions of $\Pi^{(\mathrm{II})}(z)$ and $\Pi^{(\mathrm{III})}(z)$. These expansions are lengthy, and so we omit them for the sake of brevity; instead, we present the exact (ϵ-dependent) results,

$$\begin{aligned}
\Pi^{(\mathrm{II})}(z;\epsilon) = \frac{-\alpha_s m^2 \Gamma(-\epsilon)\left(\frac{m^2}{\mu^2}\right)^{\epsilon}}{4\pi^3(4\pi)^{2\epsilon}(z-1)z\epsilon(2\epsilon+1)}\Big[&-12z(4\pi)^{\epsilon}(2\epsilon+1)+ \\
&m^{2\epsilon}\left(4z^2\epsilon(\epsilon+1)+z\left(8\epsilon^3+18\epsilon^2+13\epsilon+2\right)+1\right)\Gamma(-\epsilon-1)+ \\
&4z\left(3(4\pi)^{\epsilon}(2\epsilon+1)(2z\epsilon+1)-m^{2\epsilon}(2z(\epsilon+1)(2z+2\epsilon-1)+2\epsilon+1)\Gamma(1-\epsilon)\right)\mathrm{H}_2(z;\epsilon)- \\
&m^{2\epsilon}\left(-4z^2(\epsilon+1)(3\epsilon+2)+z\epsilon(6\epsilon+5)+2(\epsilon+1)\right)\Gamma(-\epsilon-1)\mathrm{H}_3(z;\epsilon)+ \\
&m^{2\epsilon}\left(8z^3\epsilon(\epsilon+1)-8z^2(\epsilon+1)(3\epsilon+1)+2z(\epsilon-1)(2\epsilon+1)+2\epsilon+1\right)\Gamma(-\epsilon-1)\mathrm{H}_4(z;\epsilon)\Big]
\end{aligned} \tag{3.12}$$

$$\Pi^{(\mathrm{III})}(z;\epsilon)=\frac{\alpha_s(\epsilon+1)m^{2\epsilon+2}\Gamma(-\epsilon-1)^2\left(\frac{m^2}{\mu^2}\right)^{\epsilon}}{(2\pi)^3(4\pi)^{2\epsilon}(z-1)z\epsilon(4\epsilon(\epsilon+2)+3)^2}\Bigg[$$
$$(4\epsilon(\epsilon+2)+3)(-z(-8z(\epsilon+1)+\epsilon(4\epsilon(\epsilon+2)+7)+2)-2\epsilon-3)-$$
$$8z(\epsilon+1)(2\epsilon+1)(2\epsilon+3)\left(4z^2(\epsilon+1)+z\epsilon(2\epsilon+3)+2\epsilon^2+\epsilon-1\right)\mathrm{H}_2(z;\epsilon)-$$
$$4z(\epsilon+1)(2\epsilon+1)(4\epsilon(\epsilon+2)+3)\left(1-2z(\epsilon+1)\left(2(z-1)\epsilon^2+z\epsilon+2z+\epsilon\right)\right)\mathrm{H}_2(z;\epsilon)^2+$$
$$(2\epsilon+3)(4\epsilon(\epsilon+2)+3)\left(-8z^2(\epsilon+1)^2+z\epsilon(2\epsilon+1)+2(\epsilon+1)\right)\mathrm{H}_3(z;\epsilon)-$$
$$(4\epsilon(\epsilon+2)+3)\Big(-16z^3(\epsilon+1)-8z^2(\epsilon+1)(\epsilon(2\epsilon+7)+2)-$$
$$2z(\epsilon(4\epsilon(\epsilon+2)+5)-1)+4\epsilon(\epsilon+2)+3\Big)\mathrm{H}_4(z;\epsilon)\Bigg], \tag{3.13}$$

where

$$\mathrm{H}_2(z;\epsilon)=\,{}_2F_1\left(1,-\epsilon;\frac{3}{2};z\right) \tag{3.14}$$
$$\mathrm{H}_3(z;\epsilon)=\,{}_3F_2\left(1,-2\epsilon-1,-\epsilon;\frac{1}{2}-\epsilon,\epsilon+2;z\right) \tag{3.15}$$
$$\mathrm{H}_4(z;\epsilon)=\,{}_3F_2\left(1,-2\epsilon,-\epsilon;\frac{1}{2}-\epsilon,\epsilon+2;z\right). \tag{3.16}$$

The ϵ-expanded results for the remaining terms in (3.8) can be written more concisely and are given by

$$\Pi^{(\mathrm{IV})}(z)=\frac{-3\left(8z^2-17z+6\right)+\left(2z^2-11z+6\right)\mathrm{H}_1(z)}{288\pi m^2(z-1)^3}\left\langle\alpha G^2\right\rangle \tag{3.17}$$
$$\Pi^{(\mathrm{V})}(z)=\frac{12z-15-(2z-3)\mathrm{H}_1(z)}{576\pi m^2(z-1)^2}\left\langle\alpha G^2\right\rangle \tag{3.18}$$
$$\Pi^{(\mathrm{VI})}(z)=\frac{\left\langle g^3G^3\right\rangle}{92160\pi^2m^4(z-1)^5z}\Big(416z^5-1888z^4+3078z^3-1836z^2+90z+35+$$
$$5\left(8z^5-36z^4+42z^3-20z^2+20z-7\right)\mathrm{H}_1(z)\Big) \tag{3.19}$$
$$\Pi^{(\mathrm{VII})}(z)=\frac{32z^3-89z^2+19z+8-\left(12z^4-66z^3+73z^2-37z+8\right)\mathrm{H}_1(z)}{55296\pi^2m^4(z-1)^4z}\left\langle g^3G^3\right\rangle \tag{3.20}$$
$$\Pi^{(\mathrm{VIII})}(z)=\frac{\alpha_s^2\left\langle\overline{q}q\right\rangle^2}{4860m^4(z-1)^5z}\Big(3\left(576z^5-2608z^4+4458z^3-3316z^2+765z+20\right)-$$
$$5\left(8z^5-36z^4+66z^3-74z^2+3z+12\right)\mathrm{H}_1(z)\Big) \tag{3.21}$$

$$\Pi^{(\mathrm{IX})}(z) = \frac{160z^3 - 478z^2 + 386z + 7 - (56z^4 - 196z^3 + 226z^2 - 68z + 7)\,\mathrm{H}_1(z)}{1944m^4(z-1)^4z}\alpha_s^2\langle\overline{q}q\rangle^2 \tag{3.22}$$

$$\Pi^{(\mathrm{X})}(z) = \frac{-8z^3 + 19z^2 + 7z - 3 + (4z^4 - 22z^3 + 23z^2 - 13z + 3)\,\mathrm{H}_1(z)}{55296\pi^2m^4(z-1)^4z}\langle g^3G^3\rangle \tag{3.23}$$

$$\Pi^{(\mathrm{XI})}(z) = \frac{-3\,(16z^4 - 56z^3 + 57z^2 - z - 1) - (4z^4 - 14z^3 - 5z^2 - 3z + 3)\,\mathrm{H}_1(z)}{27648\pi^2m^4(z-1)^4z}\langle g^3G^3\rangle. \tag{3.24}$$

Finally, substituting (3.9), (3.12), (3.13) and (3.17)–(3.24) into (3.8) gives us Π^{OPE}.

Renormalization-group improvement requires that the strong coupling and quark mass be replaced by their corresponding running quantities evaluated at renormalization scale μ [55]. At one-loop in the $\overline{\mathrm{MS}}$ renormalization scheme, for cc diquarks, we have

$$\alpha_s \to \alpha_s(\mu) = \frac{\alpha_s(M_\tau)}{1 + \frac{25\alpha_s(M_\tau)}{12\pi}\log\left(\frac{\mu^2}{M_\tau^2}\right)} \tag{3.25}$$

$$m \to m_c(\mu) = \overline{m}_c\left(\frac{\alpha_s(\mu)}{\alpha_s(\overline{m}_c)}\right)^{12/25} \tag{3.26}$$

and for bb diquarks,

$$\alpha_s \to \alpha_s(\mu) = \frac{\alpha_s(M_Z)}{1 + \frac{23\alpha_s(M_Z)}{12\pi}\log\left(\frac{\mu^2}{M_Z^2}\right)} \tag{3.27}$$

$$m \to m_b(\mu) = \overline{m}_b\left(\frac{\alpha_s(\mu)}{\alpha_s(\overline{m}_b)}\right)^{12/23}, \tag{3.28}$$

where [4]

$$\alpha_s(M_\tau) = 0.330 \pm 0.014 \tag{3.29}$$

$$\alpha_s(M_Z) = 0.1185 \pm 0.0006 \tag{3.30}$$

$$\overline{m}_c = (1.275 \pm 0.025)\ \mathrm{GeV} \tag{3.31}$$

$$\overline{m}_b = (4.18 \pm 0.03)\ \mathrm{GeV}. \tag{3.32}$$

For cc diquarks, $\mu \to \overline{m}_c$ and for bb diquarks, $\mu \to \overline{m}_b$. Finally, the following values are used

for the gluon and quark condensates [56, 57, 58]:

$$\left\langle \alpha G^2 \right\rangle = (0.075 \pm 0.02)\ \text{GeV}^4 \tag{3.33}$$

$$\left\langle g^3 G^3 \right\rangle = ((8.2 \pm 1.0)\ \text{GeV}^2)\left\langle \alpha G^2 \right\rangle \tag{3.34}$$

$$\left\langle \overline{q} q \right\rangle = -(0.23 \pm 0.03)^3\ \text{GeV}^3. \tag{3.35}$$

3.2.3 QCD Laplace Sum-Rules, Analysis, and Results

We now proceed with the QCD LSRs analysis of axial vector cc and bb diquarks. Laplace sum-rules analysis techniques were originally introduced in [25, 42]. Subsequently, the LSRs methodology was reviewed in [43, 118].

The function $\Pi(q^2)$ of (3.3) satisfies a dispersion relation

$$\Pi(q^2) = q^4 \int_{t_0}^{\infty} \frac{\frac{1}{\pi}\text{Im}\Pi(t)}{t^2(t-q^2)}\,\text{d}t + \cdots \tag{3.36}$$

for $q^2 < 0$. In (3.36), t_0 is an effective threshold and $\cdots$ represents a polynomial in q^2. On the left-hand side of (3.36), Π is identified with Π^{OPE} computed in Section 3.2.2. On the right-hand side of (3.36), we express $\text{Im}\Pi(t)$, *i.e.* the spectral function, using a single narrow resonance plus continuum model,

$$\frac{1}{\pi}\text{Im}\Pi(t) = 2h_+^2\,\delta(t-M^2) + \frac{1}{\pi}\text{Im}\Pi^{\text{OPE}}(t)\theta(t-s_0), \tag{3.37}$$

where M is the diquark constituent mass and h_+ is the diquark coupling defined by

$$\langle \Omega | j_{\mu,\alpha} | (cc)_\beta, 1^+ \rangle = \sqrt{\frac{2}{3}}\,\delta_{\alpha\beta}\epsilon_\mu h_+, \tag{3.38}$$

which aligns with the notation of Ref. [106]. Also, $\theta(t)$ is a Heaviside step function and s_0 is the continuum threshold parameter. Constituent diquark masses are key input parameters of Type I & II diquark-antidiquark models of tetraquarks [98, 77] (see Section 3.2.4). However, as the couplings are not parameters of Type I & II tetraquark models, we eliminate them by working with ratios of LSRs (*e.g.* see (3.45)). Though not relevant for our purposes here, we

note that knowledge of the coupling h_+ for light diquarks allows estimation of baryon matrix elements of the effective weak Hamiltonian [105, 106].

As discussed in Ref. [105], the duality relation (3.37) for diquarks is more subtle than for hadrons because diquarks are constituent degrees of freedom rather than hadron states. Ref. [105] argues that, similar to constituent quarks, the diquark mass and coupling should be regarded as effective quantities which describe the correlator at intermediate scales. Above the threshold s_0, the diquark loses its meaning as a constituent degree of freedom, and the correlator is dominated by the parton-level quark description (see Diagram I in Fig. 3.2). In the context of lattice QCD, the coupling h_+ is proportional to the signal strength, and Ref. [110] finds a remarkably clean exponential decay indicative of a single narrow resonance below the lattice cutoff $1/a^2$. In (3.37), s_0 is analogous to the lattice cutoff $1/a^2$. Thus, in the light quark sector studied in [110], there exists direct lattice QCD evidence supporting the spectral decomposition (3.37).

Laplace sum-rules are obtained by Borel transforming (3.36) weighted by powers of Q^2 (see [25, 42] as well as, *e.g.,* [119, 44]). For a function such as Π^{OPE} computed in Section 3.2.2, details on how to evaluate the Borel transform can be found in [64, 115] for instance. We find

$$\mathcal{R}_k(\tau) \equiv \frac{1}{2\pi i}\int_\Gamma (q^2)^k e^{-q^2\tau}\Pi^{\mathrm{OPE}}(q^2)\,\mathrm{d}q^2 + \int_{s_0}^\infty t^k e^{-t\tau}\frac{1}{\pi}\mathrm{Im}\Pi^{\mathrm{OPE}}(t)\,\mathrm{d}t \tag{3.39}$$

$$\implies \mathcal{R}_k(\tau) = 2h_+^2 M^{2k} e^{-M^2\tau} + \int_{s_0}^\infty t^k e^{-t\tau}\frac{1}{\pi}\mathrm{Im}\Pi^{\mathrm{OPE}}(t)\,\mathrm{d}t \tag{3.40}$$

where $\mathcal{R}_k(\tau)$ are unsubtracted LSRs of (usually non-negative) integer order k evaluated at Borel scale τ and where Γ is the integration contour depicted in Figure 3.3. Subtracting the continuum contribution,

$$\int_{s_0}^\infty t^k e^{-t\tau}\frac{1}{\pi}\mathrm{Im}\Pi^{\mathrm{OPE}}(t)\,\mathrm{d}t, \tag{3.41}$$

from the right-hand sides of (3.39) and (3.40), we find

$$\mathcal{R}_k(\tau,\, s_0) \equiv \frac{1}{2\pi i}\int_\Gamma (q^2)^k e^{-q^2\tau}\Pi^{\mathrm{OPE}}(q^2)\,\mathrm{d}q^2 \tag{3.42}$$

$$\implies \mathcal{R}_k(\tau,\, s_0) = 2h_+^2 M^{2k} e^{-M^2\tau} \tag{3.43}$$

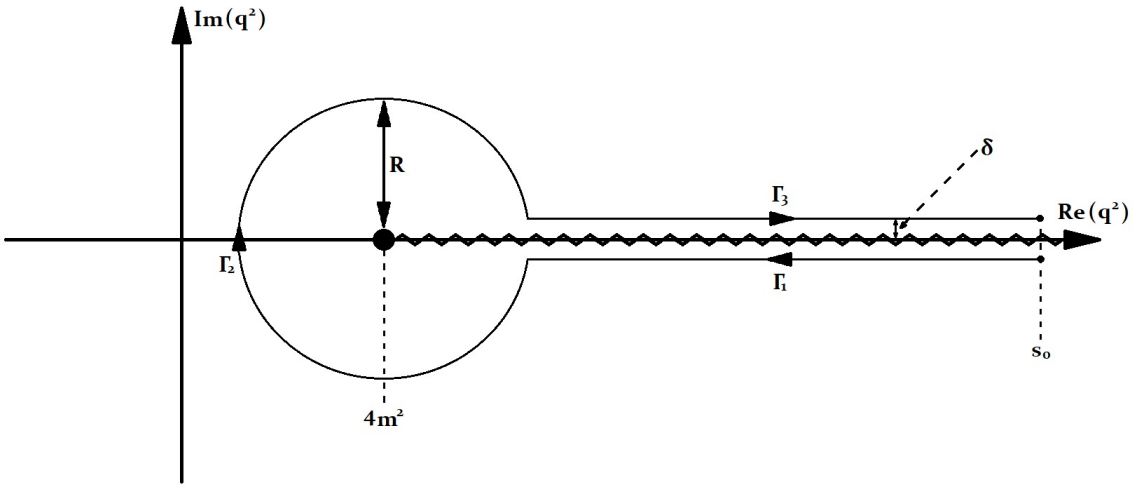

Figure 3.3: The contour of integration used in the evaluation of the LSRs (3.44). We use $\delta = 10^{-12}$ GeV^2 and R $= 2m^2$ generally in the calculation of (3.44) however other values and contour shapes were tested to verify that the code was producing contour invariant results as it must.

where $\mathcal{R}_k(\tau,\, s_0)$ are (continuum-)subtracted LSRs.

In (3.42), explicitly parametrizing each Γ_i of Γ, we have

$$\begin{aligned}\mathcal{R}_k(\tau, s_0) \equiv \frac{1}{2\pi i}\Bigg[&\int_{s_0}^{4m^2-\sqrt{\mathrm{R}^2-\delta^2}} (t-\delta i)^k e^{-(t-\delta i)\tau}\Pi^{\mathrm{OPE}}(t-\delta i)dt + \\ &\int_{2\pi-\sin^{-1}(\delta/\mathrm{R})}^{\sin^{-1}(\delta/\mathrm{R})} (4m^2+\mathrm{R}e^{\theta i})^k e^{-(4m^2+\mathrm{R}e^{\theta i})\tau}\mathrm{R}ie^{\theta i}\Pi^{\mathrm{OPE}}(4m^2+\mathrm{R}e^{\theta i})d\theta + \\ &\int_{4m^2-\sqrt{\mathrm{R}^2-\delta^2}}^{s_0} (t+\delta i)^k e^{-(t+\delta i)\tau}\Pi^{\mathrm{OPE}}(t+\delta i)dt\Bigg],\end{aligned} \tag{3.44}$$

which is then calculated numerically. In (3.44), R is set to $2m^2$. Also, it is intended that $\delta \to 0^+$. In practice, this can be achieved by setting $\delta = 10^{-12}$ GeV^2. Finally, using (3.43), we find

$$\sqrt{\frac{\mathcal{R}_1(\tau, s_0)}{\mathcal{R}_0(\tau, s_0)}} = M. \tag{3.45}$$

To use (3.45) to predict diquark constituent masses, we must first select an acceptable range of τ values, *i.e.,* a Borel window $(\tau_{\min},\, \tau_{\max})$. To determine the Borel window, we

follow the methodology outlined in [103]. To generate $\tau_{\max}$, we require OPE convergence of the $k = 0$ LSRs as $s_0 \to \infty$. By OPE convergence, we mean that the total perturbative contribution to the LSRs (pert), the total 4d contribution to the LSRs (4d), and the total 6d contribution to the LSRs (6d) must obey the inequality

$$|\text{pert}| \geq 3 \times |\text{4d}| \geq 9 \times |\text{6d}|. \tag{3.46}$$

The lowest value of τ for which (3.46) is violated as $s_0 \to \infty$ becomes $\tau_{\max}$. Additionally, $\tau_{\max}$ is constrained by the requirement

$$\frac{\mathcal{R}_2(\tau, s_0)/\mathcal{R}_1(\tau, s_0)}{\mathcal{R}_1(\tau, s_0)/\mathcal{R}_0(\tau, s_0)} \geq 1 \tag{3.47}$$

where this inequality results from requiring that individually both $\mathcal{R}_1(\tau, s_0)$ and $\mathcal{R}_0(\tau, s_0)$ satisfy the Hölder inequalities [120, 121] as per [103]. For the specific LSRs being studied here, it turns out that the condition (3.46) is more restrictive than the condition (3.47). For both diquark channels under consideration, the values of $\tau_{\max}$ obtained are given in the last column of Table 3.1. To select $\tau_{\min}$, in addition to the Hölder inequality constraint (3.47), we require that

$$\frac{\mathcal{R}_1(\tau, s_0)/\mathcal{R}_0(\tau, s_0)}{\mathcal{R}_1(\tau, \infty)/\mathcal{R}_0(\tau, \infty)} \geq 0.5 \tag{3.48}$$

i.e. that the resonance contribution to $\mathcal{R}_1/\mathcal{R}_0$ must be at least 50%. The highest value of τ which does not violate (3.47)–(3.48) becomes $\tau_{\min}$. For both diquark channels under consideration, the values of $\tau_{\min}$ obtained are given in the second-to-last column of Table 3.1.

The procedure described above for choosing a Borel window is s_0-dependent. However, s_0 is a parameter that is predicted using the optimization procedure described below. As such, choosing a Borel window and predicting s_0 are actually handled iteratively. Typically, the Borel window widens as s_0 increases. As such, we begin by selecting the minimum value of s_0 for which a Borel window exists. The corresponding Borel window is then used to predict a new, updated s_0. This new s_0 is then used to update the Borel window which, in turn, is used to update s_0 and so on until both the Borel window and s_0 settle. This iterative process has been taken into account in reporting diquark constituent masses, continuum thresholds,

and Borel windows in Table 3.1.

To predict s_0 and M, we optimize the agreement between left- and right-hand sides of (3.45) by minimizing

$$\chi^2(s_0,\, M) = \sum_{j=0}^{20} \left(\frac{1}{M} \sqrt{\frac{\mathcal{R}_1(\tau_j, s_0)}{\mathcal{R}_0(\tau_j, s_0)}} - 1 \right)^2 \tag{3.49}$$

where we have partitioned the Borel window into 20 equal length subintervals with $\{\tau_j\}_{j=0}^{20}$. For both diquark channels under consideration, the optimized values of s_0 obtained are given in the third column of Table 3.1. As a consistency check on our methodology, we require that the optimized mass M from (3.49) actually yields a good fit to (3.45) and that the left-hand side of (3.45) exhibits τ stability [103], that is

$$\frac{\mathrm{d}}{\mathrm{d}\tau} \sqrt{\frac{\mathcal{R}_1(\tau,\, s_0)}{\mathcal{R}_0(\tau,\, s_0)}} \approx 0 \tag{3.50}$$

within the Borel window. And so, in Figures 3.4 and 3.5, we plot the left-hand side of (3.45) at the appropriate optimized s_0 versus τ over the appropriate Borel window for both diquark channels under consideration. For the bb diquark, the optimized M from (3.49) does indeed yield a good fit to (3.45). Specifically, $M = 8.67$ GeV in agreement with Figure 3.5. Regarding condition (3.50), over the Borel window,

$$\frac{1}{M} \left| \Delta \left(\sqrt{\frac{\mathcal{R}_1(\tau,\, s_0)}{\mathcal{R}_0(\tau,\, s_0)}} \right) \right| \approx 0.001, \tag{3.51}$$

implying that the plot in Figure 3.5 can be considered flat to an excellent approximation. For the cc diquarks, it is clear from Figure 3.4 that the fitted value of M will be biased by the rapid increase at large τ values. We thus use the critical point $\frac{\mathrm{d}}{\mathrm{d}\tau}\sqrt{\mathcal{R}_1/\mathcal{R}_0} = 0$ for our cc diquark mass prediction, *i.e.* $M = 3.51$ GeV. For both diquark channels under consideration, predicted diquark constituent masses M are given in the second column of Table 3.1. The theoretical uncertainties associated with the mass predictions take into account the uncertainties arising from the strong coupling and mass parameters (3.29)–(3.32) as well as those associated with the QCD condensate values (3.33)–(3.35). The dominant theoretical

QQ	M_P (GeV)	s_0 (GeV^2)	$\tau_{\min}$ (GeV^{-2})	$\tau_{\max}$ (GeV^{-2})
cc	3.51 ± 0.35	17.5 ± 3.4	0.10 ± 0.02	0.71 ± 0.07
bb	8.67 ± 0.69	80.0 ± 9.2	0.02 ± 0.01	0.21 ± 0.02

Table 3.1: constituent mass predictions and sum rule parameters for axial vector cc and bb diquarks. The theoretical uncertainties are obtained by varying the QCD input parameters in Eqs. (3.29)–(3.35).

uncertainty is associated with the quark masses.

In the $s_0 \to \infty$ limit, the left-hand side of (3.45) corresponds to an upper bound on M for a wide variety of resonance shapes [122], allowing the sensitivity to the threshold s_0 and resonance model to be explored. As shown in Figs. 3.6–3.7, within the Borel window $\tau < \tau_{\max}$, we find $M \lesssim 3.6$ GeV for the cc case and $M \lesssim 8.8$ GeV for the bb case, remarkably close to the Table 3.1 predictions.

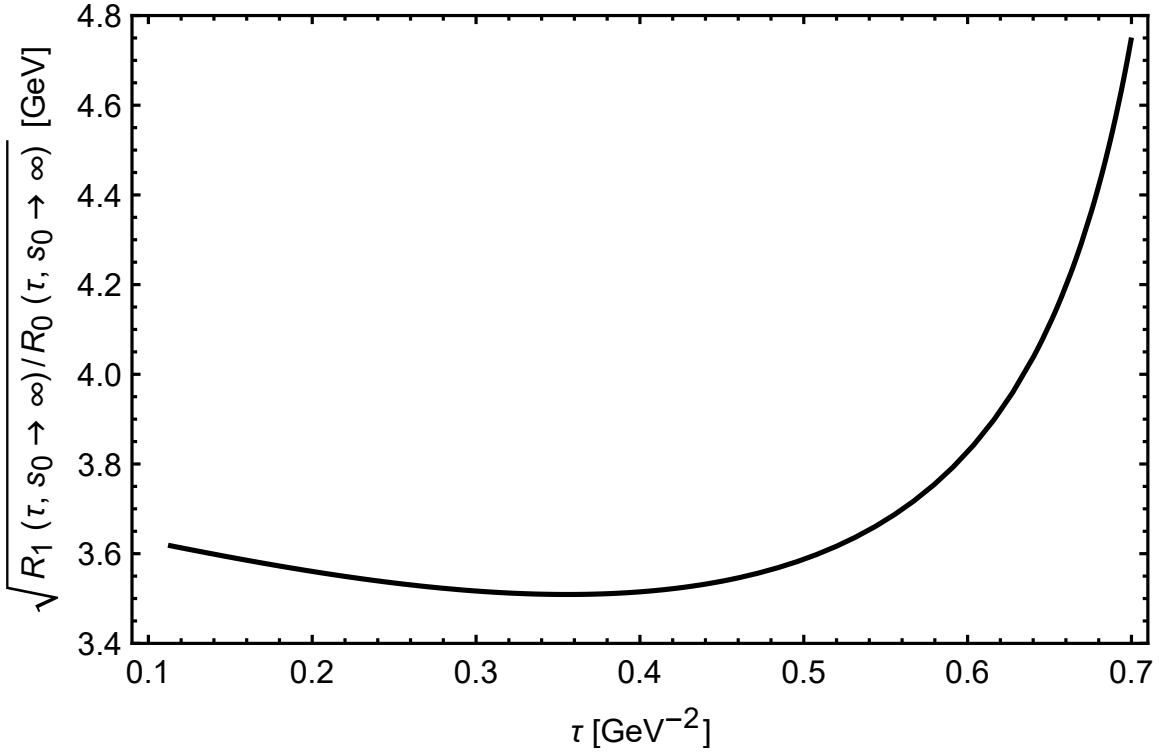

Figure 3.4: The left-hand side of (3.45) at the optimized continuum threshold parameter s_0 (see Table 3.1) versus the Borel scale τ for the cc diquark.

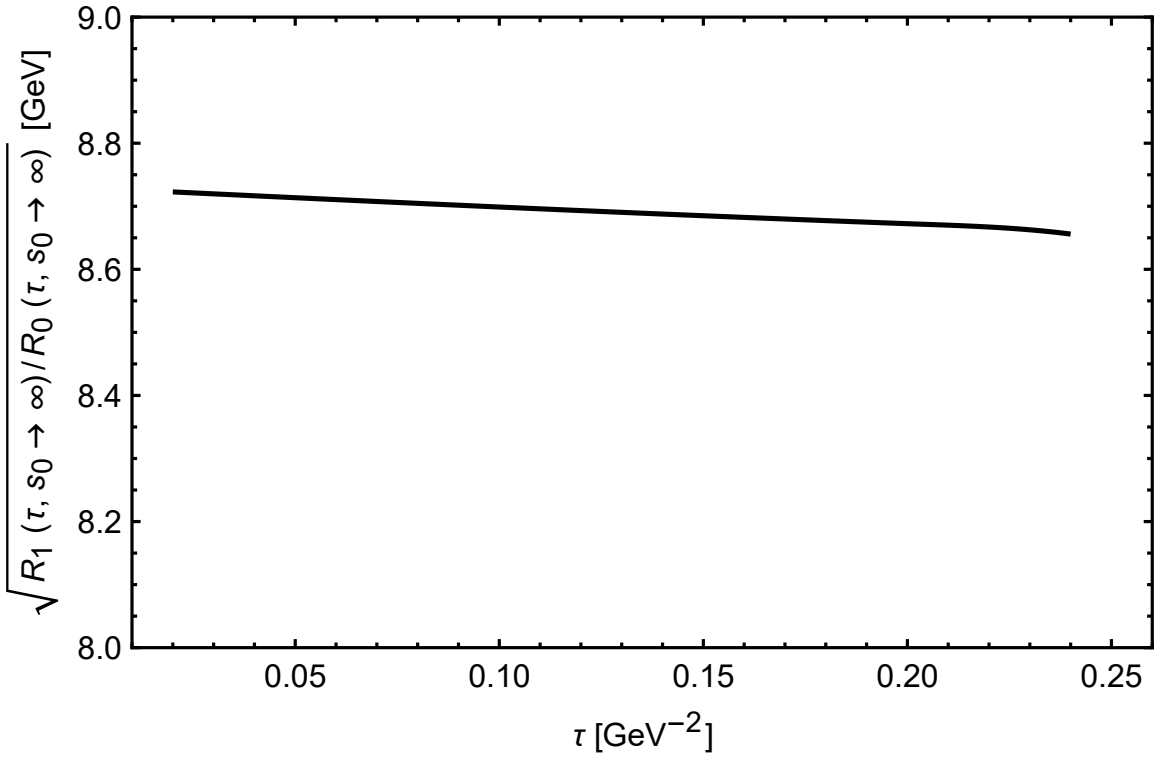

Figure 3.5: The left-hand side of (3.45) at the optimized continuum threshold parameter s_0 (see Table 3.1) versus the Borel scale τ for the bb diquark.

3.2.4 Discussion

Compared with potential model approaches [123, 124, 125] (and others cited therein) our cc central value diquark constituent mass prediction is slightly larger and bb is slightly smaller. For Bethe-Salpeter approaches [126], there is closer alignment in the cc constituent mass prediction, but the bb constituent mass prediction is still slightly smaller. However, taking into account theoretical uncertainties, we find good agreement between our QCD LSRs mass predictions and those of Refs. [123, 124, 125, 126], providing QCD evidence to support the study of diquark-antidiquark tetraquarks and doubly-heavy baryons with diquark cluster models.

Constituent diquark masses are key inputs into chromomagnetic interaction (CMI) models of diquark-antidiquark tetraquarks. For example, consider the Type-II model of Ref. [77] in which colour-spin interactions are ignored except between the quarks (antiquarks) within the diquark (antidiquark). This simplification assumes that the diquark and antidiquark

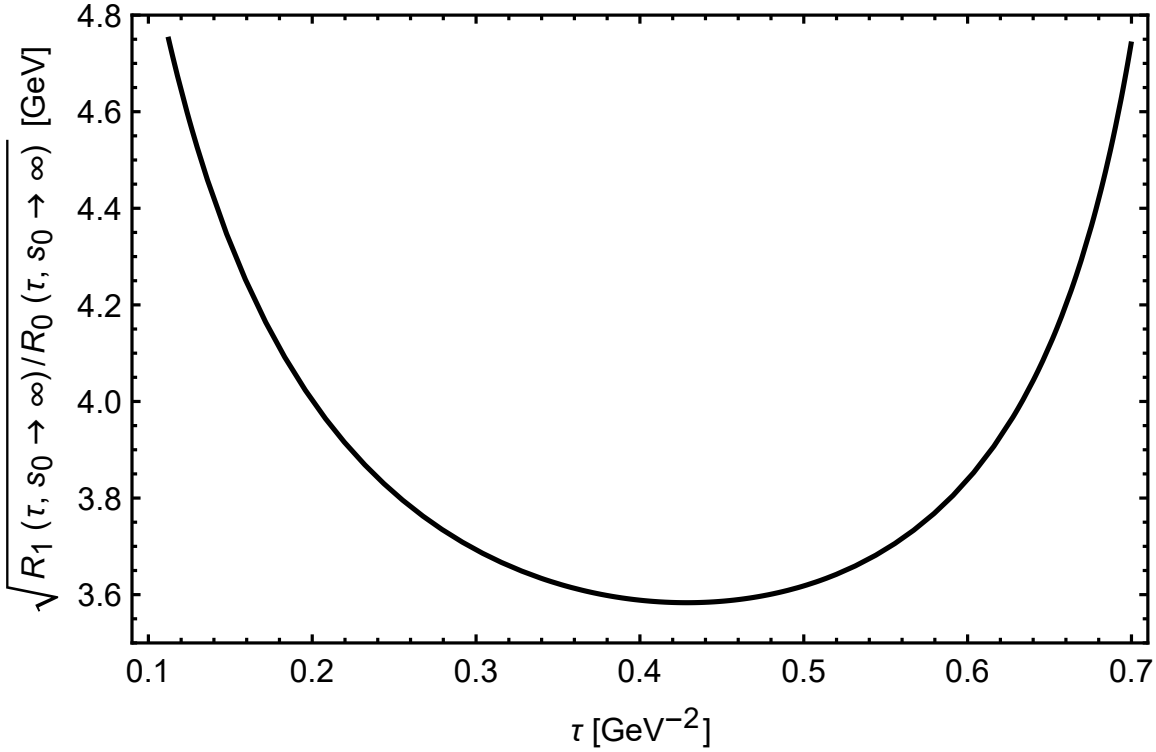

Figure 3.6: The left-hand side of (3.45) as the continuum threshold parameter $s_0 \to \infty$ versus the Borel scale τ for the cc diquark.

within the tetraquark are point-like and well-separated. Focusing on S-wave combinations of doubly-heavy, equal mass diquarks and antidiquarks, the Type-II CMI Hamiltonian reduces to [77]

$$H = m_{[Q_1Q_1]} + m_{[\bar{Q}_2\bar{Q}_2]} + 2\kappa_{Q_1Q_1}(\vec{S}_{Q_1} \cdot \vec{S}_{Q_1}) + 2\kappa_{\bar{Q}_2\bar{Q}_2}(\vec{S}_{\bar{Q}_2} \cdot \vec{S}_{\bar{Q}_2}) \tag{3.52}$$

where $m_{[Q_1Q_1]}$ and $m_{[\bar{Q}_2\bar{Q}_2]}$ are constituent diquark and antidiquark masses respectively and where $\kappa_{Q_1Q_1}$ and $\kappa_{\bar{Q}_2\bar{Q}_2}$ are colour-spin interaction coefficients. (Note that $\kappa_{\bar{Q}\bar{Q}}$ and κ_{QQ} are equal as are $m_{[QQ]}$ and $m_{[\bar{Q}\bar{Q}]}$.) As the (anti-)diquarks have $J = 1$, they must have $S = 1$ for $L = 0$ (where J, L, S are the usual angular momentum quantum numbers). Hence, the Hamiltonian (3.52) simplifies to

$$H = m_{[Q_1Q_1]} + m_{[\bar{Q}_2\bar{Q}_2]} + \frac{1}{2}\left(\kappa_{Q_1Q_1} + \kappa_{\bar{Q}_2\bar{Q}_2}\right). \tag{3.53}$$

Our predictions for $m_{[cc]}$ and $m_{[bb]}$ are in Table 3.1; however, the coefficients κ_{cc} and κ_{bb} are not known. In [77], the $X(3870)$, $Z(3900)$, and $Z(4020)$ resonances were interpreted as

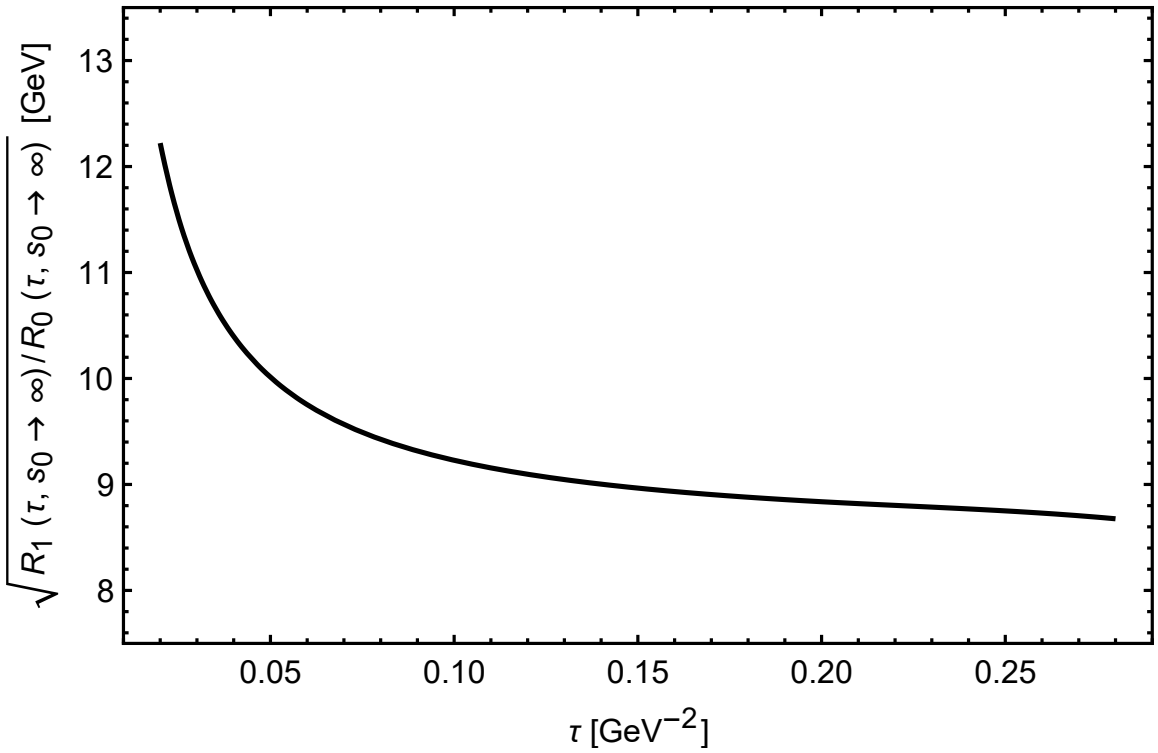

Figure 3.7: The left-hand side of (3.45) as the continuum threshold parameter $s_0 \to \infty$ versus the Borel scale τ for the bb diquark.

Type-II diquark-antidiquark tetraquarks and were used to predict $\kappa_{cq} = 67$ MeV where q is a light quark. As the κ coefficients are expected to decrease with increasing quark masses [98], we assume here that

$$0 < \kappa_{cc},\, \kappa_{bc},\, \kappa_{bb} < 67 \text{ MeV}. \tag{3.54}$$

The absolute uncertainties in our diquark constituent mass predictions in Table 3.1 are significantly larger than 67 MeV, and so, as a first approximation, we simply ignore the κ contributions to (3.53). Therefore, within the Type-II diquark-antidiquark model, we predict $J^P \in \{0^+,\, 1^+,\, 2^+\}$ tetraquark masses of 7.0 GeV for $[cc][\bar{c}\bar{c}]$, 12.2 GeV for $[cc][\bar{b}\bar{b}]$, and 17.3 GeV for $[bb][\bar{b}\bar{b}]$. The relative uncertainty in these mass predictions is roughly 10%. Furthermore, note that the $[cc][\bar{c}\bar{c}]$ and $[bb][\bar{b}\bar{b}]$ tetraquarks are charge conjugation eigenstates where $C = +$ for $J = 0$, 2 and $C = -$ for $J = 1$ [127, 128]. The $[cc][\bar{b}\bar{b}]$ tetraquarks are not charge conjugation eigenstates.

Regarding $[cc][\bar{c}\bar{c}]$ tetraquarks, taking into account 10% theoretical uncertainty, our Type-II model mass predictions are in reasonable agreement with those of [127, 128, 129], although

our central values are higher. However, our results are much higher than those of [130]. Furthermore, our tetraquark mass predictions are above both the $\eta_c(1S)$-$\eta_c(1S)$ and J/ψ-J/ψ thresholds indicating that the corresponding decay modes should be accessible as fall-apart decays.

Regarding $[cc][\bar{b}\bar{b}]$ tetraquarks, again factoring in 10% uncertainty, our Type-II model mass predictions are in reasonable agreement with those of [127, 128], although our central values are lower. With an electric charge of +2, two charm quarks, and two bottom antiquarks, such a state would be easy to identify through its decay products, and could not be misinterpreted as a conventional meson. Unfortunately, within theoretical uncertainty, we are unable to say whether or not our tetraquark mass predictions lie above or below the B_c^+-B_c^+ threshold.

Regarding $[bb][\bar{b}\bar{b}]$ tetraquarks, taking into account theoretical uncertainty, our Type-II model mass predictions are in reasonable agreement with those of [129] although our central values are lower. Our results are about 10% lower than those of [130, 131], and are much lower than those of [127, 128]. Tetraquarks with $bb\bar{b}\bar{b}$ quark composition (so-called "beauty-full" tetraquarks) have attracted considerable attention recently due to the possibility that some might have masses below the $\Upsilon(1S)$-$\Upsilon(1S)$ threshold and perhaps even the $\eta_b(1S)$-$\eta_b(1S)$ threshold. For $bb\bar{b}\bar{b}$ tetraquarks with masses below the $\eta_b(1S)$-$\eta_b(1S)$ threshold, fall-apart modes would be inaccessible and decays would instead proceed through OZI-suppressed processes. Central values of our Type-II diquark-antidiquark mass estimates put the 0^{++}, 1^{+-}, and 2^{++} states about 9% below the $\Upsilon(1S)$-$\Upsilon(1S)$ threshold and about 7% below the $\eta_b(1S)$-$\eta_b(1S)$ threshold.

In summary, we have used QCD LSRs to predict the axial vector doubly-heavy cc and bb diquark constituent masses. Our results are summarized in Table 3.1. These results were obtained from a calculation of the diquark correlation function at NLO in perturbation theory and to LO in the 4d and 6d gluon condensates as well as the 6d quark condensate. That the LSRs analyses stabilized in both the double charm and double bottom diquark channels provides QCD-based evidence for the existence of these structures. Within the Type-II diquark-antidiquark tetraquark model of Ref. [77], we predict, with an uncertainty of roughly 10%, 0^{++}, 1^{+-}, and 2^{++} $[cc][\bar{c}\bar{c}]$ tetraquarks of mass 7.0 GeV; 0^+, 1^+, and 2^+ $[cc][\bar{b}\bar{b}]$ tetraquarks of mass 12.2 GeV; and 0^{++}, 1^{+-}, and 2^{++} $[bb][\bar{b}\bar{b}]$ tetraquarks of mass 17.3 GeV.

Central values of our $[bb][\bar{b}\bar{b}]$ tetraquark mass predictions are well below the $\Upsilon(1S)$-$\Upsilon(1S)$ and $\eta_b(1S)$-$\eta_b(1S)$ thresholds, providing support for the possibility that fall-apart decay modes are inaccessible to some $bb\bar{b}\bar{b}$ tetraquarks.

Acknowledgments

We are grateful for financial support from the National Sciences and Engineering Research Council of Canada (NSERC).

3.3 Diquarks and Tetraquarks Conclusion

In [3], we began by using QCD LSRs to calculate constituent masses for $[cc]$ and $[bb]$ diquarks. These results are again collected in Table 3.2.

QQ	M_P (GeV)
cc	3.51 ± 0.35
bb	8.67 ± 0.69

Table 3.2: Constituent mass predictions for axial vector cc and bb diquarks including theoretical uncertainties from [3].

We then went on to use these diquark constituent masses as inputs into the Type-II CMI model of diquark-antidiquark tetraquarks [77] which allowed us to extract the tetraquark mass predictions collected in Table 3.3.

$[QQ][\bar{Q}\bar{Q}]$	M (GeV)
$[cc][\bar{c}\bar{c}]$	7.0
$[cc][\bar{b}\bar{b}]$	12.2
$[bb][\bar{b}\bar{b}]$	17.3

Table 3.3: Tetraquark mass predictions from [3], all uncertainties are roughly 10%.

As discussed in section 3.2.4 these tetraquarks have $J^P \in \{0^+, 1^+, 2^+\}$. Also, the $[cc][\bar{c}\bar{c}]$ and $[bb][\bar{b}\bar{b}]$ are charge conjugation eigenstates with $C = +$ for $J = 0, 2$ and $C = -$ for $J = 1$ [127, 128] and the $[cc][\bar{b}\bar{b}]$ is not charge conjugation eigenstates.

The diquark masses shown in Table 3.2 could also be used in other applications. In [3], we use them to generate the tetraquark masses shown in Table 3.3, but they could be used in a number of other hadronic systems where diquark substructure is possible. From baryons [132] to hexaquarks [133], hadrons with three or more constituent quarks have been modeled, in some cases, as though they have additional intermediate diquark substructure. Depending on the quark content of the hadron in question, these $[cc]$, $[\bar{c}\bar{c}]$, $[bb]$ and $[\bar{b}\bar{b}]$ diquark constituent masses could be used as inputs for other models.

Chapter 4

Conclusion

4.1 Closing Thoughts

The overarching goal of the work presented in this thesis was to explore several ideas related to beyond-the-quark-model hadrons. We wanted to try to shed some light on potentially allowable hadronic configurations beyond-the-quark-model. In the first two papers which we presented in Chapter 2 of this thesis [1, 2], we explored meson-hybrid mixing in vector heavy quarkonium. In the third paper [3] which we present in Chapter 3 of this thesis, we computed constituent masses for cc and bb diquarks. We then used these constituent masses to predict tetraquark masses. Let's now take a moment to collect our results and restate their implications one more time.

4.2 Results

4.2.1 Meson-Hybrid Mixing Results

When exploring meson-hybrid mixing in 1^{--} and 1^{++} charmonium and bottomonium [1, 2], we found the following results:

- In the 1^{--} charmonium sector, we saw non-zero mixing in the J/ψ, no evidence for mixing in the $\psi(2S), \psi(3770)$ cluster, and a large mixing parameter in the 4.3 GeV cluster. Again, we note that the $X(4260)$, which would be a member of this cluster at 4.3 GeV, has often been interpreted as having significant hybrid content, and our results are consistent with this idea.

- In the 1^{--} bottomonium sector, we saw non-zero mixing in all three resonances, the $\Upsilon(1S)$, the $\Upsilon(2S)$, and the two-state cluster containing the $\Upsilon(3S)$ and $\Upsilon(4S)$.

- In the 1^{++} charmonium sector, we saw almost no mixing in the $\chi_{c1}(1P)$, minimal mixing in the $X(3872)$, and significant mixing in both the $X(4140)$ and the $X(4274)$. Again, we note that the $X(3872)$ has been interpreted as having significant tetraquark content, and our result is consistent with that idea.

- In the 1^{++} bottomonium sector, we saw minimal mixing in the $\chi_{b1}(1P)$ and significant mixing in both the $\chi_{b1}(2P)$ and the $\chi_{b1}(2P)$.

4.2.2 Diquark/Tetraquark Results

In [3], we started by computing the following constituent diquark masses

$$M_{[cc]} = M_{[\overline{cc}]} = 3.51 \pm 0.35 \text{ GeV} \tag{4.1}$$

$$M_{[bb]} = M_{[\overline{bb}]} = 8.67 \pm 0.69 \text{ GeV}. \tag{4.2}$$

From these constituent diquark masses, we then went on to calculate the tetraquark masses which we have again collected in Table 4.1 (Now with accessible J^{PC}/J^{P} values listed).

$[QQ][\bar{Q}\bar{Q}]$	M (GeV)	J^{PC}/J^{P}
$[cc][\overline{cc}]$	7.0	0^{++}, 1^{+-}, 2^{++}
$[cc][\overline{bb}]$	12.2	0^{+}, 1^{+}, 2^{+}
$[bb][\overline{bb}]$	17.3	0^{++}, 1^{+-}, 2^{++}

Table 4.1: Tetraquark mass predictions from [3], all uncertainties are roughly 10%.

4.3 Error Checking

With calculations of these size there are a number of ways in which errors could be introduced into the computation. To eliminate these errors parts of the calculation are verified with

multiple methods whenever this is possible. The software that we have developed is tested against known results and, when possible, against hand calculations. Finally, whenever possible consistency checks are made against expected findings.

4.4 Future and Present Work

The work presented in this thesis also serves as a starting point for future work. Some of the techniques and results generated here could and are being used to further explore similar ideas in hadronic physics. For example, we are presently working at applying some of the tools we've developed in the calculation of diquark masses in [3] to calculate $[cb]$ diquark constituent masses. There is additional complexity introduced by the additional mass scale in the field theoretical calculation that will require more sophisticated numerical techniques to be used, but that work is ongoing. Once complete, we will again be able to use this constituent diquark mass to make further tetraquark mass predictions among other applications.

Another interesting possibility is the application of the multi-resonance analysis methodology, which we developed in [1, 2], to other hadronic spectra. This work is in the early stages, but there are several candidate hadronic spectra which we are exploring that may make good research subjects.

References

[1] A. Palameta, J. Ho, D. Harnett, and T. G. Steele, Phys. Rev. D **97**, 034001 (2018).

[2] A. Palameta, D. Harnett, and T. G. Steele, Phys. Rev. D **98**, 074014 (2018).

[3] S. Esau, A. Palameta, R. T. Kleiv, D. Harnett, and T. G. Steele, Phys. Rev. D **100**, 074025 (2019).

[4] Particle Data Group, C. Patrignani et al., Chin. Phys. **C40**, 100001 (2016).

[5] M. E. Peskin and D. V. Schroeder, An Introduction to Quantum Field Theory (Westview Press, 1995).

[6] S. L. Olsen, Front. Phys. **10**, 101401 (2015), 1411.7738.

[7] D. Binosi and L. Theussl, Comput. Phys. Commun. **161**, 76 (2004), hep-ph/0309015.

[8] A. Palameta, Vector charmonium meson-hybrid mixing: a field theoretical analysis, Master's thesis, University of Saskatchewan, 2016.

[9] M. Gell-Mann, Physics Letters **8**, 214 (1964).

[10] G. Zweig, An SU(3) model for strong interaction symmetry and its breaking. Version 2, in DEVELOPMENTS IN THE QUARK THEORY OF HADRONS. VOL. 1. 1964 - 1978, edited by D. Lichtenberg and S. P. Rosen, pp. 22–101, Cambridge University Press, 1964.

[11] H. Fritzsch and M. Gell-Mann, editors, 50 years of quarks (World Scientific, Hackensack, 2015).

[12] J. I. Friedman, H. W. Kendall, and R. E. Taylor, (1990).

[13] D. J. Gross and F. Wilczek, Phys. Rev. **D8**, 3633 (1973).

[14] H. Leutwyler, p. 29 (2014), 1211.6777.

[15] K. G. Wilson, Phys. Rev. **179**, 1499 (1969).

[16] P.Pascual and R.Tarrach, QCD: Renormalization for the Practitioner (Springer-Verlag, 1984).

[17] O. V. Tarasov, Phys. Rev. D **54**, 6479 (1996).

[18] O. V. Tarasov, Nucl. Phys. B **502**, 455 (1997).

[19] R. Mertig and R. Scharf, hep-ph/9801383 (1998).

[20] E. E. Boos and A. I. Davydychev, Theor. Math. Phys. **89**, 1052 (1991).

[21] D. J. Broadhurst, J. Fleischer, and O. V. Tarasov, Z. Phys. **60**, 287 (1993).

[22] M. A. Shifman, A. I. Vainshtein, and V. I. Zakharov, Nucl. Phys. **B147**, 385 (1979).

[23] J. Collins, Renormalization (Cambridge University Press, 1984).

[24] R. J. Eden and P. V. Landshoff, The Analytic S-Martix (Cambridge University Press, Cambridge, 1966), Bibliogr. Index.

[25] M. A. Shifman, A. I. Vainshtein, and V. I. Zakharov, Nucl. Phys. **B147**, 385 (1979).

[26] P. Colangelo and A. Khodjamirian, p. 1495 (2000), hep-ph/0010175.

[27] N. Brambilla et al., The xyz states: experimental and theoretical status and perspectives, 2019, 1907.07583.

[28] C. A. Meyer and E. S. Swanson, Prog. Part. Nucl. Phys. **82**, 21 (2015), 1502.07276.

[29] E. Kou and O. Pene, Physics Letters B **631**, 164–169 (2005).

[30] S.-L. Zhu, Phys. Rev. D **60**, 097502 (1999), hep-ph/9903537.

[31] F. E. Close and P. R. Page, Physics Letters B **628**, 215–222 (2005).

[32] BaBar, B. Aubert et al., Phys. Rev. Lett. **95**, 142001 (2005), hep-ex/0506081.

[33] BaBar, B. Aubert et al., Phys. Rev. Lett. **98**, 212001 (2007), hep-ex/0610057.

[34] Belle, C. Z. Yuan et al., Phys. Rev. Lett. **99**, 182004 (2007), 0707.2541.

[35] Belle, X. L. Wang et al., Phys. Rev. Lett. **99**, 142002 (2007), 0707.3699.

[36] S.-L. Zhu, Phys. Lett. **B625**, 212 (2005), hep-ph/0507025.

[37] W. Chen et al., QCD Sum Rule Analysis of Heavy Quarkonium Hybrids, in Meeting of the APS Division of Particles and Fields, 2013, 1310.0431.

[38] N. Brambilla et al., Eur. Phys. J. **C71**, 1534 (2011), 1010.5827.

[39] S. Eidelman, B. K. Heltsley, J. J. Hernandez-Rey, S. Navas, and C. Patrignani, (2012), 1205.4189.

[40] BESIII, M. Ablikim et al., Phys. Rev. Lett. **118**, 092002 (2017), 1610.07044.

[41] T. Barnes, F. E. Close, and E. S. Swanson, Phys. Rev. D **52**, 5242 (1995).

[42] M. A. Shifman, A. I. Vainshtein, and V. I. Zakharov, Nucl. Phys. **B147**, 448 (1979).

[43] L. J. Reinders, H. Rubinstein, and S. Yazaki, Phys. Rept. **127**, 1 (1985).

[44] S. Narison, QCD as a Theory of Hadrons, Cambridge Monographs on Particle Physics, Nuclear Physics and Cosmology Vol. 17 (Cambridge University Press, New York, 2004).

[45] S. Narison, N. Pak, and N. Paver, Phys. Lett. **B147**, 162 (1984).

[46] D. Harnett, R. T. Kleiv, K. Moats, and T. G. Steele, Nucl. Phys. **A850**, 110 (2011), 0804.2195.

[47] W. Chen et al., Phys. Rev. **D88**, 045027 (2013), 1305.0244.

[48] J. Ho, D. Harnett, and T. G. Steele, JHEP, In Press (2017).

[49] J. Govaerts, L. J. Reinders, and J. Weyers, Nucl. Phys. B **262**, 575 (1985).

[50] P. Pascual and R. Tarrach, QCD: Renormalization for the Practitioner (Springer, 1984).

[51] E. Bagán, M. R. Ahmady, V. Elias, and T. G. Steele, Z. Phys. **61**, 157 (1994).

[52] D. A. Akyeampong and R. Delbourgo, Nuovo Cimento **17**, 578 (1973).

[53] R. Mertig and R. Scharf, Comput. Phys. Commun. **111**, 265 (1998).

[54] M. Abramowitz and I. A. Stegun, Handbook of Mathematical Functions (Dover Publications, 1965).

[55] S. Narison and E. de Rafael, Phys. Lett. **103B**, 57 (1981).

[56] G. Launer, S. Narison, and R. Tarrach, Z. Phys. **C26**, 433 (1984).

[57] S. Narison, Phys. Lett. B **693**, 559 (2010), [Erratum: Phys. Lett.B705,544(2011)].

[58] W. Chen et al., J. High Energy Phys. **1309**, 019 (2013).

[59] R. Berg, D. Harnett, R. T. Kleiv, and T. G. Steele, Phys. Rev. D **86**, 034002 (2012).

[60] D. Harnett, R. T. Kleiv, T. G. Steele, and H.-y. Jin, J. Phys. **G39**, 125003 (2012).

[61] S. Narison, Int. J. Mod. Phys. **A30**, 1550116 (2015), 1404.6642.

[62] F. E. Close and P. R. Page, Phys. Rev. D **52**, 1706 (1995).

[63] E. Kou and O. Pene, Phys. Lett. **B631**, 164 (2005), hep-ph/0507119.

[64] A. Palameta, J. Ho, D. Harnett, and T. G. Steele, Phys. Rev. **D97**, 034001 (2018), 1707.00063.

[65] Belle, S. K. Choi et al., Phys. Rev. Lett. **91**, 262001 (2003), hep-ex/0309032.

[66] E. S. Swanson, Phys. Rept. **429**, 243 (2006), hep-ph/0601110.

[67] S.-L. Zhu, Int. J. Mod. Phys. **E17**, 283 (2008), hep-ph/0703225.

[68] S. Godfrey and S. L. Olsen, Ann. Rev. Nucl. Part. Sci. **58**, 51 (2008), 0801.3867.

[69] M. Nielsen, F. S. Navarra, and S. H. Lee, Phys. Rept. **497**, 41 (2010), 0911.1958.

[70] R. D. Matheus, F. S. Navarra, M. Nielsen, and C. M. Zanetti, Phys. Rev. **D80**, 056002 (2009), 0907.2683.

[71] J. H.-y. K. R. T. S. T. G. W. M. Chen, W. and Q. Xu, Phys. Rev. D **88**, 045027 (2013).

[72] M. Padmanath, C. B. Lang, and S. Prelovsek, Phys. Rev. **D92**, 034501 (2015), 1503.03257.

[73] X.-W. Kang and J. A. Oller, Eur. Phys. J. **C77**, 399 (2017), 1612.08420.

[74] J. Ho, D. Harnett, and T. G. Steele, JHEP **05**, 149 (2017), 1609.06750.

[75] S. Godfrey and N. Isgur, Phys. Rev. **D32**, 189 (1985).

[76] E. Bagan, M. R. Ahmady, V. Elias, and T. G. Steele, Z. Phys. **C61**, 157 (1994).

[77] L. Maiani, F. Piccinini, A. D. Polosa, and V. Riquer, Phys. Rev. **D89**, 114010 (2014), 1405.1551.

[78] R. J. Jaffe, Phys. Rev. D **15**, 267 (1977).

[79] R. L. Jaffe, Phys. Rev. D **15**, 281 (1977).

[80] CDF, D. Acosta et al., Phys. Rev. Lett. **93**, 072001 (2004), hep-ex/0312021.

[81] D0, V. M. Abazov et al., Phys. Rev. Lett. **93**, 162002 (2004), hep-ex/0405004.

[82] BaBar, B. Aubert et al., Phys. Rev. Lett. **93**, 041801 (2004), hep-ex/0402025.

[83] LHCb, R. Aaij et al., Eur. Phys. J. **C72**, 1972 (2012), 1112.5310.

[84] Particle Data Group, J. Beringer et al., Phys. Rev. D **86**, 010001 (2012).

[85] A. Ali, J. S. Lange, and S. Stone, Prog. Part. Nucl. Phys. **97**, 123 (2017), 1706.00610.

[86] H.-X. Chen, W. Chen, X. Liu, and S.-L. Zhu, Phys. Rept. **639**, 1 (2016), 1601.02092.

[87] Y.-R. Liu, H.-X. Chen, W. Chen, X. Liu, and S.-L. Zhu, (2019), 1903.11976.

[88] F. E. Close and P. R. Page, Phys. Lett. **B578**, 119 (2004), hep-ph/0309253.

[89] M. B. Voloshin, Phys. Lett. **B579**, 316 (2004), hep-ph/0309307.

[90] E. S. Swanson, Phys. Lett. **B588**, 189 (2004), hep-ph/0311229.

[91] N. A. Tornqvist, Phys. Lett. **B590**, 209 (2004), hep-ph/0402237.

[92] M. T. AlFiky, F. Gabbiani, and A. A. Petrov, Phys. Lett. **B640**, 238 (2006), hep-ph/0506141.

[93] C. E. Thomas and F. E. Close, Phys. Rev. **D78**, 034007 (2008), 0805.3653.

[94] X. Liu, Z.-G. Luo, Y.-R. Liu, and S.-L. Zhu, Eur. Phys. J. **C61**, 411 (2009), 0808.0073.

[95] I. W. Lee, A. Faessler, T. Gutsche, and V. E. Lyubovitskij, Phys. Rev. **D80**, 094005 (2009), 0910.1009.

[96] M. Anselmino, E. Predazzi, S. Ekelin, S. Fredriksson, and D. B. Lichtenberg, Rev. Mod. Phys. **65**, 1199 (1993).

[97] R. L. Jaffe, Phys. Rept. **409**, 1 (2005), hep-ph/0409065, [,191(2004)].

[98] L. Maiani, F. Piccinini, A. D. Polosa, and V. Riquer, Phys. Rev. **D71**, 014028 (2005), hep-ph/0412098.

[99] D. Ebert, R. N. Faustov, and V. O. Galkin, Phys. Lett. **B634**, 214 (2006), hep-ph/0512230.

[100] R. D. Matheus, S. Narison, M. Nielsen, and J. M. Richard, Phys. Rev. **D75**, 014005 (2007), hep-ph/0608297.

[101] K. Terasaki, Prog. Theor. Phys. **118**, 821 (2007), 0706.3944.

[102] S. Dubnicka, A. Z. Dubnickova, M. A. Ivanov, and J. G. Korner, Phys. Rev. **D81**, 114007 (2010), 1004.1291.

[103] R. T. Kleiv, T. G. Steele, A. Zhang, and I. Blokland, Phys. Rev. **D87**, 125018 (2013), 1304.7816.

[104] A. Zhang, T. Huang, and T. G. Steele, Phys. Rev. **D76**, 036004 (2007), hep-ph/0612146.

[105] H. G. Dosch, M. Jamin, and B. Stech, Zeitschrift für Physik C Particles and Fields **42**, 167 (1989).

[106] M. Jamin and M. Neubert, Phys. Lett. **B238**, 387 (1990).

[107] Z.-G. Wang, Commun. Theor. Phys. **59**, 451 (2013), 1112.5910.

[108] Z.-G. Wang, Eur. Phys. J. **C71**, 1524 (2011), 1008.4449.

[109] K. Kim, D. Jido, and S. H. Lee, Phys. Rev. **C84**, 025204 (2011), 1103.0826.

[110] M. Hess, F. Karsch, E. Laermann, and I. Wetzorke, Phys. Rev. **D58**, 111502 (1998), hep-lat/9804023.

[111] C. Alexandrou, P. de Forcrand, and B. Lucini, Phys. Rev. Lett. **97**, 222002 (2006), hep-lat/0609004.

[112] Y. Bi et al., Chin. Phys. **C40**, 073106 (2016), 1510.07354.

[113] R. T. Kleiv, T. G. Steele, A. Zhang, and I. Blokland, Phys. Rev. D **87**, 125018 (2013).

[114] E. Bagan, M. R. Ahmady, V. Elias, and T. G. Steele, Z. Phys. **C61**, 157 (1994).

[115] A. Palameta, D. Harnett, and T. G. Steele, Phys. Rev. **D98**, 074014 (2018), 1805.04230.

[116] M. Chanowitz, M. Furman, and I. Hinchliffe, Nucl. Phys. B **159**, 225 (1979).

[117] T. Huber and D. Maitre, Comput. Phys. Commun. **178**, 755 (2008), 0708.2443.

[118] S. Narison, (2002), hep-ph/0205006.

[119] L. J. Reinders, H. R. Rubinstein, and S. Yazaki, Phys. Rep. **127**, 1 (1984).

[120] E. F. Beckenbach and R. Bellman, Inequalities (Springer, 1961).

[121] S. K. Berberian, Measure and Integration (MacMillan, 1965).

[122] D. Harnett, T. G. Steele, and V. Elias, Nucl. Phys. **A686**, 393 (2001), hep-ph/0007049.

[123] V. V. Kiselev, A. K. Likhoded, O. N. Pakhomova, and V. A. Saleev, Phys. Rev. **D66**, 034030 (2002), hep-ph/0206140.

[124] D. Ebert, R. N. Faustov, V. O. Galkin, and W. Lucha, Phys. Rev. **D76**, 114015 (2007), 0706.3853.

[125] V. R. Debastiani and F. S. Navarra, Chin. Phys. **C43**, 013105 (2019), 1706.07553.

[126] Q.-X. Yu and X.-H. Guo, (2018), 1810.00437.

[127] G.-J. Wang, L. Meng, and S.-L. Zhu, (2019), 1907.05177.

[128] M.-S. Liu, Q.-F. Lü, X.-H. Zhong, and Q. Zhao, Phys. Rev. **D100**, 016006 (2019), 1901.02564.

[129] W. Chen, H.-X. Chen, X. Liu, T. G. Steele, and S.-L. Zhu, Phys. Lett. **B773**, 247 (2017), 1605.01647.

[130] Z.-G. Wang, Eur. Phys. J. **C77**, 432 (2017), 1701.04285.

[131] M. N. Anwar, J. Ferretti, F.-K. Guo, E. Santopinto, and B.-S. Zou, Eur. Phys. J. **C78**, 647 (2018), 1710.02540.

[132] B. Chakrabarti, A. Bhattacharya, S. Mani, and A. Sagari, Acta Phys. Polon. B **41**, 95 (2010).

[133] Z.-G. Wang, Triply-charmed hexaquark states with the qcd sum rules, 2020, 2002.06202.

[134] D. A. Akyeampong and R. Delbourgo, Nuovo Cim. **A17**, 578 (1973).

Appendix A

Identities, Definitions and Conventions

This appendix, which I also included in [8], serve as a collection of several of the identities and definitions commonly used in these calculations. I included it here as a useful reference and as clarification of the conventions used in our work. To begin with, for all calculations in this thesis we use natural units where $\hbar = c = 1$.

A.1 Colour Algebra

With regard to the use of δ functions we use a convention where a delta function appearing with Latin indices is understood to exist in gluon colour space such that

$$\delta^{ab}\delta_{ab} = \delta^a_a = 8 \tag{A.1}$$

and a delta function appearing with Greek indices is understood to exist in quark colour space such that

$$\delta_{\alpha\beta}\delta^{\alpha\beta} = \delta^\alpha_\alpha = 3 \tag{A.2}$$

finally a delta function appearing with functional arguments (such as $\delta(p-q)$) is understood to be a d dimensional Dirac delta function.

Lambdas (λ) will be understood to be Gell-Mann matrices and they relate to the generators of SU(3) (which we represent with t) as follows

$$\lambda^a = 2t^a. \tag{A.3}$$

The traces of these Gell-Mann matrices obey the following identities, additional identities can be found in [16]

$$Tr[\lambda^a] = 0 \tag{A.4}$$

$$\lambda^a_{\alpha\beta}\lambda^b_{\beta\alpha} = Tr[\lambda^a\lambda^b] = 2\delta^{ab} \tag{A.5}$$

$$\lambda^a_{\alpha\beta}\lambda^b_{\beta\delta}\lambda^c_{\delta\alpha} = Tr[\lambda^a\lambda^b\lambda^c] = 2(d^{abc} + if^{abc}) \tag{A.6}$$

where the d^{abc} are totally symmetric and the f^{abc} are totally antisymmetric structure constants.

A.2 Dirac Algebra

We use the mostly minus sign convention for our Minkowski metric tensors (g) such that

$$\text{Diagonal}(g^{\mu\nu}) = (1, -1, -1, -1) \tag{A.7}$$

and in d-dimensions they obey the following identities

$$g^{\mu\nu}g_{\mu\nu} = g^{\mu}_{\mu} = d \tag{A.8}$$

and

$$g^{\mu\nu}p_{\mu}q_{\nu} = p^{\nu}q_{\nu} = p \cdot q \tag{A.9}$$

where p and q are some four-momenta. We define γ^5 in d-dimensions by the following convention

$$\gamma^5 = -\frac{i}{24}\epsilon_{\mu\nu\sigma\rho}\gamma^{\mu}\gamma^{\nu}\gamma^{\sigma}\gamma^{\rho} \tag{A.10}$$

which is consistent with [134]. With regard to the traces of gamma matrices we use the following identities. Additional identities involving traces without γ^5's in them can be found in [5]. For the sake of brevity we omit identities with larger traces.

$$Tr[\gamma^5] = 0 \tag{A.11}$$

$$Tr[\gamma^{\mu}\gamma^{\nu}\gamma^5] = 0 \tag{A.12}$$

$$Tr[\gamma^{\mu}\gamma^{\nu}\gamma^{\rho}\gamma^{\sigma}\gamma^5] = -4i\epsilon^{\mu\nu\rho\sigma} \tag{A.13}$$

$$\begin{aligned} Tr[\gamma^{\mu}\gamma^{\nu}\gamma^{\rho}\gamma^{\sigma}\gamma^{\eta}\gamma^{\tau}\gamma^5] = -4i\Big(&\epsilon^{\mu\nu\rho\sigma}g^{\eta\tau} - \epsilon^{\nu\rho\sigma\tau}g^{\mu\eta} + \epsilon^{\rho\sigma\eta\tau}g^{\mu\nu} - \epsilon^{\nu\sigma\eta\tau}g^{\mu\rho} + \\ &\epsilon^{\nu\rho\eta\tau}g^{\mu\sigma} + \epsilon^{\nu\rho\sigma\eta}g^{\mu\tau} + \epsilon^{\mu\rho\sigma\tau}g^{\nu\eta} + \epsilon^{\mu\sigma\eta\tau}g^{\nu\rho} - \\ &\epsilon^{\mu\rho\eta\tau}g^{\nu\sigma} - \epsilon^{\mu\rho\sigma\eta}g^{\nu\tau} - \epsilon^{\mu\nu\sigma\tau}g^{\rho\eta} + \epsilon^{\mu\nu\eta\tau}g^{\rho\sigma} + \\ &\epsilon^{\mu\nu\sigma\eta}g^{\rho\tau} + \epsilon^{\mu\nu\rho\tau}g^{\sigma\eta} - \epsilon^{\mu\nu\rho\eta}g^{\sigma\tau}\Big) \end{aligned} \tag{A.14}$$

The most general contraction of two Levi-Civita symbols can be written as follows. Similar (but more compact) identities where the Levi-Civita symbols share some indices can be found in [5] among other places

$$\begin{aligned} \epsilon^{\alpha\beta\gamma\delta}\epsilon^{\mu\nu\rho\sigma} = &- g^{\alpha\sigma}g^{\beta\rho}g^{\gamma\nu}g^{\delta\mu} + g^{\alpha\rho}g^{\beta\sigma}g^{\gamma\nu}g^{\delta\mu} + g^{\alpha\sigma}g^{\beta\nu}g^{\gamma\rho}g^{\delta\mu} - g^{\alpha\nu}g^{\beta\sigma}g^{\gamma\rho}g^{\delta\mu} \\ &- g^{\alpha\rho}g^{\beta\nu}g^{\gamma\sigma}g^{\delta\mu} + g^{\alpha\nu}g^{\beta\rho}g^{\gamma\sigma}g^{\delta\mu} + g^{\alpha\sigma}g^{\beta\rho}g^{\gamma\mu}g^{\delta\nu} - g^{\alpha\rho}g^{\beta\sigma}g^{\gamma\mu}g^{\delta\nu} \\ &- g^{\alpha\sigma}g^{\beta\mu}g^{\gamma\rho}g^{\delta\nu} + g^{\alpha\mu}g^{\beta\sigma}g^{\gamma\rho}g^{\delta\nu} + g^{\alpha\rho}g^{\beta\mu}g^{\gamma\sigma}g^{\delta\nu} - g^{\alpha\mu}g^{\beta\rho}g^{\gamma\sigma}g^{\delta\nu} \\ &- g^{\alpha\sigma}g^{\beta\nu}g^{\gamma\mu}g^{\delta\rho} + g^{\alpha\nu}g^{\beta\sigma}g^{\gamma\mu}g^{\delta\rho} + g^{\alpha\sigma}g^{\beta\mu}g^{\gamma\nu}g^{\delta\rho} - g^{\alpha\mu}g^{\beta\sigma}g^{\gamma\nu}g^{\delta\rho} \\ &- g^{\alpha\nu}g^{\beta\mu}g^{\gamma\sigma}g^{\delta\rho} + g^{\alpha\mu}g^{\beta\nu}g^{\gamma\sigma}g^{\delta\rho} + g^{\alpha\rho}g^{\beta\nu}g^{\gamma\mu}g^{\delta\sigma} - g^{\alpha\nu}g^{\beta\rho}g^{\gamma\mu}g^{\delta\sigma} \\ &- g^{\alpha\rho}g^{\beta\mu}g^{\gamma\nu}g^{\delta\sigma} + g^{\alpha\mu}g^{\beta\rho}g^{\gamma\nu}g^{\delta\sigma} + g^{\alpha\nu}g^{\beta\mu}g^{\gamma\rho}g^{\delta\sigma} - g^{\alpha\mu}g^{\beta\nu}g^{\gamma\rho}g^{\delta\sigma}. \end{aligned} \tag{A.15}$$